157900-23-F

Final Report

PHASE II DEVELOPMENT OF GREAT LAKES ALGORITHMS FOR NIMBUS-7 COASTAL ZONE COLOR SCANNER

FRED J. TANIS
Applications Division

AUGUST 1984

NASA/Lewis Research Center
21000 Brookpark Road
Cleveland, OH 44135

Contract: NAS3-22892

ENVIRONMENTAL
RESEARCH INSTITUTE OF MICHIGAN
BOX 8618 • ANN ARBOR • MICHIGAN 48107

TECHNICAL REPORT STANDARD TITLE PAGE

1. Report No.	2. Government Accession No.	3. Recipient's Catalog No.
157900-23-F		

4. Title and Subtitle	5. Report Date
Phase II Development of Great Lakes Algorithms for NIMBUS-7 Coastal Zone Color Scanner	August 1984
	6. Performing Organization Code
7. Author(s)	8. Performing Organization Report No.
Fred J. Tanis	157900-23-F
9. Performing Organization Name and Address	10. Work Unit No.
Environmental Research Institute of Michigan Applications Division, P.O. Box 8618 Ann Arbor, Michigan 48107	
	11. Contract or Grant No.
	NAS3-22892
	13. Type of Report and Period Covered
12. Sponsoring Agency Name and Address	Final Report
NASA/Lewis Research Center Cleveland, OH 44135 Attn: Mr. Thom A. Coney	14. Sponsoring Agency Code

15. Supplementary Notes

16. Abstract

A series of experiments have been conducted in the Great Lakes designed to evaluate the application of the NIMBUS-7 Coastal Zone Color Scanner (CZCS). Atmospheric and water optical models were used to relate surface and subsurface measurements to satellite measured radiances. Absorption and scattering measurements were reduced to obtain a preliminary optical model for the Great Lakes. Algorithms were developed for geometric correction, correction for Rayleigh and aerosol path radiance, and prediction of chlorophyll-a pigment and suspended mineral concentrations. The atmospheric algorithm developed compared favorably with existing algorithms and was the only algorithm found to adequately predict the radiance variations in the 670 nm band. The atmospheric correction algorithm developed was designed to extract needed algorithm parameters from the CZCS radiance values. The Gordon/NOAA ocean algorithms could not be demonstrated to work for Great Lakes waters. Predicted values of chlorophyll-a concentration compared favorably with expected and measured for several areas of the Great Lakes.

17. Key Words	18. Distribution Statement
Water Reflectance Models Atmospheric Algorithms Bio-Optical Algorithms Radiative Transfer	

19. Security Classif. (of this report)	20. Security Classif. (of this page)	21. No. of Pages	22. Price
Unclassified	Unclassified		

PREFACE

This final report, as issued by the Applications Division of the Environmental Research Institute of Michigan (ERIM) under National Aeronautics and Space Administration (NASA) contract NAS3-22892 for the Lewis Research Center (LeRC), covers the contract period from September 1, 1981 through April 30, 1983. The technical representative for the contract officer was Mr. Thom Coney of LeRC. The principal investigator was Mr. Fred Tanis with important contributions made by Ms. Jacquelyn S. Ott, Mr. Thomas Wessling, and Dr. Russell Moll (University of Michigan). This research was conducted by the Resources and Technology Department of the Applications Division under the direction of Mr. Fred J. Thomson.

This contract involves developing algorithms to map chlorophyll-a and suspended sediment concentrations in Great Lakes waters using the Coastal Zone Color Scanner (CZCS). The technical approach is based upon the inherent optical characteristics of Great Lakes waters. A number of universities and institutions participated in the project. This report covers ERIM's activities in the project during the second phase of the program.

TABLE OF CONTENTS

LIST OF FIGURES

LIST OF FIGURES (continued)

LIST OF TABLES

LIST OF TABLES (continued)

1.0

SUMMARY

A series of experiments were conducted, in the Great Lakes region, to evaluate the application of the Nimbus-7 Coastal Zone Color Scanner (CZCS) to assessment of trophic state, verification and spatial refinement of whole lake models, and observation of temporal and spatial dynamics of phytoplankton. The focus of the present project is the development and testing of atmospheric and water quality algorithms appropriate to the Great Lakes as well as evaluation of existing algorithms developed for the marine environment. The quantification of chlorophyll and suspended sediment in Great Lakes waters by satellite visible radiometry is dependent on a thorough understanding of the radiative transfer processes in the atmosphere, at the water surface, and in the water column itself. It has been well established that the particulate and dissolved substance content of water affects the apparent water color. By sensing color with a high signal to noise ratio in narrow spectral bands, CZCS provides a means of mapping the water content which has been heretofore unavailable from satellite data. Since the air and water radiometric effects are coupled, removal of atmospheric effects becomes critical to the success of the Great Lakes application. Once the atmospheric path radiance has been removed, the radiance which is scattered upward from beneath the surface can be observed and used to determine water parameters. The portion of water radiance reaching the satellite from the lake surface can amount to as little as two or three percent of the total. Further, the variation due to constituent concentration can be much less than that due to atmospheric changes. In addition to these atmospheric effects, the water problem requires understanding of inherent optical properties related to measured quantities of chlorophyll-a pigment concentration, suspended mineral particles, and dissolved organics.

Previous remote sensing studies of Great Lakes waters employed less quantitative approaches and relied heavily on the available surface truth measurements [1,2]. Constituent algorithms developed in these latter studies were empirical and had little validity beyond the area of surface truth, and could not be applied when surface truth were unavailable. In the present study algorithms were sought which can be based on optical properties specific to the Great Lakes and which have reduced requirements for surface truth. Further they must be able to predict surface concentrations of chlorophyll-a and suspended sediments over a wide range of values and they must be capable of making predictions over water masses which exhibit spatial variation of both atmospheric haze and surface concentrations.

The project was carried out in two phases. The first phase involved data collection and development of CZCS geometric correction software [3]. During the summer of 1980 a series of CZCS overflights of the Great Lakes were made with the simultaneous collection of surface truth data. The surface truth data consisted of point sampling for water quality and optical parameters and airborne flightlines with the Ocean Color Scanner. The second phase consisted of data reduction and algorithm development for both atmospheric corrections and quantification of water parameters. ERIM's primary task under this second phase was CZCS algorithm development for the Great Lakes.

The investigation of possible atmospheric correction algorithms included evaluation of three existing algorithms and the development of a new algorithm based upon the available 1980 CZCS experiments. Because of the spatial variations in the concentration of aerosol particles each algorithm considered applied a correction on a pixel-by-pixel basis. Existing algorithms considered included (1) the Gordon algorithm [4], (2) the Smith and Wilson algorithm [5], and (3) the pseudo-optical depth algorithm due to Jain [6]. A fourth algorithm developed under this project was designated the residual component algorithm. Each of these

algorithms was adapted to operate in two modes. First, the algorithm could be operated in a calibration mode to extract the necessary aerosol parameters from a hazy portion of the scene. Second, the algorithm could be used with the data derived parameters to process the scene on a pixel-by-pixel basis to remove the spatially varying component due to aerosol particles. Extraction of aerosol parameters for a given scene is dependent on two basic requirements. First, there must be some water masses in the scene which have uniformly low and predictable levels of chlorophyll-a pigment concentration. It must be possible to reliably estimate the upwelling radiance for the calibration areas under a variety of illumination conditions. This need can best be satisfied with a combination of upwelling radiance measurements or reflectance model calculations. Second, the scene must contain sufficient haze over one or more of these calibration areas to provide a basis for aerosol spectral characterization.

A comparison study made with these four separate atmospheric algorithms indicated that the algorithm derived in this project was superior to the existing algorithms. Three criteria were used to evaluate the performance of each atmospheric correction algorithm. First, derived or measured local optical depths were used with an atmospheric radiance model to estimate the aerosol portion of the path radiance. These path radiances were compared with those predicted by each algorithm. Second, the upwelling CZCS spectra, or that implied from known concentrations of principal constituents, were compared with that obtained from each of the correction algorithms. Third, the spatial patterns of haze known to be present in the raw uncorrected imagery were examined to see if they were removed by the algorithm. The residual patterns in the corrected imagery were also compared with known or suspected patterns of phytoplankton productivity and suspended solids.

Results from this comparative analysis suggested that the Gordon algorithm and its assumption (that the upwelling radiance at 670 nm is

zero) are not valid for the Great Lakes waters. Acceptable performance could not be obtained even in areas with known minimum productivity. Furthermore, it was demonstrated that for extensive areas of the Great Lakes the upwelling spectra have a significant component at 670 nm which can be utilized to extract information on constituent concentrations. Under conditions of light haze each of the three other algorithms appeared to be capable of haze removal in CZCS bands one, two, and three. The project developed algorithm (4) appears to be capable of normalizing the most severe haze conditions. Conditions can exist, however, where the haze is sufficiently dense to make recovery of surface reflectance impractical. Radiance model studies showed that predicted values of the upwelling radiance produced from algorithm (4) to be the most valid, but additional surface upwelling radiance data would be helpful to further verify water radiance model calculations. For the CZCS subscenes tested, algorithm (4) developed under this project showed the best overall performance at removing the effects of aerosol haze.

The CZCS water parameter algorithm developed under this project is designed to predict both the concentration of suspended mineral particles (mg/ℓ) and the concentration of chlorophyll-a pigments (μg/ℓ). Initially, band ratio and other empirical algorithms developed for marine environments were applied to the Great Lakes waters with little success [7]. These latter water algorithms were not expected to work well for Great Lakes waters since the inherent optical properties of these waters are different from those found in an open ocean environment.

Great Lakes water algorithms were developed using a comprehensive volume reflectance/atmospheric transfer model. This model is capable of predicting CZCS measured radiances at selected viewing geometries with a flat water surface and with specified atmospheric and water absorption and scattering parameters. This model incorporates Monte Carlo

calculations of subsurface reflectance which are related to the absorption and scattering properties via a power series expansion [8]. The water reflectance model was combined with an atmospheric model so that the entire water/atmosphere radiative transfer process could be simulated. This model was used to simulate actual CZCS viewing geometries and the observed satellite measured radiances in each of the CZCS bands. Aerosol and Rayleigh optical thicknesses were estimated for each scene date and viewing geometry. Surface truth measurement data were used in the water model to estimate the subsurface reflectance. The combination of these parameters allowed simulation of the entire illuminating and viewing geometry and estimation of the expected CZCS radiance. Once the atmospheric parameters were sufficiently established, underwater absorption and scattering coefficients could be adjusted to improve the fit between model predicted and measured values of the CZCS radiance in each band.

Several different sets of water optical properties were tried based on those reported by Jain, Morel and Priur, and Gordon [6,8,9]. Underwater optical properties measured in vitro by the NASA Langley Research Center during the summer experiments were also incorporated [10]. Results from the simulation analysis indicated, as might be expected, that no single set of optical properties worked well for all waters of the Great Lakes. Optical properties of nearshore waters which are often laden with resuspended, eroded, and tributary sediments were found to be complex and different between Western Lake Erie, Southern Lake Michigan, and Western Lake Superior near Duluth, Minnesota. In addition, these waters have different optical characteristics from those associated with open waters of central Lakes Michigan, Huron, and Superior.

Surface measurements were to be obtained on all of the Great Lakes from other sources, but unfortunately they were insufficient to allow derivation of separate water algorithms for coastal and open clear

waters of each of the Great Lakes. No surface truth was collected from Lakes Huron and Ontario. Under such circumstances a compromise optical model for the entire Great Lakes was appropriate and consistent with the limited set of coincident surface truth measurements. A direct solution search technique described by Hooke and Jeeves [11] was used with the simulation model to derive a representative set of optical parameters for the Great Lakes. A water parameter extraction algorithm for CZCS was based upon this latter optical model. The algorithm consists of a series of polynomial prediction equations in the band 1/band 3, and the band 1/band 4 ratios which were derived from model simulated radiances. Comparisons made with the measurement data showed the algorithm capable of predicting concentrations with an average error of approximately 0.5 Log(C) for chlorophyll-a pigment concentration and for suspended sediment concentrations.

The derived atmospheric and water algorithms were used to extract chlorophyll-a concentrations from the available CZCS data for several open lake and coastal areas of the Great Lakes. These values were found to compare well with those reported in an earlier Upper Great Lakes Reference Study which attempted to characterize these waters from existing surface measurements [12]. The satellite and measured values compared especially well for the open clear waters for which average concentrations do not change dramatically from year to year. In productive areas such as Saginaw Bay and Western Lake Erie, the CZCS extracted values covered a broad range of values which encompassed the measured values. For such complex waters it is difficult to characterize the trophic state with a single average value without dealing with the complex spatial sampling problem. In this regard the CZCS extracted values were considered to be potentially more useful for that characterization.

While it is recognized that additional verification and field experiments are needed, a great deal of progress has been made toward

developing quantitative CZCS algorithms for the Great Lakes region and similar coastal type waters. Furthermore, it now appears feasible to develop stand alone algorithms which once calibrated would require only a minimum of surface truth data to have application to multiple scenes and location within the Great Lakes.

2.0

INTRODUCTION

The needs for monitoring and surveillance of the Great Lakes water quality have been recognized repeatedly by both Canada and the U.S. Federal agencies. This need is mandated by the Great Lakes water quality agreement of 1972. Contained within this agreement is the requirement for monitoring programs to provide for the assessment of water quality conditions and for the effectiveness of corrective actions. To meet this requirement, large scale surveillance plans, utilizing ship surveys, have been adopted and implemented throughout the Great Lakes. Present ship survey techniques are both costly and are limited in temporal and spatial resolution. Satellite remote sensing offers the potential for increasing both the efficiency and the accuracy of shipboard measurements.

The NIMBUS-7 Coastal Zone Color Scanner (CZCS) was specifically designed to quantitatively measure biomass related chlorophyll-pigment concentrations in the ocean and, therefore, represents a unique opportunity for testing the feasibility and applicability of satellite water quality monitoring in the Great Lakes. Previous research and demonstration programs have been conducted with aircraft and Landsat have shown the ability to measure certain synoptic water quality data and opportunities to extend ship sampling capabilities [2]. The present approach is a quantitative one, whereas previous studies tended to be qualitative, involving image interpretation.

Attempts to extract quantitative water quality data from Landsat were based upon empirical models which relied heavily on surface ship sampling. The validity of these relationships could not be extended to other lakes or satellite scene dates or other water masses within the same lake. These difficulties were caused at least by three separate sources of error.

First, no accounting was made of spatial or temporal variations in atmospheric optical parameters. Secondly, the inherent optical properties of Great Lakes waters were not measured, modelled or otherwise considered in the derivation of remote sensing relationships designed to predict constituent concentrations. Thirdly, the spectral bands available with Landsat MSS were not ideally placed to make such measurements. The present study has addressed each one of these issues in an effort to develop extraction algorithms representative to the Great Lakes region. Because of the complexity and diversity of Great Lakes water quality parameters a credible evaluation for CZCS requires that data be collected for the entire range of water conditions for which the CZCS data could be applied. The focus of the present program is the development and testing of atmospheric and water algorithms appropriate to the Great Lakes as well as evaluation of existing algorithms developed for the marine environment.

2.1 STATEMENT OF THE PROBLEM

The quantification of substances in Great Lakes waters by satellite visible radiometry is dependent on a thorough understanding of the radiative transfer processes in the atmosphere, at the water's surface, and in the water column itself. It has been well established that the content of water, be it particulate or dissolved substances, affects the apparent color. By sensing color with a high signal-to-noise ratio in narrow spectral bands CZCS provides a means of looking at the water content which has been heretofore unavailable from satellite data. Since the air and water effects are coupled to the CZCS radiometric data, removal of atmospheric effects becomes critical to the success of Great Lakes verification. Once these are removed, the radiance which is scattered upward from beneath the surface can be observed clearly by the satellite. Effectively, the radiance reaching the satellite from the lake surface amounts to a few percent of the total radiation and consequently much of the radiation received is from atmospheric

backscatter and surface reflectance (see Table 2.1). Furthermore the variation in radiance at the satellite due to change in constituent concentration could be on the order of 1% while the corresponding variations due to atmospheric changes can be considerably higher. The spatially varying atmospheric component is due principally to aerosol scattering. The significance of the atmospheric problem for a water target has been demonstrated by Hovis and Lung [14] and more recently by Quenzel and Kaestner [15] who compared the variability of the atmosphere with the reflected light from phytoplankton suspensions. Thus, an essential project goal and significant barrier to resolution of quantitative information from the water are the reduction of interferring atmospheric effects.

TABLE 2.1 ATMOSPHERIC INFLUENCE ON SIGNALS MEASURED OVER THE OCEAN [13]

Wavelength (nanometers)	Percent Undesired Radiance	
	Clear Water	Turbid Water
440	85.6	81.9
520	82.5	67.7
550	85.5	65.1
670	97.8	83.6

Understanding the components of the upwelling radiance which contain information on the subsurface constituents requires knowledge of both the apparent and inherent optical properties of the water and how these properties relate to measured quantities of chlorophyll-a pigments, suspended sediments, and dissolved organics. The work of Bukata et al [16] on Lake Ontario described the optical properties of these components which provided a basic model for the present study. Many previous studies relied heavily on the availability of ship collected surface truth and employed empirical techniques to relate

remote sensing derived variables to surface truth data [17]. Resulting algorithms could not be easily applied to other lakes or scene dates. For the present study algorithms were sought which could be based on optical properties specific to the Great Lakes and which would reduce the need for collection of coincident and extensive surface truth.

2.2 PROJECT PARTICIPANTS

Prior to beginning, the first phase of the project an ad hoc group was organized and coordinated by the NASA Lewis Research Center to promote cooperation among the various investigations. The group was directed by the NOAA Great Lakes Environmental Research Laboratory (GLERL). The principal participants in the project included NASA Lewis Research Center (LeRC), ERIM, University of Wisconsin, University of Minnesota (Duluth), University of Michigan Center for Great Lakes Research, NASA Langley Research Center (LaRC), Naval Oceans Systems Center (NOSC), and Science Applications Incorporated (SAI). These participants brought a wide variety of backgrounds and capabilities to the project. During the second phase of the project ERIM provided coordination services to the group by organizing a series of meetings and making personal contacts. One of the principal functions of this effort was to disseminate the data to all project participants.

2.3 OBJECTIVES AND APPROACH

The objectives of the CZCS Great Lakes Experiment were as follows:

(1) Assure the acquisition of sufficient standardized ground truth sampling and ancillary data to fully evaluate the potential of CZCS to determine and monitor Great Lakes water quality parameters.

(2) Apply the acquired data pairs to validate CZCS water quality algorithms as well as determine their limitations and accuracies when used to provide whole lake parameter maps and interlake comparisons.

(3) Apply CZCS products to demonstrate the utility of the data in the solution of particular Great Lakes water quality monitoring problems.

The approach taken to meet these objectives consisted of a multi-element program consisting of (1) surface sampling, (2) aircraft underflights, (3) algorithm developing including geometric and atmospheric correction, and (4) algorithm validation. During 1980 a series of measurements were made using point sampling from ships and area sampling by making a series of aircraft underflights with the ocean color scanner. These measurements are discussed in detail in the next section and were designated to support the refinement of subsurface volume reflectance models. Specific surface sample analysis of interest included chlorophyll and suspended mineral concentrations, spectral signatures, species identification, particle size distribution, and transmittance.

Because large portions of Great Lakes waters exhibit high concentrations of suspended particles, the volume reflectance was expected to be significant in the CZCS band 4 (670 nm). It was considered unlikely that the NOAA algorithm for atmospheric and surface reflectance corrections would be accurate for the Great Lakes area. For this reason, ancillary data collected on the surface (i.e., atmospheric optical thickness) and by aircraft were designed to support and refine an atmospheric algorithm for the Great Lakes. Correction accuracies were to be tested with a number of surface upwelling radiance measurements.

An essential element to this validation experiment was the precise geometric correction of the standard CZCS image data which would allow image-to-image registration, and registration of surface truth/satellite data pairs. Further, the geometric correction was felt necessary to develop image products accurately scaled and sized for Great Lakes conditions and applications. Development of an ephemeris driven scanner model was considered key to development of a geometric correction algorithm.

Atmospheric and bio-optical algorithms developed under this program, as well as those developed by the CZCS NET, were to be evaluated and tested with the available surface truth data pairs. To the extent possible it was planned to test the spatial and temporal limitations of specific algorithms. The applicability of CZCS data for performing Great Lakes surveillance tasks was to be evaluated by construction of suitable product map depicting chlorophyll-a pigment and suspended mineral concentrations. These maps were distributed to projected participants for evaluation and comment.

2.4 ENVIRONMENTAL CONDITIONS IN GREAT LAKES WATERS

Waters of the Great Lakes have distinctive properties from those of the deep ocean and to some extent from coastal marine environments. In general the deep ocean waters display very low levels of productivity with surface chlorophyll-a concentrations which are less than 0.5 μg/ℓ. The optical properties of these waters are dominated by the presence of phytoplankton. For these waters, suspended mineral particles are essentially not present. These waters have been classed by Morel as Type I [9]. Pigment algorithms have been developed by Clark and Gordon [7] for these waters which have applicability to large portions of the oceans with little need for surface truth calibration.

The balance of oceanic waters, consisting primarily of coastal waters are generally more productive and display values of chlorophyll-a pigment which are greater than 0.5 μg/ℓ. These waters exhibit varying concentrations of suspended sediments which have a significant and sometimes dominant impact on the optical properties. These complicated coastal waters have been designated as Type II waters.

Great Lakes waters exhibit a wide range of optical characteristics which are highly variable both temporally and spatially. Surface waters of central Lake Superior, northern Lake Huron, and Georgian Bay have very low concentrations of suspended mineral particles and have the lowest values of chlorophyll-a color pigments. These waters are probably

of the Type II class but they are very clear and certainly approach in optical characterization those classed as Type I. Waters of Green Bay of Lake Michigan, Saginaw Bay of Lake Huron, Lake Erie, and much of Lake Ontario are highly productive and have as a result high concentrations of chlorophyll-a and suspended mineral particles. These waters are frequently very turbid and highly reflective, have a shallow optical depth, and display surface concentrations which are highly variable both spatially and temporally. The balance of Great Lakes waters lie between these two extremes.

Optical characterization is complicated further by the fact that the spectral characteristics of suspended mineral particles are different for different areas of the Great Lakes. For example, red silts and clays associated with shoreline soils of western Lake Superior near Duluth influence the optical properties of off-shore waters and make them optically different than those brown and grey sediments found in western Lake Erie. Since some of these sediments reach clearer open waters of each lake, potentially these waters could also display different optical properties due to different sediment types. Possibly a greater influence in these latter open lake waters is the species distribution of phytoplankton. Many of the clear open lake waters tend to be dominated by diatoms whereas the nearshore waters are dominated by greens and the highly productive areas by blue-green algae.

Ideally one would want to derive or measure directly the optical properties of each sediment type and algal species and perhaps other components and create an optically layered model dependent on the concentration and distribution of each component. However, the implied sea truth requirements for such an analysis are far beyond the scope of the present program. Further, the differences in optical properties of algal species and suspended sediments have not been thoroughly investigated nor has their influence on apparent properties derived from remote sensing data been demonstrated. Furthermore, most studies to

date conducted with Type II waters have shown predicted concentrations which are within only a factor of two of measured values. Such results are due in part to the decreased sensitivity of the sensor to changes in concentration in more turbid and highly reflective waters and to the obvious surface sampling problem in highly productive and more turbid areas which often display large variations within the spatial resolution of CZCS.

In this context, subtle differences in optical properties will have less importance. With a modest amount of surface truth available, as described in the next section, the approach taken in the present program was to derive algorithms which would have applicability for the greatest extent of Great Lakes waters.

Because of frequent cloud cover in the Great Lakes area it usually is not possible to observe all or even most of the lakes simultaneously cloud free, further complicating the collection of adequate surface truth for validation, but underlining the need for algorithms which once calibrated have a minimum dependence on surface truth.

In addition to highly complex water optical parameters, the Great Lakes region has atmospheric aerosol components which can be expected to vary vertically and geographically in both type and concentration.

3.0

DATA COLLECTION METHODS

A multisensor approach was taken in the collection of surface truth data coincident with the collection of CZCS scenes for the Great Lakes. This approach involved surface sampling and aircraft underflights with the Ocean Color Scanner (OCS). This approach was designed to produce an extensive set of optical and biological measurements at a few positions in each lake. The aircraft underflights were conducted using an instrument similar to the CZCS allowing the collection of multiple CZCS-like signatures from multiple altitudes over the surface collection sites and cross-lake transects which were nearly coincident with the CZCS overpass. These latter data were intended to aid interpretation of the shipboard point samples and satellite data through variable spatial resolution measurements of the spectral distribution of upwelling light at both the water surface and at various altitudes.

3.1 SURFACE SAMPLING

A brief summary of the Great Lakes data sets collected during 1980 is presented in Table 3.1. Three principal experiment locations were selected: (1) Catawba area of western Lake Erie, (2) Grand Haven area in Lake Michigan, and (3) Duluth area of western Lake Superior. Surface truth data were collected by the research vessel Hydra (Ohio State University) in Lake Erie; the Shenehon (NOAA/GLERL) in Lake Michigan and the Leptadora (Univerity of Minnesota) in Lake Superior. Aircraft data were acquired by the NASA/LeRC F-106 aircraft instrumented with the OCS. Aircraft data were collected at altitudes of 500 and 41,000 feet. The 500 foot flights were flown over the surface truth vessel in order to obtain optical measurements with minimal atmospheric interference. Aircraft flights were made within one hour of local noon and usually close to the time of CZCS passes over the Great Lakes. Sun glint was a special problem for these aircraft data collected near local noon. Sun glint interference with the spacecraft sensor was largely avoided by

setting the instrument tilting mechanism. Additional aircraft flights were conducted for some dates during the morning and afternoon to correspond to solar zenith angles between 40 and 60 degrees in order to minimize the sun glint problem. The approximate areas of the Great Lakes imaged by the aircraft OCS scanner are shown in Figures 3.1 and 3.2. Figure 3.1 depicts those areas imaged while underflying the Nimbus spacecraft. Figure 3.2 shows those areas imaged during the non-satellite additional flight runs. Aircraft line orientation is dependent on the solar zenith angle. The analysis of these aircraft data was part of the University of Minnesota study effort and they were not utilized in the present phase II study.

TABLE 3.1 1980 GREAT LAKES EXPERIMENT SUMMARY DATA

No.	Date	Surface Sampling	Flight Altitudes (feet)	Time	CZCS Orbit
1	11 June	Lake Michigan	500, 500, 500, 41K 500, 41K, 41K	Noon PM	8243
2	14 July	Lake Erie	41K, 41K, 500 41K, 41K, 500	AM Noon	8699
3	17 July	Lake Erie	500, 41K, 41K, 41K 41K, 41K, 500, 500, 500	AM Noon	8740
4	23 July	Lake Michigan	41K, 41K, 500, 500, 500	Noon	8823
5	6 August	Lake Superior	41K, 41K, 500 500, 41K, 41K, 41K	AM Noon	9017

During the time period from July 15 to July 25, 1980 additional optical measurements were made at each of the surface collection areas by the Naval Oceans Systems Center (NOSC) and NASA/LaRC. The measurements included use of the NOSC in-situ submersible radiometer to measure upwelling and downwelling irradiance. Measurements were made with this radiometer during satellite and aircraft overflights. During this same time period the optical parameters, including absorption,

FIGURE 3.1 AIRCRAFT OCS FLIGHT COVERAGE COINCIDENT WITH CZCS

FIGURE 3.2. OTHER AIRCRAFT COVERAGE WITH THE OCS

attenuation, and scattering coefficients were measured on twenty-one water samples from the three primary experiment sites. Samples were also obtained from western, central and eastern Lake Erie as well as Green Bay.

The collection and analysis of all of the bio-chemical data were supervised by the University of Michigan Great Lakes Research Center Laboratories. Surface truth measurements are summarized in Table 3.2.

3.2 CZCS DATA COLLECTION

The CZCS data collected under the 1980 validation experiment included five scene dates where substantiating surface truth data were collected. These include June 11, July 14, July 17, July 23, and August 6. The validation analysis conducted for this study included each of these five scene dates. Weather conditions for these five dates are reported in Table 3.3. Additional CZCS scenes were collected on April 18, May 22, June 30, July 18, July 25, August 1, September 8, September 11, and September 18. The June 11 and July 23 scene dates provided the best overall cloud free coverage of the Great Lakes. Cloud coverage limited the analysis to Lake Erie for July 14 and 17 and to Lake Superior for August 6. These latter scenes were not requested by LeRC for analysis under the present project.

TABLE 3.3 WEATHER CONDITIONS AT PRIMARY SAMPLING SITES

Date	Visibility/ Cloud Cover	Wind Speed	Wind Direction	Wave Height
June 11	Clear with haze	0-3 knots	180-200°	< 0.5'
July 14	Clear with haze	7 knots	225°	< 0.5'
July 17	20% Cumulus clouds	9 knots	240°	1-2'
July 23	Clear with light haze	5 knots	315°	1-2'
August 6	Clear with light haze	calm	calm	< 1.0'

TABLE 3.2 SURFACE TRUTH MEASUREMENTS

Measurements	Instrument Method	Sampling Method	Spectral Range
Downwelling Diffuse and Global Irradiance	Tracor Northern Spectroradiometer	Multiple Deck Samples	400-800 nm
Subsurface Up/Down Radiance	NOSC Subsurface Multiband Radiometer	Subsurface Measurements at 0, 0.5, 1.0 secchi depths	440-670 nm
Secchi Depth	30 cm Secchi Disk		
Volume Scattering Function	Modified Brice Phenoix Scatterometer	Large volume water sample to Secchi depth	450-800 nm
Beam Attenuation	NASA/LaRC Transmissometer	Same as above	450-800 nm
Absorption Coefficient	NASA/LaRC Absorption Meter	Same as above	450-800 nm
Chlorophyll-a and Photo-Pigments	Spectrophotometric with acetone extraction	Samples at 0.01, 0.5, and 1.0 Secchi depths Triple Alignots	
Total Suspended Solids	Gravimetric Ash-free dry weight	Same as above	
Particulate Organic Carbon	HP-CHN Analyzer Gas Chromatography	Same as above	
Temperature	BT-Type/Electronic	Profile	

3.3 COLLECTION AND ANALYSIS OF THE NASA LaRC OPTICAL DATA

The inherent optical properties measured by the NASA/Langley group of scientists included absorption, beam attenuation, and the scattering phase function. The scattering function was subsequently integrated to estimate the total and back scattering coefficients. A few additional measurements of this type were made by NASA/LeRC using a separate set of instruments which supported those made by the Langley group. The measurement instrumentation could not be placed on board the sampling vessel so large volume water samples (50 gal.) were transported to the NASA/LeRC facilities. For each of the twenty-one optical data sets the measured properties pertain to a particular mix of constituents in the lake sample. These latter optical data are included in Appendix A. If sufficient number of measurements are made in this manner and if the principal constituents are known then multivariate regression analysis can be used to derive the inherent optical cross sections for a common constituent.

Of the twenty-one optical data sets taken, three Lake Erie samples contained sufficient quantities of sediment to saturate the optical measurement instrumentation. Samples collected from Green Bay in Lake Michigan and from western Lake Superior were found to have distinctive local optical properties. Four of the six samples collected from the Grand Haven area were essentially sediment free and the presence of low concentrations of phytoplankton made absorption measurements difficult and the results uncertain. Attempts to include these latter samples in the statistical analysis proved to be unproductive.

The most representative samples, in our opinion, included nine samples from western Lake Erie and two samples from Lake Michigan. Measured optical properties for these samples are given in Table 3.4. Several regression models were formulated and tested against these selected optical measurement sets. Regression models were based upon chlorophyll-a, phaeophytins, total residue, and ashed residue. These models are discussed further in section 6.1.

TABLE 3.4. NASA LaRC MEASURED INHERENT OPTICAL PROPERTIES [10]

Sample ID*	Sample Location	Chlorophyll-a + Phaeophytins (μg/ℓ)	Ashed Residue (mg/ℓ)	Optical Properties a-absorption Bb-backscatter (m^{-1}) 450 nm		520 nm		550 nm		670 nm	
				a	Bb	a	Bb	a	Bb	a	Bb
1 RR-1	Lake Erie, Rocky River Mouth	16.1	1.03	.66	.111	.42	.108	.41	.0988	.44	.0841
2 HYD-I-1	Lake Erie, West Basin	18.4	2.01	.87	.140	.62	.136	.55	.118	.55	.1026
3 HYD-I-2	Lake Erie, West Basin	21.0	1.61	.73	.128	.51	.130	.44	.110	.45	.0932
4 CATT-1	Lake Erie, East Basin	14.9	15.1	1.40	.335	1.12	.326	1.04	.312	1.03	.274
5 CATT-2	Lake Erie, East Basin	11.2	9.29	.79	.159	.70	.157	.71	.142	.64	.124
6 NS-1	Lake Erie, Central Basin	10.5	7.57	1.10	.277	.86	.256	.88	.233	.85	.202
7 NS-2	Lake Erie, Central Basin	6.98	10.2	1.41	.421	1.22	.385	1.15	.349	1.12	.297
8 HYD-II-1	Lake Erie, West Basin	43.0	22.2	2.68	.900	2.12	.817	1.79	.820	1.75	.697
9 HYD-II-2	Lake Erie, West Basin	22.9	2.73	.77	.146	.51	.145	.52	.129	.48	.108
10 GH-1	Lake Michigan, Grand Haven	173.4	7.53	2.89	.246	2.06	.261	1.46	.252	1.35	.213
11 GH-6	Lake Michigan, Grand Haven	113.9	1.80	1.80	.125	1.17	.126	.80	.124	.80	.104

*Samples reported here were used to determine optical cross sections

3.4 SUBMERSIBLE RADIOMETER DATA

The NRSC submersible radiometer was used to make upwelling downwelling irradiance measurements just above the surface, at the surface, and at one and two meters below the surface. Due to wave action the subsurface data were found to be absent or inconsistent. The above surface radiance measurements and the estimate of the subsurface reflectance are compiled in Table 3.5 for Lake Erie sampling stations on July 14 and July 17 as well as the Lake Michigan Grand Haven stations on July 23, 1980 [18]. Results are reported at 488 and 500 nm in addition to the first four CZCS wavelengths. The upwelling measurements made on July 14 and 17 are generally consistent both in spectral shape and in magnitude with model predicted radiances based upon the measured water constituents. The Lake Michigan July 23 measurements, on the other hand, were found to lack expected spectral shape and were somewhat higher than expected. While these data were found useful in the verification of optical models and extraction algorithms for the Great Lakes there were insufficient measurements for purposes of model development. Further comments on these data can be found in the discussion of results in section 5.9.

3.5 DOWNWELLING IRRADIANCE DECK MEASUREMENTS

A TRACOR Northern spectrophotometer was instrumented on the deck of the sampling vessel for purposes of collecting frequent measurements of the diffuse and direct solar irradiance. Presurvey calibrations were made with an integrating sphere. Preliminary analysis of these data indicated that while the measured spectral irradiance was of the approximate correct value the shape of the irradiance spectra were peak at a longer wavelength than would be expected from model calculations. Since measurements were not made precisely at the time of CZCS overflight no direct application to the present studies was made.

TABLE 3.5 NOSC SUBMERSIBLE RADIOMETER DATA

Upwelling Radiance ($mW/cm^2 \cdot sr \cdot \mu$) (1)
Subsurface Reflectance (2)

Date (1980)	Station	Sample Location	Local Time	Solar Zenith Angle	Data Type	WAVELENGTH (nm) 440	488	500	520	550	670
July 14	1	L. Erie, W. Basin	10:30a	38.0	(1)	.852	1.21	1.25	1.54	1.85	
					(2)	.0152	.0291	.0342	.0469	.0566	0
	2		12:30p	22.5	(1)	1.29	1.29	1.30	1.42	2.56	.81
					(2)	.0141	.0263	.0291	.0389	.0499	0
July 17	1	L. Erie, W. Basin	9:16a	54	(1)	2.10	2.36	2.42	2.77	3.46	2.40
					(2)	.0115	.0218	.0254	.0364	.0143	.0037
	2		12:33p	23	(1)	2.28	4.04	3.85	4.43	5.02	3.10
					(2)	.0370	.0654	.0633	.0745	.0825	.0577
July 23	4	L. Michigan, G. Haven	12:50p	25.1	(1)	2.97	2.68	2.62	2.69	2.61	.84
					(2)	.0187	.0328	.0374	.0484	.0586	0
	6		16:45p	48.0	(1)	1.69	1.75	1.23	1.68	2.36	.83
					(2)	.0053	.0102	.0106	.0165	.0253	0

3.6 ATMOSPHERIC OPTICAL THICKNESS MEASUREMENTS

A NASA/LeRC developed solar radiometer was used to make atmospheric total optical thickness measurements. These measurements were made at each of the primary sampling sites. The estimate of optical thickness was made from a series of solar radiance measurements made over a five or six hour period. By measuring only the radiance of the solar disk and the solar elevation one can estimate the total optical thickness from the following transmittance equation

$$E = rE_0 \, e^{-\tau/\mu_0} \qquad (1)$$

where τ is the total optical thickness, μ_0 is the cosine of the solar zenith angle, E_0 is the extraterrestrial irradiance, and r is the responsivity of the radiometer. The optical thickness can simply be estimated by plotting log E versus $1/\mu_0$ where the slope becomes the estimate of τ. Measurements were made at 380, 450, 500, 610, 749, 873, and 1040 nm using selected interference filters. Linear interpolation was used to estimate the atmospheric optical thickness at CZCS wavelengths. Radiometer optical thicknesses derived by this method are shown in Table 3.6 [19]. Subsequent radiometric analysis showed these measurements to have the proper spectral shape but incorrect magnitude. This result was not surprising since the instruments were not properly recalibrated prior to the experiment.

TABLE 3.6 MEASURED TOTAL OPTICAL THICKNESS

Date	Location	443 nm	520 nm	550 nm	670 nm
June 11	Lake Michigan, Grand Haven	0.605	0.417	0.380	0.284
July 14	Lake Erie, Catawba	0.733	0.506	0.449	0.317
July 17	Lake Erie, Catawba	0.632	0.412	0.375	0.285
July 23	Lake Michigan, Grand Haven	0.441	0.440	0.400	0.284
August 6	Lake Superior, Duluth	0.529	0.403	0.373	0.283

Note: Values reported here have been estimated by linear interpolation from those reported by NASA LeRC [19].

3.7 COLLECTION AND ANALYSIS OF WATER SAMPLES

Water samples were collected from a series of offshore stations and as close as possible to the time of CZCS overpass. The original plan was to collect samples from stations located at the apex of a triangular array. In actuality the stations were laid out along a line perpendicular to the shoreline. Figure 3.3 shows the approximate location of sampling stations at each of the primary sampling sites. At each station samples were collected in triplicate from each of three depths. These depths were one meter, one half the Secchi depth, and the Secchi depth. When the Secchi depth was less than two meters samples were also collected at one third and two thirds this depth. Water samples were split into three aliquots and filtered for determination of chlorophyll, particulate organic carbon, and suspended solids. Chlorophyll was analyzed spectrophotometrically using an acetone extraction procedure. Pigments were analyzed for A, A2, B, and C fractions. Suspended solids were estimated gravimetrically by weighing prepared oven dried filters and then ashing the filters to obtain the ash-free dry weight. Particulate organic carbon samples were analyzed with an HP-CHN analyzer. Dry filters were analyzed by infrared gas chromatography for C, and gas chromatography for N and H [20].

In addition to the primary sampling sites, samples were also gathered from the non CZCS sampling sites in Lake Erie, Green Bay, etc. which were associated with the collection of large volume samples for the NASA/LaRC optical parameter analysis. Results from these laboratory analyses are reported in Appendix A.

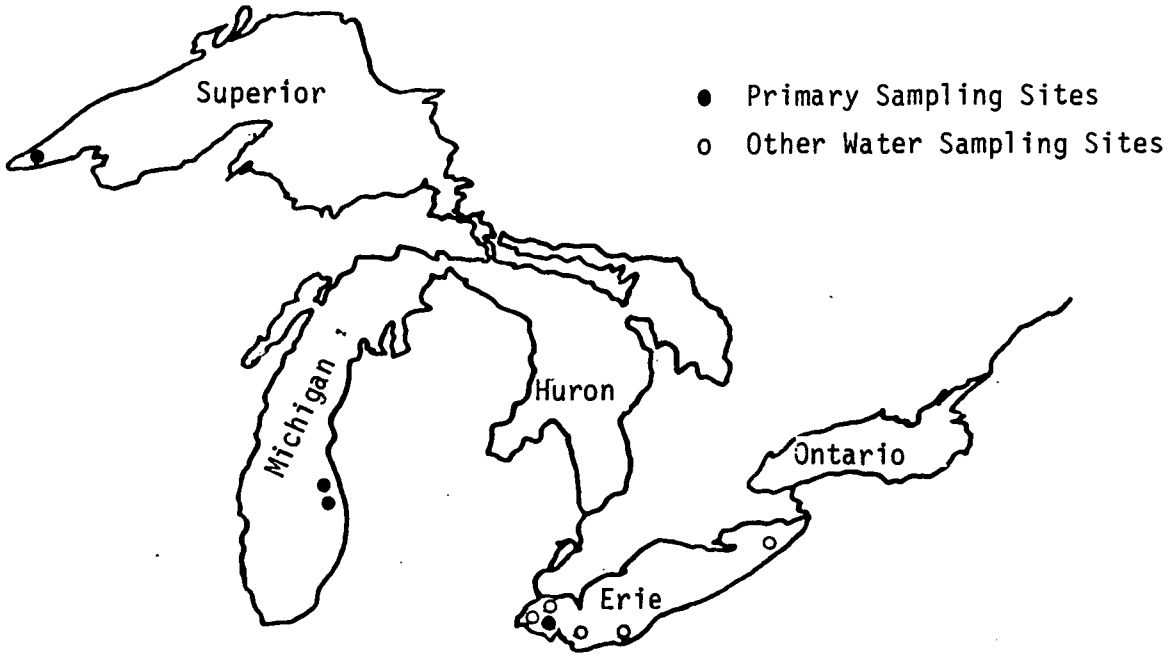

FIGURE 3.3 PRIMARY SURFACE SAMPLING SITES

4.0

GEOMETRIC CORRECTION METHODS

During phase I of this projejct a scanner model was developed which permitted the transformation of CZCS line and point coordinates to earth latitude and longitude. CZCS scanning geometry includes variable tilt angle for Great Lakes viewing combined with ground control points to derive the appropriate transformation matrix. Existing mapping software was modified to accommodate the CZCS frame size and mapping polynomials. Geometric correction of an image results from two operations. First mapping polynomials are generated to define the transformation from raw original image to the corrected image. Second, the corrected image is created from the uncorrected image using these mapping polynomials. Two fifth-order, twenty-one term polynomials were used in this process, one for each dimension of the image. These polynomials defined the transformation which makes the corrected image conform to a given map projection as well as adjust for viewing distortions such as satellite position, satellite motion, and earth motion.

The scanner model developed for CZCS is based upon the ERIM experience with Landsat and in its present form takes each image control point in turn and proejcts it to the earth's surface. The line number for each point is used to interpolate for the latitude, longitude, and altitude from the values supplied with the tape reference data for each scene. The point number is used to calculate the mirror scan angle which together with the reported tilt angle determines the scanner line of sight vector in spacecraft coordinates. A series of single angle rotations through the angles of roll, pitch, heading provide the transformation to earth centered coordinates.

There are two basic uses for the derived scanner model. First, the image control points and their corresponding map control points may be easily evaluated for consistency with other points and any outliers rejected. Second, the coefficients for global mapping polynomials used

in the resampling process can be derived by a fit to the model rather than to the points themselves.

A number of scanner variables including satellite altitude and longitude are converted to line and pixel location in the resulting image via the equations which define the desired map projection. The process used to resample a corrected image works in the reverse direction. For each pixel location in the resulting image the software calculates the corresponding location in the original image. Operation of the scanner model in reverse so as to select original pixel locations which correspond to a given location in the corrected image is most difficult. Alternatively the pair of twenty one term polynomials is generated to satisfy this mapping requirement. One polynomial describes the east-west position and the other the north-south position. The selected set of image control points are used to generate coefficients for each term in the polynomial. The complete set of coefficients defines the mapping from the original image to the correct projected image.

4.1 RESAMPLNG OF THE CZCS 1980 IMAGERY

Each of the five scenes collected during the summer 1980 CZCS Validation Experiment as listed in Table 3.1, were resampled with the same polyconic projection space with the central meridian set of 84.0 degrees. Thus, each resampled image was coregistered to within the scene to scene resampling errors. A data file with one hundred and twenty-four control points was compiled for the Great Lakes region. Most of these points could be easily identified in the CZCS imagery and were somewhat evenly distributed throughout the region. Control points were selected from this data file for each scene which could be identified in the raw image. In the case of the June 11 and July 23 scenes (orbits 8243 and 8823) most of the Great Lakes were visible and multiple frames (two or three) from the same orbit were required to cover the entire

region (see Figure 4.1). In this case resampling polynomials were generated for the frame with greatest coverage and extended to apply to the entire data set. The resampling software did not permit generation of mapping polynomials based upon a variable size input space. The possibility existed to independently generate mapping polynomials for each frame but the resulting problems of boundary matching made the approach impractical. Results from independent polynomial mapping compared well with that obtained by domain extension.

All of the CZCS frames were resampled with a 500 meter pixel size, but the pixel size in the input space, of course, varies with scan position. Radiometric resampling employed a nearest neighbor algorithm. Spatial accuracy of this resampling procedure is thus a function of scan position and ground point control. The approximate position of the nadir track in the resampled space for each of the scene date is shown in Figure 4.1. In some cases only a few control points could be applied since most of the Lakes were cloud covered. The lack of control points was generally compensated by selecting a smaller area for resampling and one where the resampling polynomial was considered to be representative. The worst case occurred with the July 17 date where only a portion of Lake Erie containing the surface sampling site was cloud free. The rest of the Great Lakes region were essentially cloud covered. This condition coupled with the large scan angle produced the largest resampling RMS errors (approximately 5000 meters E-W and 2100 meters N-S). Typical resampling errors were estimated to be 200 meters in the N-S direction and 1875 meters in the E-W direction [3]. Since the scanning direction of CZCS is nearly east and west at this latitude the RMS east-west errors were found to be much larger than the north-south errors.

Subsequent radiometric analyses of the resampled CZCS data sets were made on individual pixels corresponding to ship sampling sites and on subscenes containing a single Great Lake or sublake (e.g., Green Bay, western Lake Superior, etc.). The individual pixels were extracted

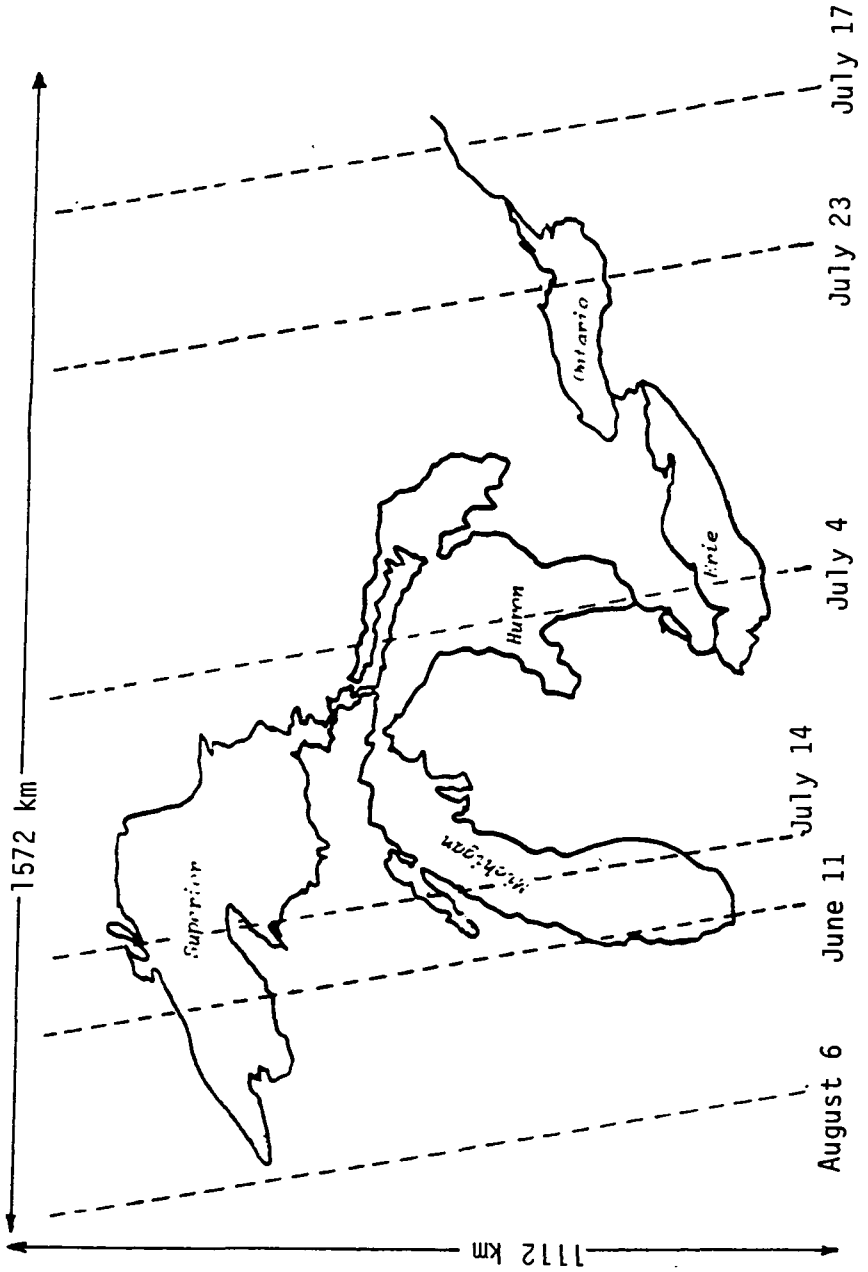

FIGURE 4.1 CZCS NADIR TRACKS AND RESAMPLED IMAGE COVERAGE

based upon the lat/long line/point relationship implied by the polyconic projection space and the reported ship position at the sampling site. Because of the resampling errors and the high variability of lake waters, some of these pixels are more representative of the radiometry of the sampling position then others.

5.0

DEVELOPMENT OF AN ATMOSPHERIC CORRECTION ALGORITHM FOR THE GREAT LAKES

Before CZCS data can be effectively used to distinguish between and monitor coastal water types, methods are needed for removal of spatial variations in aerosol path radiance which dominate radiance measurements made by the satellite sensor. In the present study efforts were focussed on the comparison and evaluation of existing atmospheric algorithms for use with Great Lakes data and the development of improved algorithms. Algorithms were sought which would have minimum requirements for surface truth and which would produce scene independent results. The abilities of three existing algorithms and one developed under the present study to quantitatively remove haze effects when applied to Great Lakes scene data where evaluated and compared.

The atmospheric algorithms considered are (1) the Gordon Algorithm [4], (2) the Smith and Wilson iterative algorithm [5], (3) the pseudo optical depth method [6], and (4) the residual component algorithm. Each of these algorithms was adapted to extract required scene dependent parameters during an initial pass through the data set. The performance of each algorithm was evaluated on the basis of four comparisons: (1) derived upwelling radiance spectra with water radiance model calculations, (2) derived aerosol path radiance spectra with atmospheric model predictions, and (3) predicted radiance in the form of color coded images with uncorrected data. These latter maps show the extent that spatial features of the aerosol haze were removed by each algorithm.

Atmospheric path radiance is produced by a combination of Rayleigh and aerosol scattering. The amount of path radiance generated by Rayleigh molecular scattering is a function of viewing and solar geometries and can be calculated directly from an analytical model. The radiance due aerosol particles varies spatially and cannot be predicted by analytical means unless local atmospheric optical thicknesses are

well known. Because of spatial variations in the concentration of aerosol particles it is necessary to use an atmospheric correction procedure that applies corrections on a pixel-by-pixel basis. Effective correction algorithms of this type have been demonstrated by Gordon, et al [7] for the open ocean. The ocean waters for which these algorithms work are classified as type I by Morel and Prieur [9]. These algorithms will not work in the more turbid case II coastal waters. The waters of the Great Lakes are by in large of type II but cover a wide range of optical properties and concentrations of suspended particles. Waters of central Lakes Superior and Huron approach those designated as type I.

5.1 RADIATIVE TRANSFER PROCESS IN THE LAKE ATMOSPHERE SYSTEM

The components of the radiative transfer model for a lake atmosphere system are described by the equation below.

$$L(\lambda) = L_R^1(\lambda) + L_R^2(\lambda) + L_A(\lambda) + L_S(\lambda) + L_U(\lambda) \cdot T(\lambda) \qquad (2)$$

where $L(\lambda)$ is the radiance measured at the satellite; $L_R^1(\lambda)$ is the Rayleigh path radiance as generated by molecular backscattering of solar irradiance; $L_R^2(\lambda)$ is the Rayleigh path radiance due to scattering of irradiance after it has reflected from the surface toward the sensor, $L_A(\lambda)$ is the aerosol path radiance, $L_S(\lambda)$ is the reflected sky radiance, $L_U(\lambda)$ is the upwelling radiance from beneath the water surface, and $T(\lambda)$ is the atmospheric transmittance.

The $L_U(\lambda)$ term contains the information on the water constituents and may only represent a small fraction of the total signal received at the satellite. The Rayleigh scattering phase function and the sensor view geometry can be used together to directly calculate the Rayleigh components at each pixel. Unlike the Rayleigh scattering process it is not possible to approximate the aerosol path radiance explicitly since aerosol concentration is highly variable. In principle, however, the radiance added by aerosol scattering could be calculated if the concentrations and optical properties were known throughout the scene. Each

algorithm must, therefore, use the data itself to derive the aerosol component at each pixel in order to subsequently estimate the L_U term. This approach relies on making two assumptions. The first of these assumptions is that the band ratio of aerosol path radiances is independent of pixel position within the scene. This statement is equivalent to saying the aerosol concentration varies from pixel-to-pixel but aerosol type remains constant. This assumption is largely supported by the fact that the aerosol scattering phase function is essentially independent of wavelength. In addition, it is necessary to assume some characteristic of the upwelling radiance spectra which is invariant over the entire scene.

The approach taken to calibrate the algorithm involves collecting sea truth data at one position within the scene. First, the downwelling irradiance or atmospheric optical thickness is measured at each of the CZCS wavelengths. Second, the upwelling radiance just below the surface is measured directly or model estimated from the measured chlorophyll pigment concentration. Together these two measurements can be used to estimate the aerosol path radiance ratios. The atmospheric correction is then adjusted over the calibration region so that the satellite derived upwelling radiances (or reflectances) match the surface measured or model estimated values. Gordon has refined this approach for studies of the open ocean with his concept of normalized clear water radiances [15]. For this study normalized water radiances for Great Lakes waters were developed for a Lake Superior calibration area.

5.2 SOLAR IRRADIANCE AND ATMOSPHERIC TRANSMITTANCE

The mean extraterrestrial solar spectral irradiance, E_o, has been determined experimentally for each Julian Day. Values of E_o for each of the CZCS wavelengths are given in Table 5.1. The solar irradiance is attenuated during the passage through the atmosphere caused by interaction with air molecules and aerosols during which photons are either scattered or absorbed. The quantity of radiance transmitted depends on

TABLE 5.1 ATMOSPHERIC OPTICAL PARAMETERS

Wavelength (nm)			
443	520	550	670
Extraterrestrial Irradiance (mW/cm^2 . sr)			
186.42	185.34	184.76	151.52
Rayleigh Optical Thickness			
0.2316	0.1224	0.0964	0.0442
Ozone Optical Thickness			
0.0069	0.0237	0.0390	0.0226
Initial Aerosol Optical Thickness			
0.320	0.300	0.280	0.250

the optical thickness and the slant path. The optical thickness characterizes the attenuation properties in a vertical path and can be separated into molecular and aerosol optical thicknesses as given in the equation below.

$$\tau(\lambda) = \tau_R(\lambda) + \tau_A(\lambda) + \tau_{O3}(\lambda) \qquad (3)$$

where $\tau(\lambda)_{O3}$ is the optical thickness of the ozone layer, $\tau_R(\lambda)$ is the Rayleigh optical thickness due to molecular scattering and $\tau_A(\lambda)$ is the aerosol optical thickness due to scattering and absorption by aerosols. The ozone optical depth varies with season and latitude and the values used for this study are given in Table 5.1. Because the quantity of molecules in the atmosphere is essentially constant, the Rayleigh optical thickness varies approximately inversely with the fourth power of wavelength. The aerosol optical thickness, on the other hand, varies throughout the scene.

The diffuse transmittance, $T_D(\lambda)$, is usually applied to components of radiance between the water surface and the sensor. This transmittance is given by

$$T_D(\lambda) = EXP[-(a_R \cdot \tau_R(\lambda) + \tau_{O3}(\lambda) + a_A \cdot \tau_A(\lambda))/\mu] \qquad (4)$$

where μ is the cosine of the viewing zenith angle. The diffuse transmittance is essentially the same as the beam transmittance except that each component of the optical thickness has been multiplied by a factor to account for scattering of radiance from adjacent pixels which are scattered into the sensor field of view. The ozone layer absorbs and does not scatter photons so there is no change for the diffuse calculation. The Rayleigh scattering phase function $\rho(\psi)$ is symmetrical as given below and, therefore, one half of the photons scattered from the beam will be replaced by those scattered into the beam and a factor of one half is, therefore, appropriate to this calculation.

$$\rho(\psi) = 3/4(1 + \cos^2(\psi)) \qquad (5)$$

The aerosol scattering is asymmetric with a large forward component and, therefore, the diffuse transmittance is only weakly dependent on the aerosol optical thickness. A coefficient of 0.1 has been proposed but 0.0 can be effectively used where haze levels are very low.

5.3 CALCULATION OF THE RAYLEIGH PATH RADIANCE COMPONENTS

The radiative transfer equation can be solved using the Rayleigh scattering phase function to derive closed form solutions for each of the components. Only single scattering is considered since multiple scattering is negligible for this case. The Rayleigh path radiance for directly scattered radiance is given by the following equation.

$$L_R^1(\lambda,\mu,\mu_0) = \frac{E_0(\lambda)\ \mu_0}{4\pi} \cdot \frac{\rho(\psi)\cdot\tau_R}{(\mu + \mu_0)} [1 - \exp(-\tau_R \cdot \frac{\mu + \mu_0}{\mu \cdot \mu_0})] \cdot T_{03}(\lambda, \mu, \mu_0) \quad (6)$$

where $T_{03}(\lambda, \mu, \mu_0)$ is the transmittance for a combined downward and upward trips through the ozone layer, μ and μ_0 are cosines of the view and solar zenith angles and E_0 is the extraterrestrial irrradiance. The scattering angle (as shown in Figure 5.1) is given by the following cosine equation where θ and θ_0 are, respectively, the view and solar zenith angles and ϕ and ϕ_0 are the view azimuth and solar azimuth angles to the solar plane.

$$\cos(\psi_-) = -\cos\theta \cdot \cos\theta_0 + \sin\theta \cdot \sin\theta_0 \cdot \cos(\phi - \phi_0) \quad (7)$$

This approximate solution is the quasi-single scattering solution which is discussed in section 5.5. It has been assumed by some investigators that multiple scattering is negligible in which case the above solution can be approximated by

$$L_R^1(\lambda,\mu,\mu_0) = \frac{E_0(\lambda)\ \rho(\psi_-)}{4\pi\ \mu} \cdot \tau_R \cdot T_{03}(\lambda,\mu,\mu_0) \quad (8)$$

which is essentially the double delta solution [17].

The Rayleigh component $L_R^2(\lambda)$ of direct radiance which is first reflected from the water surface and then scattered to the sensor is the same as the equation above, but includes a Fresnel factor for the solar zenith angle. The scattering angle is given by the following cosine equation.

$$\cos(\psi_+) = \cos\theta \cdot \cos\theta_0 + \sin\theta \cdot \sin\theta_0 \cdot \cos(\phi - \phi_0) \quad (9)$$

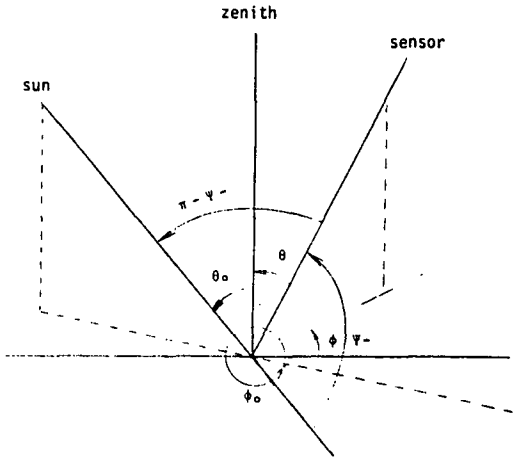

FIGURE 5.1 GEOMETRY OF RAYLEIGH SCATTERING ANGLE

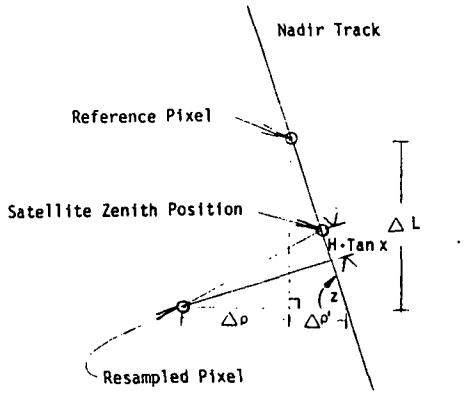

FIGURE 5.2 CZCS VIEWING GEOMETRY IN THE RESAMPLED IMAGE

The last term accounts for the photons which are scattered on the downward side and reflected directly to the sensor. The equation for this term is the same as above, but where the solar Fresnel factor is replaced with one for the view angle. These three components together constitute the Rayleigh path radiance, and were included in each of the algorithms tested.

In making these calculations for resampled CZCS data one must relate the resampled pixel coordinates to the sensor viewing geometry. This relation is most easily acquired by locating at least two nadir points in the resampled scene. The nadir track can be assumed to be approximately linear with line number in the resampled space (see Figure 5.2). Because of rotation, the track will have angle ζ with the geographically orientated resampled space. For a sensor tilt angle χ, the view angle θ, and view azimuth ϕ are given by the equations below.

$$\theta = \tan^{-1}[\tan^2 \chi + (\Delta P + \Delta L \cdot \tan \zeta) \cos \zeta / H^2]^{1/2}$$

$$\phi = \tan^{-1}[(\Delta P + \Delta L \cdot \tan \zeta) \cos \zeta / H \cdot \tan \chi] - \zeta - \phi_0 \qquad (10)$$

where ζ is the angle between the nadir track, and the resampled scan line, ΔP and ΔL are the point and line offsets (in km) from a reference point on the nadir track, and H is the spacecraft altitude.

5.4 CALCULATION OF AEROSOL PATH RADIANCE

Theoretically we can calculate the aerosol path radiance components in the same as those for Rayleigh scattering if we knew the aerosol optical thickness, absorption coefficient (or single scattering albedo) and the scattering phase function. Since the aerosol optical properties are highly variable in both time and space such analytical calculations are not possible for algorithm calculations. Thus the calculation must

be accomplished by some indirect means which will be the focal point of each of the correction schemes discussed below.

5.5 ATMOSPHERIC WATER RADIANCE MODEL

The radiance at any point in the lake atmosphere system can be obtained in principle by the solution of the radiative transfer equation with proper knowledge of critical optical properties. A full description of the optical properties of a medium include the absorption coefficient and volume scattering function. An exact solution is not obtainable in close form for this integral equation even for the simplest geometry. Under this circumstance two approaches are possible. First, we can develop an exact numerical solution with Monte Carlo simulation techniques. This method is especially powerful and can incorporate spatially varying optical properties. The chief disadvantage to this approach is the large number of iterations required to obtain a solution for a single case. Further, a large number of cases need to be examined in order to gain proper insight into the problem. A more practical approach and the one taken here, is to develop approximate solutions which give good results over a range of conditions. Insight can sometimes be gained by merely examining the functional form of the approximate solution.

Using this approach radiative transfer model was developed to predict the CZCS radiances at the top of the atmosphere which includes photon interaction in the atmosphere, through the water surface and beneath the water surface. A flow diagram for this model is shown as Figure 5.3. The model was designed to accept specific view and solar geometries as well as aerosol type characteristics giving it the capability to simulate any selected CZCS pixel radiance.

The atmospheric portion is based upon a previous model developed by Turner et al [21]. The extraterrestrial irradiances, Rayleigh optical thicknesses, and ozone optical thicknesses are the same as reported above. The Turner code was modified to include the ozone layer, the

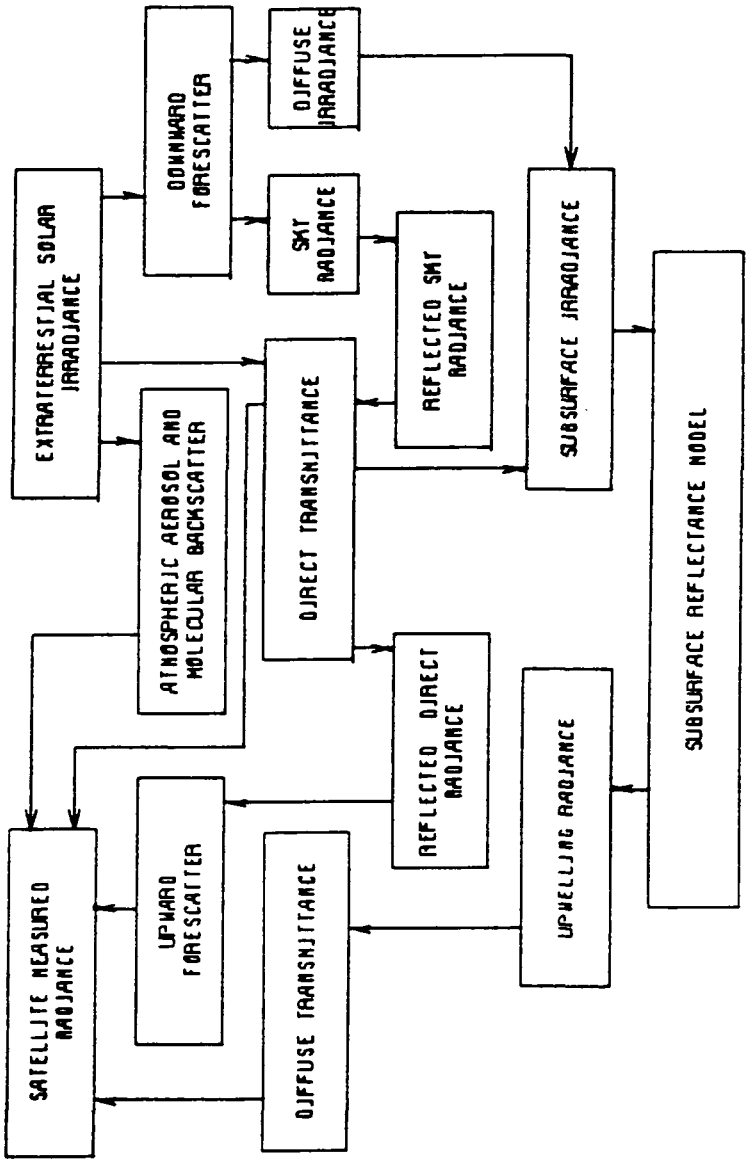

FIGURE 5.3 WATER RADIANCE MODEL FLOW CHART

reflected diffuse sky radiance, and the reflected direct irradiance which is scattered to the sensor. The aerosol phase function was based upon an Elterman type atmosphere [22]. Turner used the following aerosol scattering phase function which allows direct solution of the radiative transfer equation.

$$\rho(\mu, \phi; \mu', \phi') = 4\pi F \cdot \gamma(\mu - \mu')\,\gamma(\phi - \phi') + 4\pi B \cdot \gamma(\mu + \mu')\,\gamma(\phi - \phi' + \pi) \quad (11)$$

where F and B are the forward and backward scattering constants and γ is a delta function. The solution was re-entered into the transfer equation to get a second order solution in what is referred to as the double delta method. The Turner solution has been compared to exact Monte Carlo solutions by Lyzenga [23] and found to give acceptable results in the forward direction but overestimated the radiance in the anti-solar direction and underestimated the radiance in other directions. The double delta solution thus gives a good solution for the downward irradiance and the reflected upward scattered direct radiance. The double delta solution will, in general, work poorly for strongly forward scattering functions which are characteristic of aerosols, but give good results for disymmetric Rayleigh scattering. These solutions were then incorporated into the present model. A quasi-single scattering solution was used to estimate the radiance that is backscattered to the sensor during the downward leg. The quasi-single scattering solution uses the following phase function which includes the actual aerosol scattering function in the backward direction as given by the following equation.

$$\rho(\mu, \phi; \mu', \phi') = 4\pi F \cdot \gamma(\mu-\mu')\,\gamma(\phi-\phi') + \rho(\mu, \phi; \mu',\phi')\,\mu\,\mu' \leq 0 \quad (12)$$

The quasi-single scattering solution yields a hemispherical reflectance which agrees well with exact calculations. While this solution estimates the backward scattered radiance it does not predict forward scattered radiance. In addition, the errors in the backscattered radiance increase as

the single scattering albedo approaches one (i.e., a highly turbid atmosphere). The quasi-single scattering solution does account in part for multiple scattering of photons. The Turner model was also modified to include the diffuse transmittance as defined previously for the component upwelling from beneath the surface and for the reflected diffuse sky radiance. The diffuse transmittance also partially accounts for possible multiple scattering effects.

In developing a water radiance model, it is generally assumed that the inherent optical properties arer linear functions of concentration of each constituent in the medium. Under these circumstances the total absorption, backscatter, and total scattering coefficients can be expressed by the following relationships.

$$a = a_w + \sum_{i=1}^{N} a_i c_i$$

$$Bb = Bb_w + \sum_{i=1}^{N} Bb_i c_i \qquad (13)$$

$$b = b_w + \sum_{i=1}^{N} b_i c_i$$

where a_w, Bb_w, and b_w are the absorption backscattering and total scattering coefficients for pure water and a_i, Bb_i, and b_i are the absorption, backscattering, and total scattering cross sections, respectively for constituent i with concentration c_i. These relationships are approximations since the actual optical properties depend on other factors such as particle size distribution. Having made these approximations a useful relationship can be made between these inherent optical properties and the apparent optical properties of the medium including volume reflectance. The water reflectance model used for this study was

that developed by Gordon, et al. [8] which is commmonly referred to as the power series approximation and is given below.

$$R_H^-(\chi) = 0.0001 + 0.3244\chi + .1425\chi^2 + .1308\chi^3 \qquad (14)$$

where χ is Bb/(a+Bb) and R_H^- is the subsurface hemispherical reflectance and the (-) signifies a subsurface component. The coefficients were obtained by fitting the power series to Monte Carlo calculations of the subsurface water reflectance for solar zenith angles less than thirty degrees. These calculations were made for hemispherical irradiance reflectance and for this model we assume a uniform reflectance distribution so that the subsurface radiance reflectance can be estimated. There have been some studies to indicate that the relationship between these quantities is somewhat greater than π [8]. However, for this study it was assumed that the radiance reflectance r can be approximated as

$$r^-(\mu, \mu_o) = R_H^-(\mu_o)/\pi \qquad (15)$$

The above surface upwelling radiance from beneath the surface can then be calculated using the following relationship.

$$r^+(\mu, \mu_o) = \frac{T_1 T_2}{2\pi n^2} r^-(\mu, \mu_o) \qquad (16)$$

where T_1 and T_2 are the surface transmittances (i.e,. 1 - ρ, ρ = Fresnel reflectance) for the incoming and outgoing light.

Derivation of optical properties for the water reflectance models are discussed in section 6.1.

5.6 EXISTING ATMOSPHERIC ALGORITHMS

Three existing algorithms were selected for comparison and evaluation with CZCS data collected over the Great Lakes. These included (1) the NOAA NET algorithm developed by Gordon et al. [4], (2) the iterative algorithm of Smith and Wilson [5], and (3) the pseudo-optical depth algorithm developed for the Great Lakes by Jain et al. [6]. Each of these algorithms was adapted to operate in two modes. First, the algorithm can be used in the calibration mode to extract necessary aerosol parameters from a hazy portion of the scene. Second, the algorithm can, with these data derived parameters, process the scene on a pixel-by-pixel basis for removal of aerosol and Rayleigh path radiance.

1. Gordon Algorithm

The NOAA atmospheric correction algorithm for CZCS developed by Gordon assumes the upwelling radiance at 670 nm is zero for all pixels to be corrected. This assumption has been shown to be valid for ocean waters and using the aerosol ratio values the direct calculation of t^*L_w by way of the following equation. Here L_w is the sum of the upwelling radiance L_u plus the reflected sky radiance.

$$L(\lambda_i) = L_R(\lambda_i) + T_D(\lambda_i) \cdot L_u(\lambda_i) + k_{ij}(L(\lambda_i) - L_R(\lambda_i)) \qquad (17)$$

where $k_{ij} = \varepsilon(\lambda_i, \lambda_j)[F_o(\lambda_i)/F_o(\lambda_j)]$ and F_o is the instantaneous extra-terrestrial solar irradiance reduced by the two way transmittance through the ozone, and ε is the ratio of $\tau_a \cdot \omega_a$ and the aerosol scattering phase function at the two wavelengths, λ_i and λ_j. In this manner one has separated out the factor ε which does not change with respect to pixel position. Once the ε value is determined for a particular scene the aerosol path radiance can in principle be estimated for each pixel and subsequently the water leaving radiance. The determination of ε is accomplished by having at least one pixel in the

scene where the value of L_w has been measured or estimated using the concept of clear water radiances [24]. In equation 17 k_{ij} is the band ratio of the aerosol path radiances.

2. Smith and Wilson Algorithm

In coastal waters the subsurface upwelling radiance at 670 nm is non-zero largely because sediment concentrations are relatively high. Smith and Wilson [5] developed an iterative procedure for these waters which is based upon known spectral characteristics and which allows L_w at 670 nm to be non-zero. The algorithm utilizes the following relationship determined from measured upwelling radiance data.

$$L_w(670\ nm) = 0.0829\ L_w(443) \cdot R_{13}^{-1.661} \tag{18}$$

where $R_{13} = L_w(443\ nm)/L_w(550\ nm)$. Initially one assumes that $L_w = 0$ and uses the above equation to calculate the upwelling radiance at each of the other wavelengths per the NET algorithm. The values of L_w at 443 and 550 nm are then substituted back into the above equation and a new estimate of L_w is obtained. This process is repeated until there is acceptable convergence to constant values of $L_w(\lambda)$.

3. Pseudo-optical Depth Algorithm

In this algorithm path radiance is assumed to be a linear function of surface albedo for a specific aerosol optical depth. The discrete ordinate method (DOM) solution to the radiative transfer equation is used to derive the linear relationships between surface albedo R_w and total path radiance L_p including the aerosol and Rayleigh components.

$$L_p = C_1 + C_2 \cdot R_w \tag{19}$$

The computation assumes the ozone and Rayleigh standard atmosphere of Elterman and a Deirmendjian haze (L) continental aerosol [21]. The Elterman aerosol optical depth is scaled according to the experimentally

derived values. Absorption was assumed to be small and not included in these calculations. For fixed values of the surface albedo and view angle these calculations were fitted to a second order polynomial in the aerosol optical thickness. Accuracy of the computed L_p with the approximate equations was reported by Jain [6] to be within 1.1% of the actual DOM calculations. A linear equation was used to describe the relationship between L_p and the solar zenith angle for $R_w \leq 0.25$ and with cos θ for $0.25 < R_w < 0.50$. These relationships together provided a means to determine L_p from R_w, θ_o, and τ_a. In addition, these relationships can be inverted to approximate τ_a from a measured L_p, R_w, and θ_o. The algorithm procedure is as follows. For each pixel the path radiance is estimated at the reference wavelength (670 nm or 750 nm) and the upwelling radiance is assumed to be known. A pseudo aerosol optical depth is then estimated from the DOM based relationships.

The ratio between this pseudo optical depth to a previously measured optical thickness at some location within the scene is used to estimate by proportion the aerosol optical depth at each of the other wavelengths. The underlying assumption here is, of course, equivalent to that common to all algorithms as discussed above. These aerosol optical depths are then used with the derived relationships to calculate the path radiance as a linear function of the surface albedo. The surface albedo can be estimated as

$$R_w(\lambda) = \frac{\pi \cdot L_w(\lambda)}{E_o(\lambda) \cdot T_o(\lambda)} \tag{20}$$

In this case the satellite radiance is

$$L(t) = L_w(\lambda) \cdot T_D(\lambda) + C_1 + C_2 \cdot \pi \cdot L_w(\lambda) \tag{21}$$

where T_0 is the downwelling beam transmittance which can be calculated using the previously estimated aerosol optical depths. The above equation can now be solved for L_w which does include the radiance from reflected diffuse sky irradiance.

5.7 DEVELOPMENT OF A NEW CORRECTION ALGORITHM FOR THE GREAT LAKES

A fourth algorithm considered in this study was centered around the need to extract the needed algorithm parameters from the data itself. In this approach the characteristic CZCS spectra are used to develop a diagnostic for haze type which is directly related to the previous approach but which avoids the necessity of assuming zero upwelling radiance in the 670 nm band. Basically the algorithm assumes that over a uniform small patch of water the upwelling radiance will be essentially constant as will the Rayleigh components of path radiance. In this case the pixel-to-pixel variations are due solely to the variations in the aerosol path radiance components. The orientation of this radiance vector can be determined from the scene data independent of actual measurements of the upwelling subsurface radiance. The aerosol vector direction cosines are obtained as the eigenvector of the first principal component. These cosines are related directly to the k-ratios of the aerosol path radiances by

$$\cos \gamma_i = (1 + \sum_{\substack{j=1 \\ j \neq i}}^{4} k_{ij}^2)^{-1/2} \qquad (22)$$

where γ_i is the angle between the aerosol vector and the aerosol path radiance axis for band i. The orientation of the aerosol vector is assumed to be constant throughout the scene or portion to be atmospherically corrected. This assumption is equivalent to assuming a constant aerosol type with the length of the aerosol vector allowed to vary from pixel-to-pixel. Example first component eigenvectors are listed in

Table 5.2 for the Great Lakes scenes with the percent of total variance. Our analysis of these results suggest that a good estimate accounts for over ninety percent of the variance. In cases where the aerosol path radiance components are small the eigenvector is not uniquely determined and surface measurements of the optical thickness and/or measurements of the upwelling radiance are required to estimate proper eigenvector components. Like algorithms one and two the residual component algorithm relies on a scene invariant relationship between the upwelling radiance in each band such that

$$F(L_u(\lambda_i),\ i = 1,2,3,4) = 0 \tag{23}$$

In principle we will not know the length of the aerosol vector at any pixel and, therefore, must estimate this value with the algorithm. The water radiance vector, hopefully is always oriented in some other direction from that of the aerosol vector. Previous model simulation studies have indicated that 18.7 to 26.1 degrees separate the aerosol vector and suspended minerals and chlorophyll-a vectors respectively [3]. There is, in any case, a large component of the water radiance vector cooriented with the aerosol vector. A relationship was, therefore, developed between the projected modulus (brightness) of the water radiance vector, $|\vec{L}_w(\lambda)|$, and a spectral characteristic R* which is invariant throughout the scene. The spectral characteristic selected for the residual component algorithm was the following combination of upwelling radiances.

$$R^*(L_w(\lambda)) = \frac{L_w(550\text{ nm}) \cdot L_w(520\text{ nm})}{L_w(443\text{ nm})} \tag{24}$$

Figure 5.4 shows the water radiance model derived relationship for a June 11, 1980 aerosol vector orientation. The water radiance values were calculated using the Great Lakes optical model described in section 6.3.

TABLE 5.2. FIRST PRINCIPAL COMPONENTS DERIVED FROM CZCS DATA SETS

Scene Date	Location	Eigenvector λ_1=443	λ_2=520	λ_3=550	λ_4=670	Percent of Total Variance
11 June 1980	Upper Lake Michigan*	-.0112	.352	.771	.530	96%
	Central Lake Michigan	.699	.569	.368	.228	76%
	Lower Lake Michigan	.814	.389	.370	.221	61%
	Lake Michigan (Grand Haven)	.214	.569	.761	.224	98%
	Central Lake Huron	.480	.547	.587	.355	92%
	Lower Lake Huron	.412	.654	.625	.108	80%
	Western Lake Superior	.702	.429	.437	.365	78%
	Central Lake Superior	.606	.521	.487	.353	96%
	Eastern Lake Superior	.712	.509	.380	.298	78%
	Central Lake Erie	.954	.202	.211	.069	63%
23 July 1980	Central Lake Michigan	.582	.771	.243	.090	86%
	Lower Lake Michigan	.774	.516	.136	.341	77%
	Lake Michigan (Grand Haven)	.487	.541	.533	.433	58%
	Central Lake Huron	.975	.205	.681	.564	71%
	Central Lake Superior	.547	.609	.488	.302	99%
	Eastern Lake Superior	.478	.505	.519	.497	99%
	Central Lake Erie	.789	.458	.368	.178	94%
6 August 1980	Western Lake Superior	.997	.0577	-.0172	.0372	44%
	Central Lake Superior	.994	.656	.913	-.0013	62%
	Eastern Lake Superior	.971	.183	.118	.0955	62%

*May include islands in test area

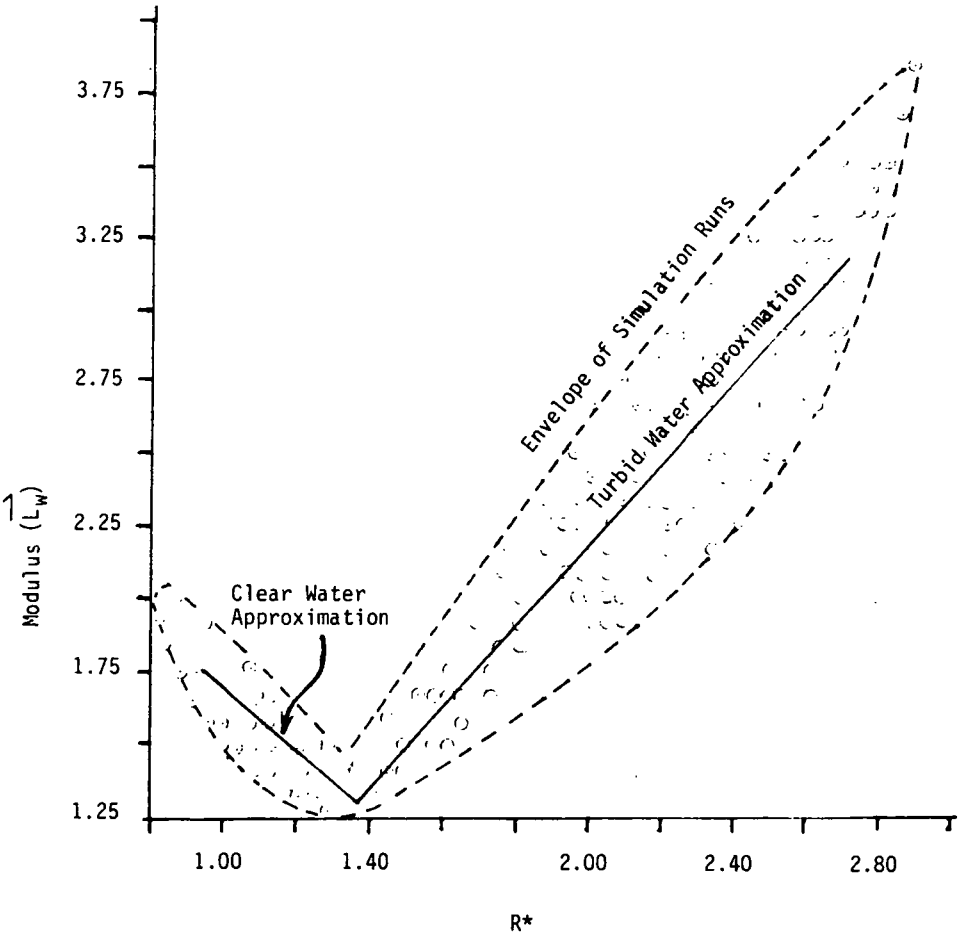

Figure 5.4 R* vs. brightness (modulus) of the upwelling radiance spectra using simulated cases generated with the Great Lakes optical model.

For small values of R* the L_w(550 nm) . L_w(520 nm) product ratio is correspondingly small and the water radiance brightness is dominated by the contribution from the 443 nm band. Waters in this case have very low concentrations of chlorophyll and are essentially free of suspended minerals and dissolved organics. As R* increases so do the constituent concentrations. Surprisingly the corresponding water radiance brightness values decreases, passes through a minimum, and then increases asymmtotally to a maximum. These data imply a higher order polynomial in R* would describe the relationship. A study by Austin and Petzold [25] of a large number of ocean upwelling radiance measurements showed that the radiance in each band can be expressed as a power function in R* suggesting as in the present study that some higher order polynomial would describe the vector modulus of the water radiance. For the residual component algorithm the following linear approximation was used to describe this relationship.

$$\begin{aligned} |\vec{L_w}(\lambda)| &= 0.517 - 0.097\ R^*(L_w(\lambda))\ R^* < 1.4 \\ |\vec{L_w}(\lambda)| &= 1.318 + 1.17\ R^*(L_w(\lambda))\ R^* \geq 1.4 \end{aligned} \tag{25}$$

In applying the residual component algorithm the Rayleigh path radiance components are first calculated and subtracted from the total satellite measured radiance. The Rayleigh components are estimated here using the double delta solution rather than the QSS approximation. Next, the aerosol path radiance is estimated at 443 nm and the previously derived a-ratios are used to estimate the corresponding path radiance at each of the other wavelengths. These radiances are then subtracted at each wavelength from the balance and the length of the residual component vector as projected on the aerosol vector is calculated. The residual radiances are used to also calculate R* and make a model predicted estimate of the brightness value. The two moduli are then

compared and the length of the aerosol vector is modified so as to reduce the difference in these two estimates. In effect we are adding or subtracting the amount of aerosol haze present while keeping the type constant. The procedure is conceptually illustrated in Figure 5.5. Two or three iterations are usually sufficient for convergence to a constant set of residual component radiances which are then equal to

$$T_D(\lambda) \cdot L_w(\lambda). \tag{26}$$

5.8 CONVERSION OF DIGITAL COUNTS TO RADIANCE VALUES

Since each of the above algorithms operates on CZCS measured radiances the computer code for each algorithm contained a section to convert count data to radiance values. These conversion relationships are critical to obtaining any meaningful results where a quantitative approach has been made to understand the radiometric components.

The necessary radiometric calibration constants are nomially reported in the header of each NOAA processed CCT. However, NET calibration studies have shown that use of such constants would produce incorrect radiance values primarily because these constants do not account for sensor deterioration.

Two independent investigations were made by H. Gordon and R. Austin et al [26] into the calibration problem using repeated CZCS measurements over predictable very clear waters such as those of the Sargasso Sea. In both studies the objective was to start with the original prelaunch gain correction constants and determine an adjustment factor $G(\lambda,j)$ for each orbit k. The sensor radiances $L(\lambda)$ are then related to the digital counts $N(\lambda,j)$ by

$$L(\lambda) = (A(\lambda) \cdot N(\lambda,j)K) + B(\lambda))G(\lambda,j) \tag{27}$$

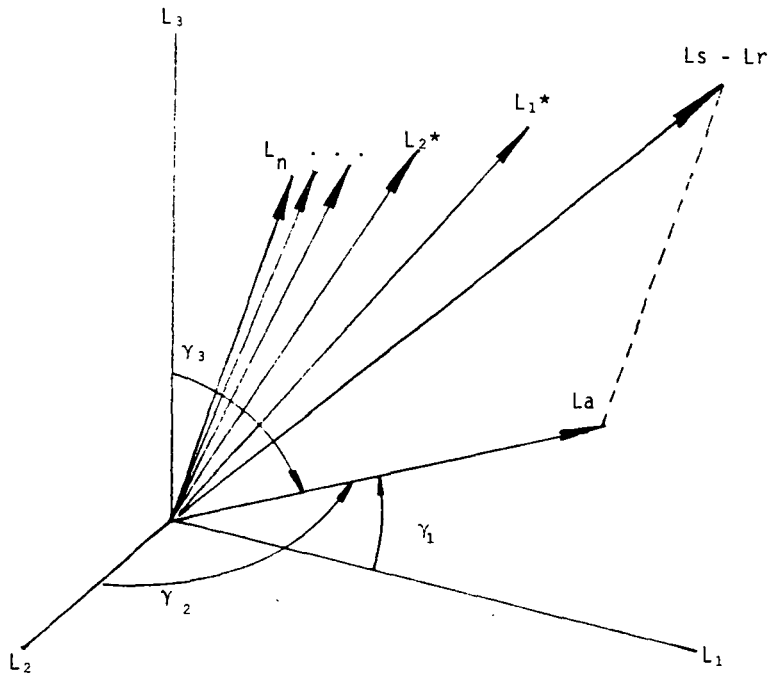

Figure 5.5 Vector Illustration of Residual Component Algorithm. Successive iterations $\overrightarrow{L_1^*}$, $\overrightarrow{L_2^*}$, . . ., $\overrightarrow{L_n^*}$ reduce $\overrightarrow{Ls - Lr}$ by $\Delta \cos \gamma_i$ to estimate $\overrightarrow{L_w \bullet T}$ with $\overrightarrow{Ln^*}$

where A and B are the gain correction constants. Unfortunately, the two investigations, which used tens of scenes over deep ocean targets with uniform upwelling radiance, came up with different results. The two studies produced two fits of G with orbit number with different mathematical form. The G values were found to be similar at some orbit numbers and quite different at others. The G calibration factors used in this study were based upon a set of formulas developed by H. Gordon [27] which are listed with the gain 1 and 2 correction constants in Table 5.3. Also given are the G values for orbits 8243, 8699, 8740, 8823, and 9017 (June 11, July 14, July 17, July 23, and August 6, respectively.

TABLE 5.3 RADIOMETRIC CALIBRATITON CONSTANTS

		G(λ,j) values wavelenth (λ)			
1980 Dates	Orbit(j)	443 nm	520 nm	550 nm	620 nm
June 11	8243	1.189	1.022	0.969	1.00
July 14	8699	1.201	1.025	0.969	1.00
July 17	8740	1.202	1.025	0.969	1.00
July 23	8823	1.204	1.025	0.969	1.00
August 6	9017	1.209	1.027	0.971	1.00
A(λ)	(Gain 1)	.0445	.0310	.0247	.0114
B(λ)	(Gain 1)	.0396	.0636	.0799	.0114
A(λ)	(Gain 2)	.0359	.0249	.0202	.0897
B(λ)	(Gain 2)	.0528	.0883	.0625	.0359

Above Calibration Constants from H. Gordon [26].

5.9 ALGORITHM CALIBRATION

Each of the existing atmospheric correction algorithms and the residual component algorithm developed as part of the present study were

applied to the June 11, 1980 scene for purposes of comparison and evaluation. Large quantities of aerosol haze were present over Lakes Michigan and Superior on this date. These aerosol concentrations were highly variable and easily identifiable in each CZCS band especially over a major portion of Lake Superior where conditions ranged from clear to haze sufficiently heavy to optically obscure the upwelling radiance.

The algorithms were implemented by making two passes through the data set. In the first pass the necessary scene dependent parameters were estimated for each algorithm as discussed below. The second pass removed the aerosol components of path radiance on a pixel-by-pixel basis and transformed the corrected radiances to a nadir viewing geometry. The results of this algorithm processing were summarized in products which consisted on numerical transects and color coded radiance maps.

The four algorithms were individually calibrated for the Lake Superior subscene using a block of 100 pixels located north of Michigan's Keewanaw Peninsula in the central part of the Lake (see Figure 3.4). Typical chlorophyll-a pigment levels have been reported by Munawar et al. [28], 1978 to average 1.1 mg/m^3 for all but the nearshore waters with an expected lower seasonal value for the calibration area of 0.8 mg/m^3. Chlorophyll levels are very stable for this part of Lake Superior and perhaps the most predictable for all of the lakes. Year-to-year productivity cycles in Lake Superior are not expected to change dramatically based upon year-to-year measurements made at the same time over a period of several years, including 1980, in the open waters of Lake Huron [20]. While no surface truth data were collected from this area on June 11, 1980 the estimated concentration of 0.8 mg/m^3 is considered to be within chlorophyll-a measurement error of actual values. Surface truth collected on this date were collected in Lake Michigan near Grand Haven, Michigan. This area displayed little radiometric effects from haze and had highly variable concentrations of

chlorophyll-a and suspended mineral particles associated with the discharge from the Grand River. For these reasons the Grand Haven surface truth data could not be used to calibrate the algorithms to be applied over the whole of Lakes Superior and Michigan. However, the optical thickness measurements were used to estimate the a-ratio coefficients which were considered to be valid for much of the southern portion of Lake Michigan.

Estimation of the upwelling radiance for the Lake Superior calibration area was accomplished using the water radiance model discussed above and in section 5.5. A normalized upwelling radiance was estimated for Lake Superior which was independent of solar elevation and view geometry. These radiance values were then used to estimate the upwelling radiance from beneath the surface at the calibration area. The viewing geometry and normalized radiances are shown in Table 5.4. In the case of the Gordon algorithm the average satellite radiance, estimated upwelling water radiance, and average calculated Rayleigh path radiance were used to estimate the average aerosol path radiance at each wavelength and subsequently the epsilon constants which are related to the k-ratios and which account for scene-to-scene differences in aerosol type. A similar set of epsilons were derived for the Smith and Wilson iterative algorithm but were determined to be slightly different since the upwelling radiance at 670 nm was not assumed to be zero. In the case of the pseudo optical depth algorithm the average path radiance over the calibration area was used to estimate the corresponding aerosol optical depth from the DOM derived relationships. These aerosol optical depths were then used as described above to estimate the aerosol optical depths at other pixels within the scene. For the residual component algorithm the calibration area data were used to derive a first principal component eigenvector containing the direction cosines of the aerosol vector. The model generated upwelling radiance values were not needed for this latter algorithm calibration. The scene dependent parameters derived for the four algorithms are given in Table 5.5.

TABLE 5.4 VIEWING GEOMETRY FOR LAKE SUPERIOR CALIBRATION AREA

Solar zenith angle:	25.4 degrees
Solar azimuth:	152.4 degrees
Average view angle:	25.6 degrees
Sensor tilt angle:	20.0 degrees
Calibration area size:	100 pixels

Normalized radiances $L_u(mW/cm^2.sr.\mu)(1...4)$ = (1.495, 0.980, 0.725, 0.042)

TABLE 5.5 DERIVED SCENE DEPENDENT ALGORITHM PARAMETERS FOR CZCS CHANNELS 1-4

ALG. 1: Gordon's Epsilons (1...4) = (0.665, 0.886, 0.744, 1.00)

ALG. 2: Smith and Wilson Epsilons (1...4) = (.0790, 0.972, 0.816, 1.00)

ALG. 3: Aerosol Optical Depths, (1...4) = (0.327, 0.367, 0.350, 0.521)

ALG. 4: Aerosol Vector Direction Cosines, $V_A(1...4)$ = 0.605, 0.540, 0.433, 0.315)

5.10 ALGORITHM COMPARISON AND PERFORMANCE ANALYSIS

Three criteria were used to evaluate the performance of each atmospheric correction algorithm. First, derived or measured local optical depths were used with an atmospheric radiance model to estimate the aerosol portion of path radiance. These path radiances were compared with those predicted by each algorithm. Second, the upwelling CZCS spectra or that implied from known concentrations of constituents were compared with that obtained from each of the atmospheric correction algorithms. Third, the spatial patterns of haze known to be present in the raw uncorrected imagery were examined to see if they were removed by each algorithm. The residual patterns in the corrected imagery were also compared with known or suspected patterns of phytoplankton productivity and suspended particles.

Algorithm derived aerosol path radiances are compared with model estimates in Figure 5.6. The modified atmospheric water radiance model was used to estimate the aerosol path radiance over the Lake Superior calibration area. The atmospheric model values are shown here and they correspond closely to those produced by algorithm (4). The shape of the aerosol path radiance curve approximates theoretical considerations which suggest that aerosol path radiance is inversely proportional to wavelength. It is apparent from these results that both algorithms (1) and (2) severely underestimate the aerosol path radiance components. All four algorithms produced and equivalent estimate of the Rayleigh components of the satellite radiance.

Upwelling radiance spectra were obtained for two test areas, one in southern Lake Michigan and the other in Lake Superior. These were compared with the spectra for each test site produced by the atmospheric correction algorithm. The upwelling radiance spectra used for the southern Lake Michigan test site were produced from water reflectance model using data collected coincidently with the CZCS's overflight.

A comparison of the model predicted and algorithm predicted upwelling radiance for the southern Lake Michigan test site for algorithm (4) is presented in Table 5.6. Relative to Lake Superior these waters contained high concentrations of chlorophyll-a pigments (4-29 mg/m^3) and suspended minerals (0.4-3.0 mg/1). Algorithm (3) produced similar results with the exception of band 4. Algorithm (1) produced the worst match to the model predictions.

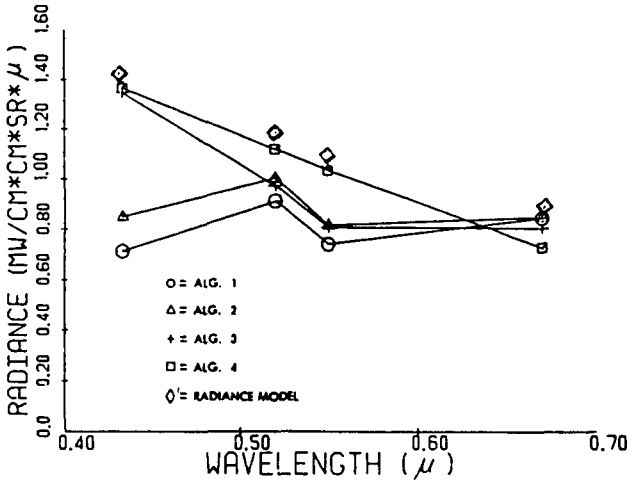

Figure 5.6 Aerosal path radiance predicted by algorithms and atmospheric model calculations.

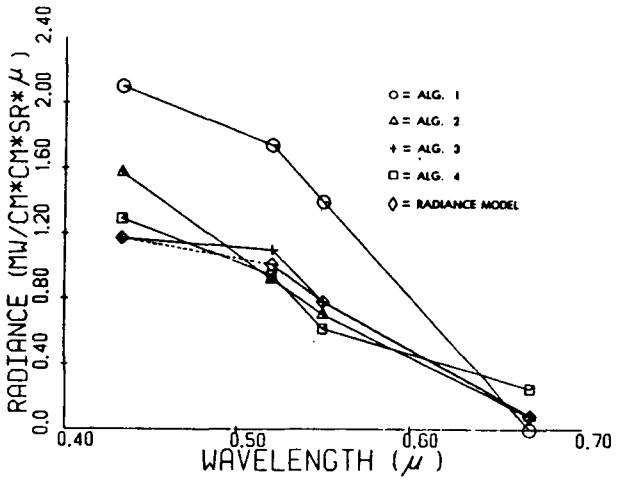

Figure 5.7 Upwelling radiance predicted by algorithms and water radiance model calculations.

TABLE 5.6. MODEL PREDICTED AND ALGORITHM PREDICTED UPWELLING RADIANCE (MW/CM^2 . SR . μ)

	WAVELENGTH (NM)			
STATION*	443	520	550	670
1 Model	1.16	1.39	1.38	0.40
ALG. 4	1.39	1.58	1.58	0.49
2 Model	0.93	1.07	1.07	0.25
ALG. 4	0.93	0.93	0.76	0.19
3 Model	1.01	1.16	1.13	0.25
ALG. 4	1.07	0.92	0.73	0.23
4 Model	0.89	0.81	0.85	0.25
ALG. 4	0.92	0.88	0.78	0.20
5 Model	0.95	1.22	1.33	0.57
ALG. 4	0.95	1.31	1.41	0.43

*All stations located near Grand Haven, Michigan

Comparison of upwelling radiance predicted by each algorithm with that obtained from model calculations is shown in Figure 5.7 for the Lake Superior calibration area. Algorithms (2), (3), and (4) all approximate model values. Exceptions noted are that algorithm (2) produced a slightly higher value of $L_U(\lambda)$ at 443 nm and algorithm (4) a slightly higher value at 670 nm. The Gordon algorithm produced the poorest fit to the modeled radiances.

The other means used for algorithm comparison and evaluation included transect and image analysis. A 50 km image transect was laid out in a west-east direction oriented perpendicular to the apparent haze pattern over Lake Superior. Figure 5.8 shows the uncorrected radiance at 443 nm along this transect with the corrected values generated by each algorithm. Algorithm (1), as applied, did not normalize the impact of aerosol haze. Each of the other three algorithms produced nearly the same result which appears to be free of the radiometric variations due

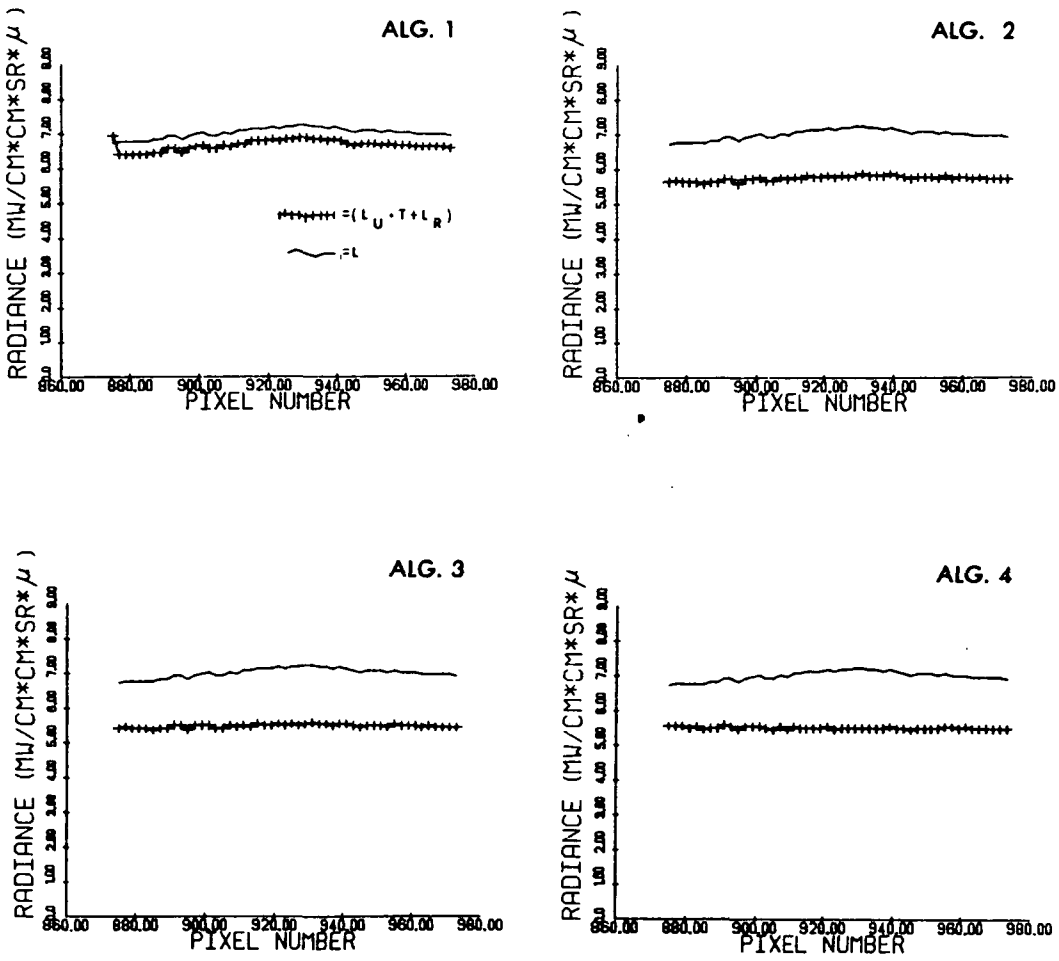

Figure 5.8 Comparison of uncorrected CZCS Band 1 (λ = 443 nm) radiance values for the Lake Superior transect with those produced using correction algorithms.

to aerosol path radiance. Similar plots made for 520 nm and 550 nm produced comparable results. Transect plots for 670 nm are shown in Figure 5.9. The corrected radiance for algorithm (1) contains no upwelling contribution and clearly shows the effects of haze. The corresponding results for algorithm (2) and (3) imply haze normalization with only a very small upwelling radiance component. Algorithm (4) produced slightly higher radiance values implying a larger upwelling component. Transects selected for Lake Michigan waters produced similar comparisons between the four algorithms. Since these transect studies were made ovoer waters with minimum productivity these results suggest that the Gordon algorithm (Alg. 1) has little application for the Great Lakes region.

Another type of spatial comparison of algorithm performance was made for algorithms (2), (3), and (4) by producing color-coded radiance maps in each band for both corrected and the original uncorrected data. A set of maps were made for both the Lake Superior and Lake Michigan test sites. These maps are shown respectively, as plates 1 and 2 of Appendix B.

These maps illustrate the patterns of aerosols over each lake and the extent to which each algorithm was able to correct the subscene on an area wide basis. Examination of the uncorrected data indicated that large radiometric variations exist in both the aerosol and water components. The same water details were essentially absent in the 750 nm band where the variations due to aerosols were greatly attenuated. Algorithms (2) and (3) both used an aerosol radiance estimate in the 670 nm band to estimate the corresponding radiance at the shorter wavelength bands. This process tended to eliminate spatial details in the upwelling radiance at 670 nm. An attempt was made to correct this situation by using the 750 nm band instead of 670 nm to estimate the aerosol component. However, the aerosol variations were represented by fewer signal counts at 750 nm than at 670 nm. The process caused stairstep

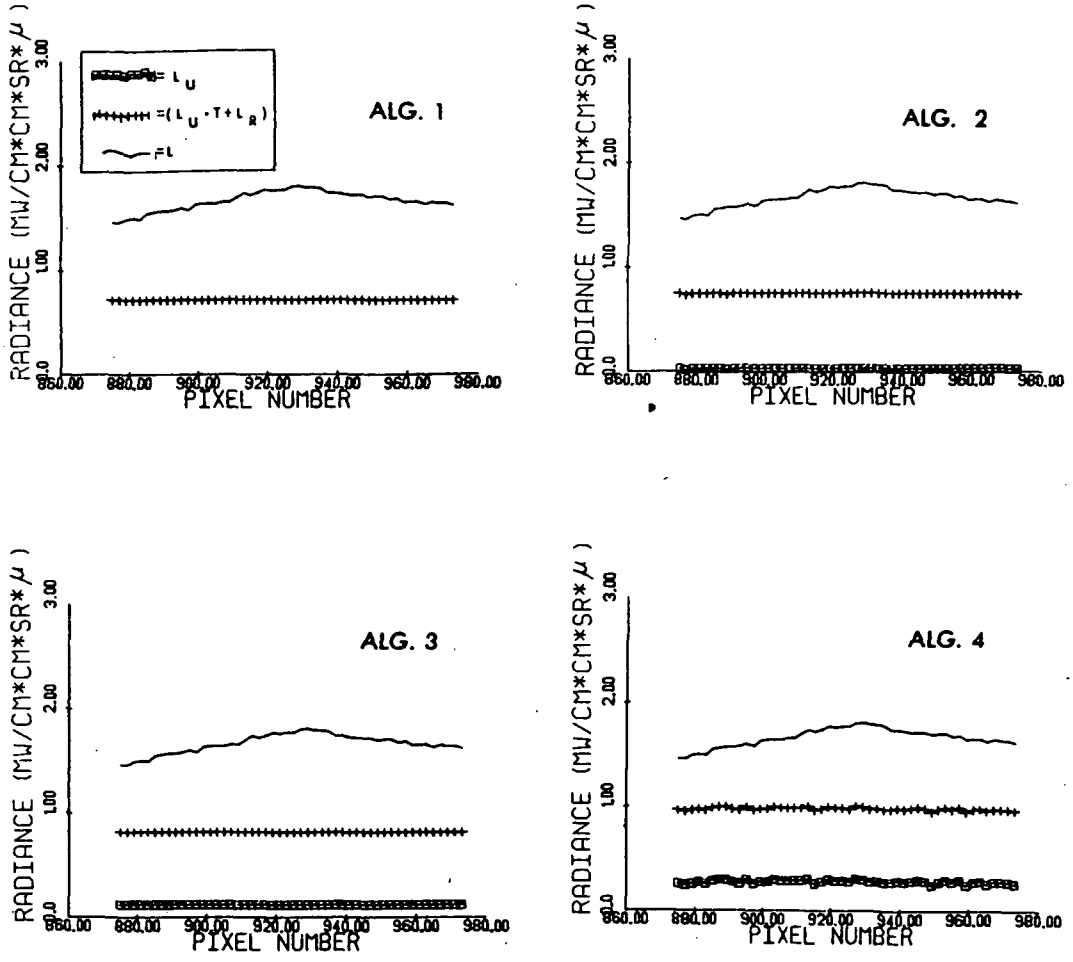

Figure 5.9 Comparison of uncorrected CZCS Band 4 (λ = 670 nm) radiance values for the Lake Superior transect with those produced using correction algorithms. Also shown are the algorithm calculated upwelling radiance values just above the water surface.

anomalies to appear in each of the first four CZCS bands. By comparison, the approach used in the residual component algorithm (4) preserved much of the water radiance with Lake Superior. Algorithms (2), (3), and (4) all removed the haze patterns at 443, 520, and 550 nm. The residual patterns of upwelling radiance seem to be consistent with our expectations, based upon suspected patterns of productivity and suspended sediments. As with the transect comparisons only algorithm (4) produced acceptable results at 670 nm.

Results from these algorithms for Lake Superior displayed varying degrees of haze removal capability. Some residual haze features are apparent in the radiance corrected images produced by each algorithm. These features correspond to those portions of the subscene with the greatest concentration of haze. Algorithm corrected radiance compared well for portions of the east end of Lake Superior where the quantity of haze was the lowest. Over the entire lake residual variations due to haze were greatest for algorithm (3) and least for algorithm (4) which showed the best performance overall for the Lake Superior data set.

6.0

DEVELOPMENT OF BIO-OPTICAL ALGORITHMS FOR THE GREAT LAKES

A primary objective in this validation study is the development of working algorithms which are capable of transforming the satellite measured radiance into surface concentrations of chlorophyll-a pigment and suspended sediment (minerals). In the previous section the development of atmospheric correction algorithms were discussed. This section focuses on the development of the companion water algorithms. These algorithms together are sufficient to convert spacecraft radiances in water constituent concentration values. The bio-optical algorithm is designed to transform the upwelling radiance values as estimated for a position just above the surface into concentration values for the selected biochemical constituents. The fundamental relationship developed in the bio-optical algorithm are based upon the absorption and scattering optical properties of each constituent. By contrast many previous algorithms were based upon empirical relationships between concentration values and remotely sensed radiances. This latter approach is usually valid for a limited range of environmental conditions since the optical properties are implicitly expressed in the algorithm. For example the NOAA chlorophyll algorithms derived for the open ocean are sensitive to small changes in chlorophyll concentrations in those open waters of the ocean, but have little application to coastal waters where a highly variable suspended particulates and dissolved organics can greatly influence and possibly dominate the observed radiance.

The relationship between upwelling radiance and component concentration $[c_i]$ is usually expressed by the following equation.

$$\mathrm{Log}[c_i] = A_1 + A_2 \, \mathrm{Log}(L_u(\lambda_1)/L_u(\lambda_2)) \qquad (28)$$

where A_1 and A_2 are determined by a least squares fit of a set of chlorophyll-a [C] or suspended sediment [SM] data and the radiometric data acquired at two appropriate wavelengths λ_1 and λ_2. For CZCS a band 1/band 3 ratio has been most commonly used where band 1 at 440 nm is highly sensitive to changes in pigment concentration and band 3 at 550 nm is located near the hinge point of the chlorophyll absorption curves. In principle these algorithms cannot be applied without modification in waters having optical properties differing from the algorithm calibration sites. The goal is to model the influence of these components on the reflectance in order to solve the inverse which would allow the derivation of component concentrations from reflectance.

In order to systematically approach the development of new algorithms it is necessary to understand the underlying radiative transfer processes and optical properties which influence the observed radiometry. The inherent optical properties of a passive medium include the absorption coefficient and the volume scattering function. From a practical standpoint it is necessary only to specify the total scattering coefficient and the backscatter coefficient which is obtained by integrating the volume scattering function. For a water medium it is assumed that these inherent optical properties are a linear function of concentrations of various constituents. Thus, the total coefficient can be expressed as shown by the equation in section 5.4.

There are several possible approaches to the determination of absorption and scattering cross sections for each of the constituents. First, one could isolate each constituent and measure the inherent optical properties for different concentrations and thereby estimate the cross section value. The principal problem with this approach is that the isolation may be difficult and could possibly alter the samples such that the measured conditions might not be representative of the natural waters. A second approach for determining optical cross sections is to measure the in situ apparent or inherent optical properties and

constituent concentrations for a large number of samples. Apparent properties can be transformed to inherent properties. Multiple linear regression can then be used to estimate the scattering cross sections for each component. However, biases could be introduced if there exists covariance between constituents. A third approach is to extract the optical cross sections indirectly from measured radiances and concentration data. A radiative transfer model is used with numerical methods to interrelate the two sets of data and to extract the optical parameters.

The advantage of this latter method is that it does not require extensive absorption and scattering measurements which are difficult to perform. The disadvantage is that the method may not converge to a correct or precise determination of the optical cross sections. Having prior knowledge of optical properties for one or more of the constituents present can greatly improve chances of obtaining good approximations for the others. Thus, while the specification of optical cross sections is recognzied to be a difficult task, one gains the necessary information to model the affect of constituent concentration on upwelling radiance and thereby, can gain a great deal of insight on water types throughout the Great Lakes. The empirical model, on the other hand, could not easily account for simultaneous changes in multiple parameters and may have little validity beyond the immediate area of surface truth collection.

In principle the upwelling radiance at any point can be defined by the solution of the radiative transfer equation with proper boundary conditions and specified inherent optical properties. An analytical solution is not possible, but at least two approaches exist for obtaining an approximate solution. First, an exact numerical solution can be obtained using Monte Carlo and/or matrix operator methods [29]. Accuracy from these methods can be excellent but the costs make examination of a large number of solutions impractical. For the present study, the development of specific bio-optical algorithm for the Great

Lakes was based upon the Gordon power series model described previously in section 5.4.

6.1 ANALYSIS OF OPTICAL PROPERTIES FOR THE GREAT LAKES

The inherent optical data available to this project consisted of values reported in the literature, those produced from the Canadian Lake Ontario Study [16], and that measured by NASA/LaRC on the present program [10]. Previous to the present work and that for Lake Ontario several analyses [9, 20, 31] have been performed with marine waters to estimate the optical cross section for chlorophyll-a pigments using both laboratory and insitu optical measurements. Initially the greatest weight was logically given to the LaRC data since it was collected coincident with the 1980 sampling program.

The optical measurements made by NASA/LaRC during the 1980 summer experiments were for lake samples. In this case the measured optical properties pertain to the particular mix of constituents in the lake sample. If sufficient number of measurements are made in this manner and if the principal constituents present are known then multiple regression can be used to derive the optical cross sections for a common parameter. While the present data are considered limited for this purpose a preliminary set of optical properties were derived for the Great Lakes. Of the twenty-one optical data set collected three Lake Erie samples contained sufficient quantities of sediment so as to saturate the optical measurement instrumentation. Samples collected from Green Bay in Lake Michigan, from western Lake Erie, and from western Lake Superior indicated that all these waters have somewhat distinctive local optical properties. Four of the six samples collected from Grand Haven area were essentially sediment free and the presence of low chlorophyll-a concentrations made absorption measurements difficult and results uncertain. For these reasons many of the original twenty-one samples were not considered suitable to be included in the regression analysis.

In fact only eleven samples were used, nine from Lake Erie and two from Lake Michigan. Several linear regression models were formulated and tested against these selected optical measurements. These models utilized the available surface truth data including chlorophyll-a, phaeophytins, total residue, ashed residue, and volatiles [20]. Of these chlorophyll-a, chlorophyll-a plus phaeophytins (i.e., corrected values), total residue, and ashed residue were selected for regression analysis. Each regression model consists of four equations pertaining to the backscatter cross section and four equations pertaining to the absorption cross section. In each case the four equations correspond to the first four CZCS wavelengths (443, 520, 550, 670 nm). The optical model considered for these analyses describes the surface water mass to be a combination of unique organics as represented by chlorophyll-a and phaeophytin pigments and concentrations of unique inorganics as represented by the measurement of suspended minerals (SM). In addition each of the models contains a constant which includes absorption and scattering of pure water, dissolved organics, and possibly other unmeasured components. The two component model equations are written as follows.

$$a = a_1 \cdot [C] + a_2 \cdot [SM] + a_o$$
$$Bb = Bb_1 \cdot [C] + Bb_2 \cdot [SM] + Bb_o \qquad (29)$$

Where [C] and [SM] are the concentrations of chlorophyll-a and suspended minerals, respectively and a and Bb are the absorption and backscatter cross sections. Statistics from these regressions are summarized in Table 6.1. Also included was a case where only the measurements for suspended minerals as ashed weight have been used. Corresponding optical cross sections derived from these regression analyses are given in Table 6.2.

TABLE 6.1

TWO COMPONENT REGRESSION MODELS FOR WATER OPTICAL DATA

(Absorption)

Wavelength (nm)	a-C(m^2/mg)	a-SM(m^2/mg)	Constant m^{-1}	Regression Coefficient	Standard Error of the Estimate
450	0.0162	0.0764	0.309	0.961	0.240
520	0.00835	0.0636	0.248	0.952	0.181
550	0.00529	0.0577	0.303	0.983	0.162
670	0.00450	0.0556	0.390	0.942	0.157
	(Backscatter)				
	Bb-C(m^2/mg)	Bb-SM(m^2/mg)			
450	0.000152	0.0312	0.0424	0.900	0.113
520	0.000372	0.0284	0.0370	0.911	0.0958
550	0.000469	0.0287	0.0232	0.911	0.0967
670	0.000428	0.0250	0.0197	0.013	0.0830

[1]C - Chlorophyll-a

[2]SM - Suspended Minerals as Sample Ashed Weight

TABLE 6.2

SUSPENDED MINERALS REGRESSION MODEL FOR BACKSCATTER

Wavelength	Bb-SM(m^2/mg)	Constant	Regression Coefficient	Standard Error of the Estimate
450	0.0314	0.0116	0.099	0.0210
520	0.0283	0.0127	0.0999	0.0137
550	0.0287	-0.0021	0.999	0.0111
670	0.0250	-0.0012	0.999	0.0105

[1]SM equals sample ashed weight.

The cross sections as derived for chlorophyll have the correct spectral shape but are only about one half the size of those derived for the Ontario Model and other reported results as summarized in Table 6.3. All of the samples included in this analysis were from very turbid waters with a high suspended sediment component which perhaps sufficiently dominated the measured optical properties so as to make these data less correlated to values of chlorophyll-a concentration. This dominance is confirmed by the single component regression results for suspended minerals (Table 6.2). Notice that the derived cross sections for suspended minerals are approximately the same as those obtained in the two component cases and where the multiple regression coefficient is 0.999 and the standard error is greatly reduced. For this latter case the standard error of the estimate coefficient was approximately .02 of the coefficient value. Repetition of the two component model using total chlorophyll-a plus phaeophytin pigments produced almost the same cross sections for suspended minerals and slightly smaller values for chlorophyll-a than reported in Table 5.3. The large constant term in each regression equation also suggests that we have not properly accounted for the absorption due to chlorophyll-a and possibly other components as well. In any case the correlation with suspended sediment concentration is high and the cross sections are considered to be representative for the waters sampled.

TABLE 6.3. CHLOROPHYLL ABSORPTION CROSS SECTIONS (m^2/mg)

Wavelength (nm)	443	520	550	670
Smith and Baker [27]	0.0293	0.0143	0.0090	0.0113
Morel and Prieur [9]	0.0253	0.0159	0.0102	0.0203
Bukata, Jain et al [15]	0.0354	0.0240	0.0173	0.0086
Present Work*	0.0162	0.0936	0.0053	0.0045

*As derived from NASA/LaRC optical measurement.

The Canadian Lake Ontario optical water quality model was based upon a more comprehensive set of water quality parameters than available under the present program. This set allowed the specification of two additional components in the optical model for dissolved organics and non-living organics. The optical cross sections were not derived from measurements of the inherent properties as described above but rather were inferred from in situ measured apparent properties using the Gordon reflectance model [8]. The measured apparent properties included the diffuse reflectance, the irradiance attenuation, and the beam attenuation. Once the inherent properties of absorption and scattering were estimated they were deconvolved into their cross sections using regression techniques.

In constructing an optical model for the present study the available data were recognized to be insufficent to characterize any one of the Great Lakes. As discussed above the measured inherent optical data were insufficient to characterize local areas or single lakes, but altogether provided optical cross sections for suspended sediments. Further there was no complete set of optical data reported outside of that contained in the Lake Ontario model and it was not known how representative this model would be for all of the Great Lakes. Under these circumstances a single set of optical cross sections was sought to represent the waters of the Great Lakes. It was conjectured that if the CZCS radiances can be predicted by a model at the positions where surface measurements of water parameters were collected, then the model optical cross sections are representative of those lake waters. The approach taken was to use a direct search method for unconstrained optimization where the water optical model which appeared to best fit the observed CZCS radiances could then be used for further investigation and algorithm development.

Starting point for this modeling process was central Lake Superior where the chlorophyll-a concentrations are known to be very low. Typical

chlorophyll-a pigment levels for Lake Superior [27] average 1.1 mg/m^3 while in the water radiance calibration area the level is typically lower at 0.8 mg/m^3. Chlorophyll-a concentrations are also very stable in this area during the spring to mid-summer period. Year to year productivity cycles in central Lake Superior are not expected to change dramatically based upon year to year measurements taken in similar waters of Lake Huron [20]. These latter samples represent the low range of chlorophyll-a and suspended mineral concentration values where as the measured boat values from the five CZCS dates represent mid to high concentrations. Because of cloud cover open lake samples of CZCS radiance at satellite altitude could be extracted for Lakes Michigan, Superior, and Huron for the June 11 and July 23 images and also for Lake Superior for the August 6 scene for a total of six samples. The measured data available for this analysis consisted of the Lake Erie sites (July 14, 2) and July 17, 2), Lake Michigan at Grand Haven (June 11, 5 and July 23, 5), and Lake Superior (August 6, 5) for a total of 19 sampling stations. It was assumed that at each station there was a variable concentration of atmospheric aerosols and the aerosol type could also vary from scene date to scene date. The concentrations of chlorophyll-a, suspended minerals, and dissolved organics were known or assumed. The unknown optical cross sections constitute eight unknowns and the unknown concentration of aerosol at each measurement site contributes a total of twenty five unknowns. Under these circumstances it is possible to write 25 x 4 non-linear differential equations in the 25 + 8 unknowns and any acceptable solution must be first bounded in the parameter space. One can start with an existing optical model or some notion of how the cross section spectra should appear although these cross sections would be expected to change if suspended sediments have different particle size distributions or absorption properties connected to differing parent soil materials (i.e., sand, silt, blue clay, and red clay). Further complexities to finding a solution are the uncertainties in the CZCS radiance measurements and possible insensitivities of

measured radiance to changes in constituent concentration. These latter insensitivities can occur at high concentrations of chlorophyll or suspended sediment. Although any attempt to obtain a general solution appears difficult an approximate solution is possible in the neighborhood of a suitable optical model.

There are many well known approximate solution methodologies including LaGrange multipliers, Runge Kutta, and steepest descent. However, all of these methods require computation of derivative at each iteration. Since our solution to the radiative transfer equation is in the form of a computer model the computation of derivatives is a formidable task. An approach was sought which would find a solution without involving derivatives. The method selected was essentially that due to Hooke and Jeeves [11] which is a sequential technique where each step comprises two types of moves: EXPLORATORY and PATTERN. The first kind of move is designed to explore the local behavior of the objective function which can be written as

$$F(a_{ij}, Bb_{ij}, C_j) = G(a_{ij}, Bb_{ij}, C_j) - L_{si} \quad i = 1,2,3,4; \; j = 1,2 \qquad (30)$$

where G is the model function and A_{ij} and B_{ij} are the absorption and backscattering coefficients for wavelength i and constituent j with concentration C_j and L_{si} is the satellite measured radiance. Introducing a starting point (a_{ij}, Bb_{ij}) we prescribe step lengths ΔA and ΔBb in each of the directions e_i, i=1, 2, 3, 4. The exploratory stage is performed as follows. Set i=1 and compute $F(a_1 + \Delta a, a_2, a_3, a_4, Bb_1 + \Delta Bb, Bb_2, Bb_3, Bb_4)$ where $\Delta a/\Delta Bb$ is constant. If $F < F^*$ accepts the trial point, set i=i+1, and repeat new trial point. Here F^* is the value of the objective function from the previous base point (i.e., optical model). If $F > F^*$ reject trial point and compute $F(a_1 - \Delta a, a_2, a_3, a_4; Bb_1 - \Delta Bb, Bb_2, Bb_3, Bb_4)$. If again $F < {}^*F$ reject trial point, set i=i+1, and repeat from the beginning. After a series of exploratory moves we arrive at a new base point. If our objective function is less

at the base point then from the starting point F* then we substitute this new base point (i.e., pattern move) and restart the exploratory stage. Otherwise we return to the previous base point restart the exploratory moves reducing the size of Δa and ΔBb. These sequential moves are continued until satisfactory convergence is obtained.

The solution methodology employed in the present study consisted of the following steps.

1. Utilize principal component analysis to extract the spectral shape of the aerosol path radiance (i.e., as the first eigenvector) for each date and Great Lake. Use spectral shape factors to estimate atmosphere aerosol optical thicknesses produces the original extracted eigenvector.

2. Set the initial optical cross section coefficients to those reported for the Lake Ontario five component model [16]. Set absorption and backscatter coefficients for background waters to match oceanic clear water radiances as developed by Gordon [24].

3. Set model view geometry and solar geometry at each test pixel. Set concentration levels to expected or measured values. Iterate the atmospheric water radiance model over aerosol optical thickness until a best match is obtained between the observed and calculated CZCS band spectra at satellite altitude. Check the consistency and reasonableness of aerosol optical thicknesses derived for a sampling area (i.e., Lake Michigan, Grand Haven Stations).

4. Investigate suitability of optical cross sections estimated from the NASA/LaRC optical measurements and as reported in the literature.

5. Use the results from the above analyses to define the initial base point of the Great Lakes optical model. Apply the Hooke

and Jeeves exploratory and pattern search technique to converge on an acceptable optical model.

6.2 DISCUSSION OF ANALYSES AND RESULTS

Although this approach has a heuristic nature it is one which can produce a single Great Lakes optical model representative of the available surface measurement and CZCS data sets. The optimality of this approach remains intuitive rather than that which can be substantiated easily by mathematical proof. While it is recognized that the derived model is based upon very little actual data for the size of the system and that a single model for the entire system is less appropriate than a series of models designed for each lake or sublake area the limitations of the present data set left little alternative. The extraction of needed optical parameters from the actual data sets by model search techniques is considered appropriate since there is little likelihood that extensive measurements of inherent optical properties can ever be obtained for a complex "coastal" system such as the Great Lakes. Thus, we view our approach to be consistent with the theoretical aspects of the water atmospheric radiative transfer process and to be practical in consideration of scarce optical and biological measurements.

The inherent optical properties for the models considered are shown in Table 6.4 where model (I) is the Lake Ontario optical model, model (II) is the Lake Ontario model modified to include inherent absorption and scattering properties as measured in Lakes Erie and Michigan, and model (III) which is the result of five iteration steps from model (II) using the direct search methodology described above. Comparison of modelled and measured CZCS satellite radiances are made in Table 6.5 for each of the three models. A measure of the goodness of the fit of the measured and modeled data are the unbiased RMS errors computed for each of the CZCS wavelengths over the twenty-three stations and sites as shown in Table 6.6. The process of fitting the modeled to the measured data was done so initially to minimize the different at 443 nm. Because

TABLE 6.4

OPTICAL CROSS SECTIONS FOR GREAT LAKES WATER RADIANCE MODELS

MODEL I

Wavelength(nm)	a-C(m^2/mg)	a-SM(m^2/mg)	a-DO(m^2/mg)	a_w
443	0.0354	0.0557	0.0730	0.020
520	0.0240	0.0281	0.0390	0.028
550	0.0173	0.0185	0.0390	0.037
670	0.0100	0.0225	0.0042	0.370

	Bb-C(m^2/mg)	Bb-SM(m^2/mg)	Bb-SM(m^2/mg)	Bb_w
443	0.00199	0.0328	0.00	0.0065
520	0.00182	0.0474	0.0	0.00370
550	0.00241	0.0525	0.0	0.00296
670	0.00175	0.0333	0.0	0.0014

MODEL II

Wavelength(nm)	a-C(m^2/mg)	a-SM(m^2/mg)	a-DO(m^2/mg)	a_w
443	0.0354	0.0764	0.0730	0.020
520	0.0240	0.0636	0.0390	0.028
550	0.0173	0.0577	0.0390	0.037
670	0.0100	0.0556	0.0042	0.370

	Bb-C(m^2/mg)	Bb-SM(m^2/mg)	Bb-SM(m^2/mg)	Bb_w
443	0.00199	0.0312	0.0	0.0065
520	0.00182	0.0284	0.0	0.00370
550	0.00241	0.0287	0.0	0.00296
670	0.00241	0.0250	0.0	0.0014

TABLE 6.4 (Cont'd.)

MODEL III

Wavelength	a-C(m^2/mg)	a-SM(m^2/mg)	a-DO(m^2/mg)	a_w
443	0.0350	0.0764	0.0730	0.020
520	0.0240	0.0636	0.0390	0.028
550	0.0170	0.0577	0.0390	0.037
670	0.0280	0.0556	0.0042	0.370
	Bb-C(m^2/mg)	Bb-SM(m^2/mg)	Bb-SM(m^2/mg)	Bb_w
443	0.00200	0.0315	0.0	0.0065
520	0.00190	0.0285	0.0	0.00370
550	0.00180	0.0240	0.0	0.00296
670	0.00175	0.0200	0.0	0.0014

Model I Lake Ontario Model

Model II Lake Ontario Model modified to include suspended mineral absorption and backscatter. Cross sections measured for Lakes Erie & Michigan.

Model III Modified Lake Ontario - Chlorophyll-a absorption and backscatter with measured absorption and backscatter for suspended mineral particles.

C - Chlorophyll-a

SM- Suspended Minerals

a_w, BB_w - absorption and backscatter for background water

TABLE 6.5 COMPARISON OF MODELLED AND MEASURED CZCS SATELLITE RADIANCES

$L(mW/sr\ cm^2\ \mu)$

	λ(nm)	Model I	Model II	Model III	CZCS
June 11, 1980 - Lake Michigan Near Grand Haven					
Station 1	443	6.73	6.84	6.84	6.83
	520	5.20	4.60	4.60	4.71
	550	5.04	4.09	3.84	4.07
	670	1.81	1.73	1.57	1.64
Station 2	443	6.71	6.67	6.67	6.67
	520	4.70	4.33	4.33	4.24
	550	4.29	3.77	3.57	3.45
	670	1.57	1.51	1.43	1.45
Station 3	443	6.62	6.56	6.56	6.61
	520	4.73	4.27	4.27	4.18
	550	4.35	3.71	3.50	3.36
	670	1.50	1.43	1.35	1.43
Station 4	443	6.68	6.65	6.65	6.67
	520	4.65	4.31	4.31	4.24
	550	4.26	3.77	3.56	3.50
	670	1.59	1.53	1.44	1.48
Station 5	443	6.71	6.65	6.85	6.77
	520	5.02	4.45	4.59	4.71
	550	4.95	4.06	3.91	4.12
	670	2.47	2.16	1.82	1.70
July 14, 1980 - Lake Erie Near Sandusky					
Station 1	443	6.63	6.69	6.69	6.67
	520	5.01	4.60	4.60	4.76
	550	4.76	4.09	3.86	4.22
	670	2.37	2.19	1.89	1.61
Station 2	443	6.86	6.86	6.82	6.83
	520	5.17	5.17	4.69	4.89
	550	4.91	4.91	3.95	4.41
	670	2.53	2.30	1.95	1.71

TABLE 6.5 (Continued)

	λ(nm)	Model I	Model II	Model III	CZCS
August 6, 1980 (Continued)					
Station 4	443	6.05	5.83	5.83	5.92
	520	4.01	3.67	3.67	3.83
	550	3.28	2.95	2.82	3.12
	670	1.33	1.21	1.16	1.15
Station 5	443	6.14	5.99	5.98	5.87
	520	5.14	4.03	4.03	3.67
	550	4.75	3.38	3.18	2.95
	670	1.36	1.21	1.12	1.12
July 23, 1980 - Central Lake Michigan					
Station 1	443	7.36	7.33	7.33	7.33
	520	4.67	4.44	4.44	4.40
	550	3.79	3.52	3.43	3.37
	670	1.24	1.23	1.22	1.26
July 23, 1980 - Central Lake Huron					
Station 1	443	6.74	6.70	6.70	6.62
	520	4.29	4.04	4.04	4.02
	550	3.49	3.22	3.12	3.16
	670	1.09	1.07	1.06	1.32
July 23, 1980 - Central Lake Superior					
Station 1	443	7.03	7.09	7.09	7.04
	520	4.44	4.29	4.29	4.25
	550	3.60	3.41	3.31	3.24
	670	1.16	1.19	1.17	1.32
June 11, 1980 - Central Lake Michigan					
Station 1	443	6.82	6.79	6.79	6.85
	520	4.43	4.22	4.21	4.31
	550	3.70	3.44	3.32	3.46
	670	1.30	1.29	1.27	1.49
June 11, 1980 - Central Lake Huron					
Station 1	443	6.43	6.40	6.40	6.56
	520	4.38	4.15	4.14	4.11
	550	3.64	3.37	3.27	3.26
	670	1.42	1.40	1.39	1.28
June 11, 1980 - Central Lake Superior					
Station 1	443	7.18	7.15	7.15	7.14
	520	4.96	4.72	4.72	4.55
	550	4.20	3.93	3.83	3.64
	670	1.73	1.71	1.70	1.78

TABLE 6.5 (Continued)

	λ(nm)	Model I	Model II	Model III	CZCS
July 17, 1980 - Lake Erie Near Sandusky					
Station 1	443	8.48	8.36	8.36	8.38
	520	7.41	5.81	5.81	6.77
	550	7.56	5.18	4.87	5.67
	670	4.43	3.20	2.58	2.69
Station 2	443	7.82	7.89	7.88	7.84
	520	5.60	5.16	5.16	5.72
	550	5.24	4.52	4.29	4.71
	670	2.66	2.43	2.08	1.80
July 23, 1980 - Lake Michigan Near Grand Haven					
Station 1	443	7.15	7.17	7.12	7.15
	520	4.78	4.47	4.47	4.38
	550	4.32	3.87	3.67	3.57
	670	1.59	1.52	1.42	1.37
Station 2	443	7.13	7.11	7.10	7.10
	520	4.67	4.42	4.42	4.34
	550	4.12	3.78	3.60	3.52
	670	1.49	1.44	1.37	1.32
Station 3	443	7.18	7.18	7.17	7.15
	520	4.47	4.44	4.40	4.41
	550	3.97	3.92	3.70	3.64
	670	2.10	2.08	1.68	1.41
August 6, 1980 - Lake Superior Near Duluth					
Station 1	443	6.03	5.96	5.96	5.92
	520	4.64	3.96	3.96	3.92
	550	4.50	3.49	3.25	3.28
	670	1.89	1.64	1.38	1.31
Station 2	443	6.10	5.96	5.96	5.87
	520	5.06	4.00	4.00	3.73
	550	4.69	3.37	3.17	3.02
	670	1.36	1.21	1.12	1.09
Station 3	443	6.02	5.98	5.98	5.97
	520	4.26	3.88	3.88	3.99
	550	3.80	3.26	3.07	3.31
	670	1.49	1.40	1.29	1.38

TABLE 6.6. RMS ERRORS FOR MODEL PREDICTED RADIANCE*

Wavelength (nm)	Model I	Model II	Model III
443	0.0988	0.0574	0.596
520	0.413	0.272	0.267
550	0.851	0.265	0.265
670	0.497	0.319	0.156

*Calculated RMS errors based upon results reported in Table 6.5

of the larger radiance values at this wavelength and the sensitivity of any subsequent predictive technique to the radiances in this band. The initial adjustments were made by varying the atmospheric aerosol optical thickness at each measurement site. An estimate of the aerosol optical thickness for each scene date can be obtained by subtracting the known Rayleigh and ozone optical thicknesses from the measured total value as reported in Table 3.6 of Section 3.6. These estimates are compared in Table 6.7 with model derived values of the aerosol path radiance as obtained with the final optical model. As would be expected the model predicted station to station variations in the aerosol optical thickness were very small or nil for each of the primary sampling sites. The RMS errors associated with the Lake Ontario model I are large especially at CZCS wavelengths 520, 550, and 670 nm. The inclusion of optical cross sections for suspended sediments derived from the NASA/LaRC data as model (II) represented a substantial reduction in the RMS errors and especially in bands 1 and 3. The least reduction was made in the 670 nm band. Between models (II) and (III), four exploratory moves were made at each wavelength in attempt to reduce the RMS errors. Little reduction was obtained except for the 670 nm band where RMS errors were reduced further by about 50% in model (III). Attempts to further reduce these errors in band 2 and 3 were fruitless and suggest that major differences in optical properties exist at these wavelengths throughout the Great Lakes. These differences seemed most apparent with July 14 and 17 Lake Erie sampling sites, the radiance values for which implied

TABLE 6.7

COMPARISON OF MODEL PREDICTED AND MEASUREMENT DERIVED AEROSOL PATH RADIANCE

$L_w(nw/cm \cdot^2 \cdot sr \cdot \mu)$

Date	Site Location	Wavelength(nm) 443	520	550	620
June 11	Grand Haven, Lake Michigan				
	Model Predicted	1.76	1.33	1.13	0.840
	Measurement Derived	0.723	0.557	0.465	0.341
July 14	Catawba, Lake Erie				
	Model Predicted	2.06	1.54	1.26	0.832
	Measurement Derived	2.38	1.26	1.44	0.958
July 17	Catawba, Lake Erie				
	Model Predicted	1.29	0.895	0.754	0.567
	Measurement Derived	1.89	1.30	1.10	0.831
July 23	Grand Haven, Lake Michigan				
	Model Predicted	0.366	0.274	0.230	0.157
	Measurement Derived	1.94	1.44	1.22	0.830
Aug 6	Duluth, Lake Superior				
	Model Predicted	0.212	0.191	0.106	0.038
	Measurement Derived	1.40	1.26	1.09	0.833

an exceptionally large backscatter component at 550 nm. Adjusting to these samples would throw all the others off greatly increasing the RMS errors for these bands. Thus, optical properties of model (III) were considered for all practical purposes to have the greatest "overall representativeness" of the optical properties of the Lakes with little opportunity to improve the result using this direct solution search methodology.

6.3 USE OF THE GREAT LAKES OPTICAL MODEL TO DERIVE A BIO-OPTICAL ALGORITHM

The optical cross sections derived above provided a means to simulate the upwelling radiance from Great Lakes waters with a wide variety of component concentrations. Further the irradiance reflectance can be readily calculated for each CZCS band as a function of the concentration of chlorophyll-a pigments and suspended sediments. The spectral characteristics of the irradiance reflectance function can be depicted with iso-chloropleths for each pair of wavelengths. Figure 6.1 and 6.2 show calculated subsurface reflectance for the Great Lakes Optical model (III). Dissolved organics are assumed, for this case, to be 2.0 mg/ℓ. Each of the panel figures has nine curves of increasing suspended mineral concentration and constant value of chlorophyll pigment concentration (0.0, 1.0, 2,0, 5.0, 10.0, 20.0, and 1000.0 μg/ℓ). Each figure also contains four curves of increasing chlorophyll with constant values of sediment (0.0, 2.0, 10.0, and 50.0 mg/ℓ). Each panel figure is a projection of the reflectance space and together suggest the reflectance space is a three dimensional hyperplane which is nearly perpendicular to the 520/550 plane as shown in Figure 6.2 as panel 3. This result suggests that there is little bio-optical information in this latter band pair which is contrary to the results obtained for the clear ocean where these bands were successfull used to predict chlorophyll-a concentration [20].

SUBSURFACE IRRADIANCE REFLECTANCE MODEL III

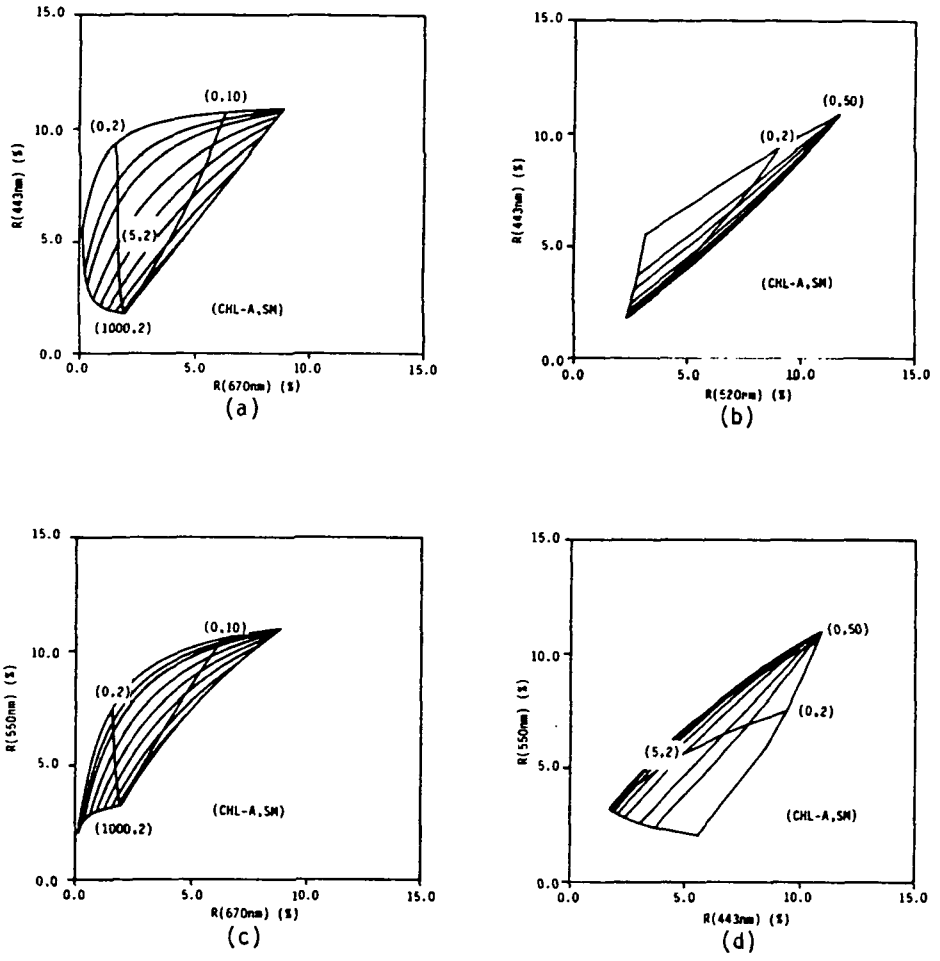

Figure 6.1 Subsurface irradiance reflectance (percent) at CZCS wavelengths (443 nm, 520 nm, 550 nm, 670 nm) as predicted by the Great Lakes Optical model. Each figure has eight parametric curves of increasing suspended mineral concentration (0.0-50.0mg/ℓ) with constant values of chlorophyll pigment concentration (0.0, 1.0, 2.0, 5.0, 10.0, 20.0, or 1000 μg/ℓ). Each figure also contains four parametric curves of increasing chlorophyll a (0.0-1000.0g/ℓ) at constant values of suspended mineral concentration (0.0, 2.0, 10.0, 50.0 mg/ℓ).

C-2

SUBSURFACE IRRADIANCE REFLECTANCE MODEL III (Continued)

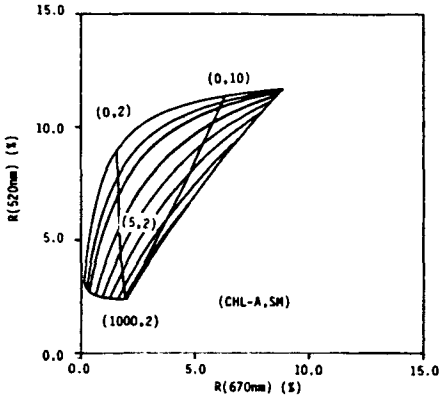

(a)

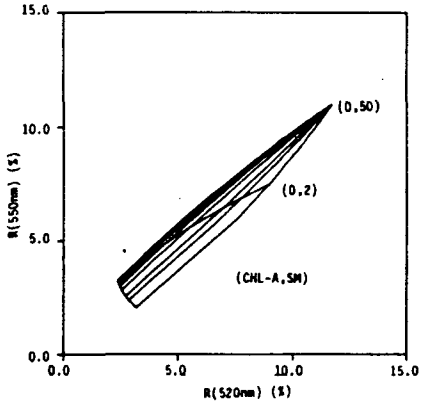

(b)

Figure 6.2 Subsurface irradiance reflectance (percent) at CZCS wavelengths (443 nm, 520 nm, 550 nm, 670 nm) as predicted by the Great Lakes Optical model. Each figure has eight parametric curves of increasing suspended mineral concentration (0.0-50.0 mg/ℓ) with constant values of chlorophyll pigment concentration (0.0, 1.0, 2.0, 5.0, 10.0, 20.0, 50.0, 1000 µg/ℓ) at constant values of suspended mineral concentration (0.0, 2.0, 10.0, 50.0 mg/ℓ).

The orientation of the band pair projection and the corresponding spacing between iso-chloropleths curves suggests the potential of that individual band pair to resolve various constituent concentration levels. For example the (1,3) band pair (panel 2, Figure 6.1) provides the greatest resolution of chlorophyll and suspended sediment concentrations in the concentration range of 0 to 10 μg/ℓ chlorophyll and 1 to 10 mg/ℓ of suspended sediments. For greater concentrations of suspended sediments it appears that resolution of the chlorophyll concentration would become more difficult especially for low concentration values. It is apparent from the spatial features of the subsurface irradiance reflectance function that each band pair coordinate represents a unique concentration of chlorophyll-a and suspended sediments. If the concentration of dissolved organics were also involved then a triple in 3-space would be necessary to describe a set of unique concentrations. While the reflectance model provides a one to one mapping from component concentration space to band pair reflectance space the inverse mapping function is needed for purposes of extracting component concentrations. The complexity of the reflectance model makes any analytical form of the inverse function an impractical for purposes of extracting constituent concentrations. Since the model is essentially a numerical approximation to Monte Carlo calculations a numerical approximation to the inverse function seems appropriate.

Points in the two band reflectance space (1,3) representing constituent concentrations can be located with a vector of length equal to $(R_1)^2 + (R_2)^2$ and orientation equal to $\tan^{-1}(R_1/R_3)$. Thus, two spectral variables, i.e., two band brightness and band ratio, are needed to resolve the two concentration components. The strong non-linearities in mapping reflectance to concentration values suggests that approximation functions are needed over subregions of the reflectance space. The approach taken was to partition the space using the brightness variable and then obtain polynomial approximations in the band ratio variable to the desired concentration pair. The approximation polynomials were

derived as follows first the Great Lakes optical model III was used to simulate the irradiance reflectance such that the simulation data set (3000 samples) was representative of the two band projection space and constituent combinations found in Great Lakes waters. These data were then categorized into ten separate regions as level ranges of the band pair reflectance brightness (i.e., two band vector modulus). Multivariate regression techniques were then used to estimate constituent concentration polynomial coefficients using the (1,3) band ratio as the independent variable. Polynomial coefficients were derived for both suspended sediments and chlorophyll-a pigments. A third degree, three term polynomial was found to be sufficient to describe constituent concentrations. Figure 6.3 shows an example of radiance versus concentration curves for chlorophyll-a pigment. Each of the concentration polynomials has the following form.

$$C(R_1/R_2) = a_1 R^1(1,3) + a_2 R^2(1,3) + a_3 R^3(1,3) \qquad (31)$$

Where R(1,3) is the band 1/band 3 irradiance reflectance ratio. Each of the curves essentially applies to a separate range of suspended sediment concentration. Note that for small concentrations of chlorophyll the curves of Figure 6.3 approximately overlay one another since the concentration of suspended sediment can be expected to be very small. At the other extreme the curves are highly separated based on the influence suspended sediments. As these polynomials curves become more vertical the ability of the band ratio to resolve chlorophyll concentration becomes greatly diminished as was apparent with the plots shown in Figure 6.1.

Polynomials were also derived for a band 1/band 4 ratio algorithm which also appears from the simulation analysis to have capabilities of identifying chlorophyll suspended sediment constituent concentration pairs. Examination of simulation data sets for band ratios (1,2), (2,4), and (3,4) all were shown to have much less capability to extract

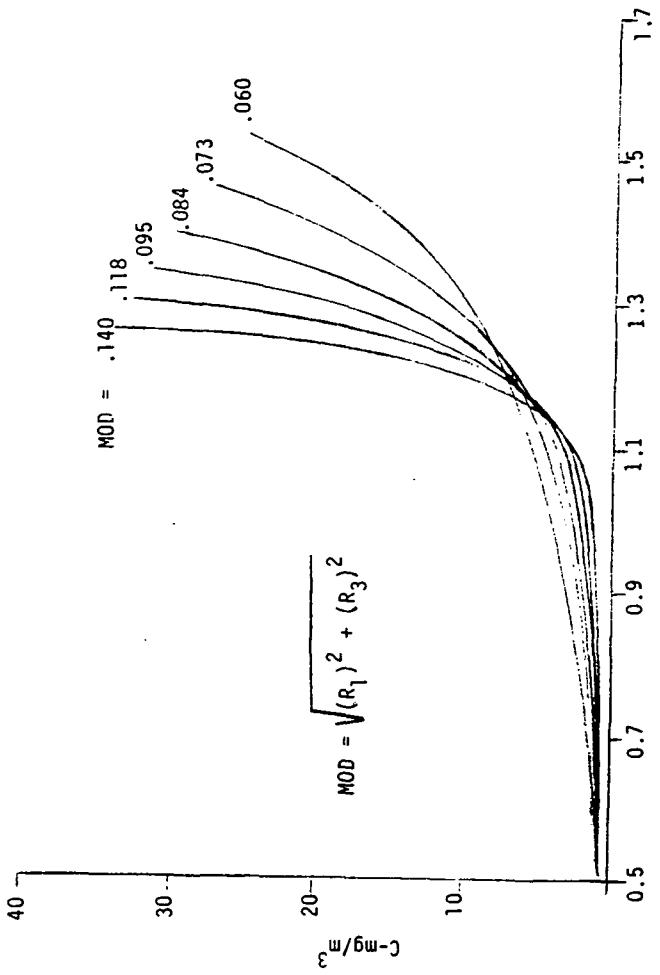

FIGURE 6.3 ALGORITHM PREDICTION CURVES FOR CHLOROPHYLL-A PIGMENT CONCENTRATION (C-mg/m^3) AS BASED UPON THE BAND 3/BAND 1 REFLECTANCE RATIO AND THE TWO BAND MODULUS.

the desired concentrations levels, as indicated from the band pair reflectance space projections. The polynomials generated above were incorporated into a bio-optical algorithm as described below.

6.4 CZCS IMAGE PROCESSING FOR CHLOROPHYLL-A AND SUSPENDED SEDIMENT CONCENTRATIONS

The five CZCS scenes were processed for two types of output. First a 3 x 3 array of pixels for each sampling site was processed on a pixel by pixel basis and the results averaged to produce a CZCS extracted concentration value for chlorophyll-a pigments and suspended sediments. Comparisons were then made to the available surface truth data. Second, a series of twelve subscenes were processed with individual scene, solar geometrical, and atmospheric aerosol characteristic parameters (as made available from pass 1 or by surface measurements). The approximate coverage of each subscene is shown in Figure 6.4 and subscene processing parameters are listed in Table 6.8. Processed subscenes were subsequently used to create color coded level slice constituent concentration maps for chlorophyll-a pigment, < 1.0 to 40 mg/m^3, and suspended sediments, < 0.1 to 20 mg/ℓ. The overall processing scheme is outlined with the data flow diagram shown as Figure 6.5. Pixel by pixel processing was performed using the ERIM QLINE image processing software with major sequential processing steps handled by individual image processing modules. Modules developed specifically for this CZCS validation study included:

1. SPLIT - Cloud/land/water discrimination module. Option to black out land and cloud features.
2. ATMOS - Atmospheric correction routine which removes the spatially varying aerosol path radiance and view angle effects. Pass 1 calculates proper byte to radiance conversion factors and aerosol characteristic parameters. Pass 2 is used to calculate upwelling water radiance or nadir radiance normalized and corrected to the top of a Rayleigh atmosphere.

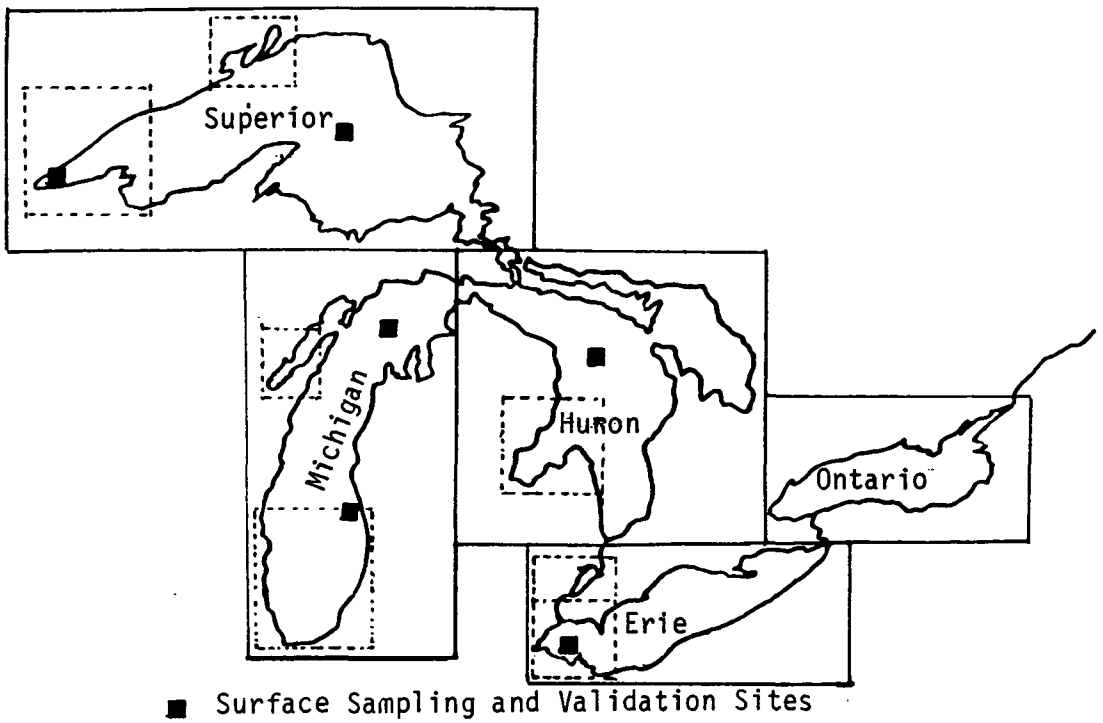

FIGURE 6.4 CZCS GREAT LAKES SUBSCENES

TABLE 6.8

CZCS GREAT LAKES PROCESSING PARAMETERS

Subscene	Date (1980)	Solar Zenith Angle	Solar Azimuth Angle	Aerosol Vector Direction Cosines	Line Range	Point Range	Pixel Sampling Frequency
Lake Superior	August 6	31.60	155.10	0.601, 0.541, 0.468, 0.357	230- 790	200-1400	5
Thunder Bay	August 6	32.29	155.19	0.601, 0.541, 0.468, 0.357	220- 380	630- 880	1
W. Lake Superior	August 6	31.36	155.07	0 601, 0.541, 0.468, 0.357	460- 710	210- 460	1
Lake Michigan	June 11	22.17	151.88	0.699, 0.569, 0.368, 0.228	840-1840	800-1350	4
Green Bay	June 11	23.06	152.25	0.699, 0.569, 0.368, 0.228	1030-1190	800-1050	2
S. Lake Michigan	June 11	22.17	151.88	0.674, 0.510, 0.433, 0.318	1400-1840	800-1050	2
Lake Huron	June 11	22.83	152.16	0.606, 0.521, 0.487, 0.353	800-1540	1300-2120	4
Saginaw Bay	June 11	22.33	151.95	0.606, 0.521, 0.487, 0.353	1190-1410	1440-1680	1
Lake St. Clair	June 11	20.97	151.39	0.480, 0.547, 0.587, 0.355	1600-1700	1520-1740	1
Lake Erie	July 14	23.00	149.15	0.694. 0.513, 0.420, 0.229	1530-1900	1520-2300	3
W. Lake Erie	July 14	22.61	148.83	0.694, 0.513, 0.420, 0.299	1710-1900	1520-1740	1
Lake Ontario	July 14	24.59	150.48	0.694, 0.513, 0.420, 0.299	1190-1500	2090-2720	3
Lake Erie	July 17	22.98	150.42	0.632, 0.412, 0.375, 0.284	1530-1900	1520-2300	3
S. Lake Michigan	July 23	25.71	151.17	0.685, 0.509, 0.431, 0.294	1400-1840	800-1050	2

1. Processed only at primary sampling site.

2. Subscene dimensions equivalent to 0.5x pixel span in km.

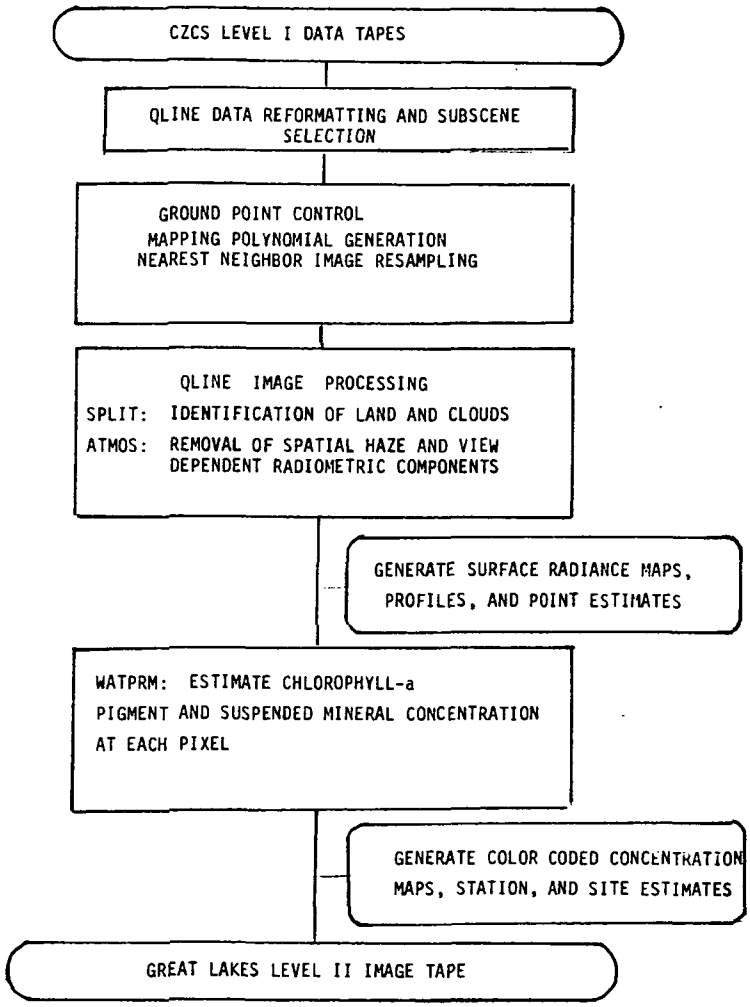

FIGURE 6.5 DIAGRAM OF IMAGE PROCESSING SCENE

3. WATPRM - Uses output from ATMOS to estimate concentration of chlorophyll-a pigments and suspended sediments. Options for bands (1,4) and (1,3) estimates and selected outputs as four channels.

Input CCTs were geometrically corrected and resampled at 500 meters in a polyconic projection. Output tapes contained image files of chlorophyll-a and suspended sediment concentration values. Data flow diagrams for each of the above modules are shown as Figures 6.6, 6.7, and 6.8.

6.5 ANALYSIS AND INTERPRETATION OF RESULTS

Measured and algorithm predicted concentrations for chlorophyll-a pigments and suspended sediments for each of the sampling stations are listed in Table 6.9. Results are shown for both the (1,3) and (1,4) band ratios. While in many cases the predicted concentrations from these ratios are similar the (1,3) ratio was felt to give better results and have a wider application to Great Lakes waters and especially in clear waters where the radiance in 670 nm band is very low and unreliable for extraction of concentration values. The average accuracy of NOAA type ocean CZCS chlorophyll algorithms have been reported to be within 0.5*log(C) [7]. The average log(C) coefficients for the present study were determined to be:

June 11, 1980	Grand Haven, Lake Michigan	0.51LOG(C)
July 14, 1980	Western Lake Erie	0.13LOG(C)
July 17, 1980	Western Lake Erie	0.68LOG(C)
August 6, 1980	Duluth, Lake Superior	0.53LOG(C)

While the above results are based upon a small number of stations where surface truth data were gathered, they suggest that these Great Lakes CZCS algorithms may have comparable performance characteristics to that reported for the ocean experience.

The results shown in Table 6.9 for July 23, 1980, Grand Haven, Lake Michigan are considered to be anomalous. Examination of the CZCS data

Function: Separate cloud haze and land pixels
Required Inputs: Faw count values for Bands 5 and 6

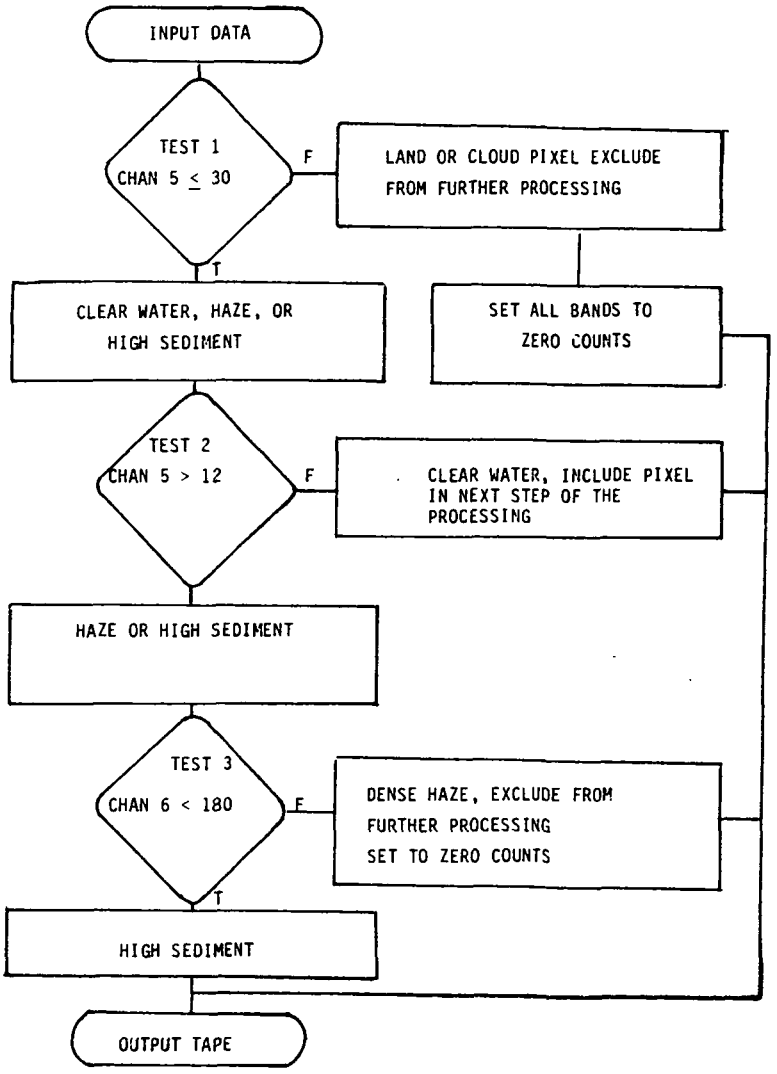

FIGURE 6.6 DIAGRAM OF SPLIT QLINE MODULE

Function: Pass 1: Extraction of Scene Dependent Atmospheric Parameters
Pass 2: Remove Spatial Haze and View Dependent Components

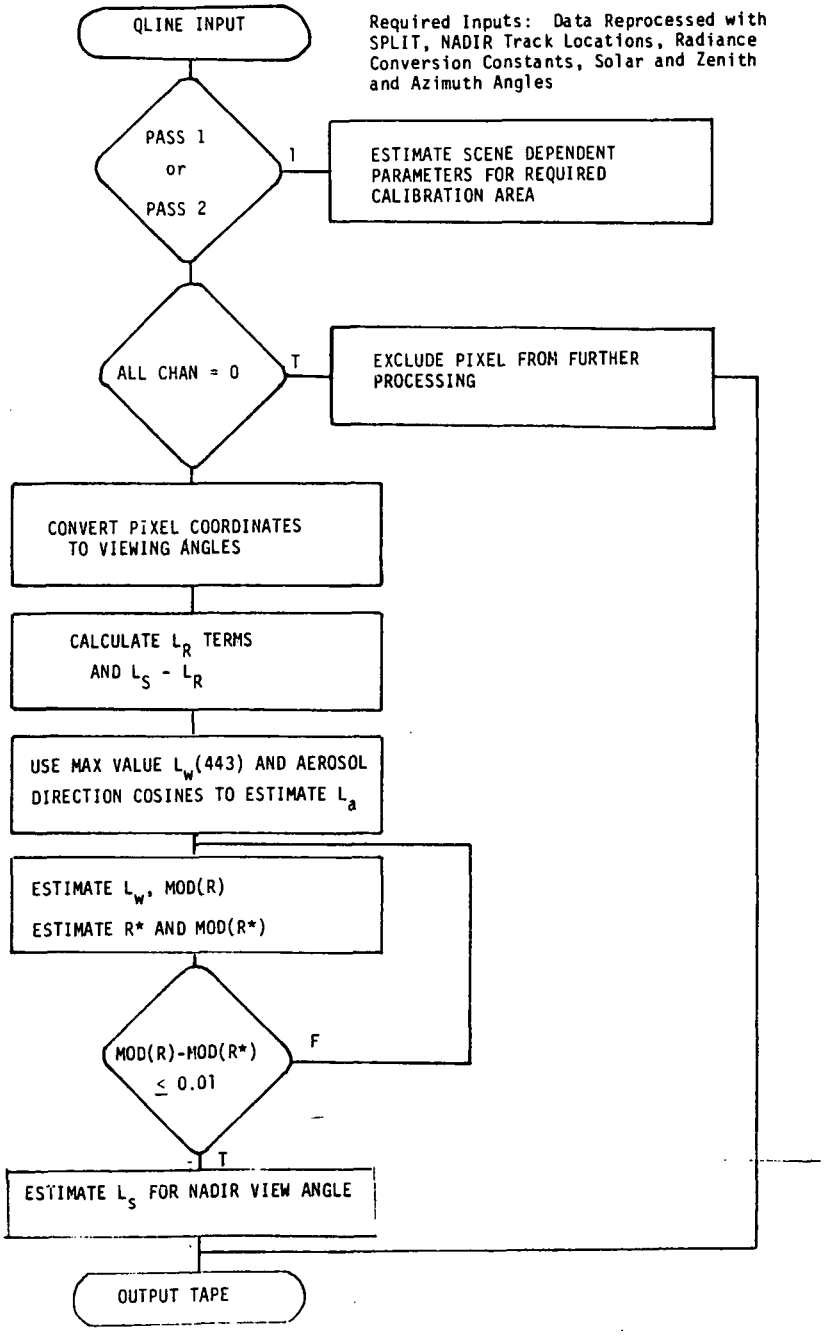

FIGURE 6.7 DIAGRAM OF ATMOS: ALGORITHM 4 QLINE MODULE

Function: Convert ATMOS corrected data to estimate of Chlorophyll-a and Suspended Mineral Concentrations

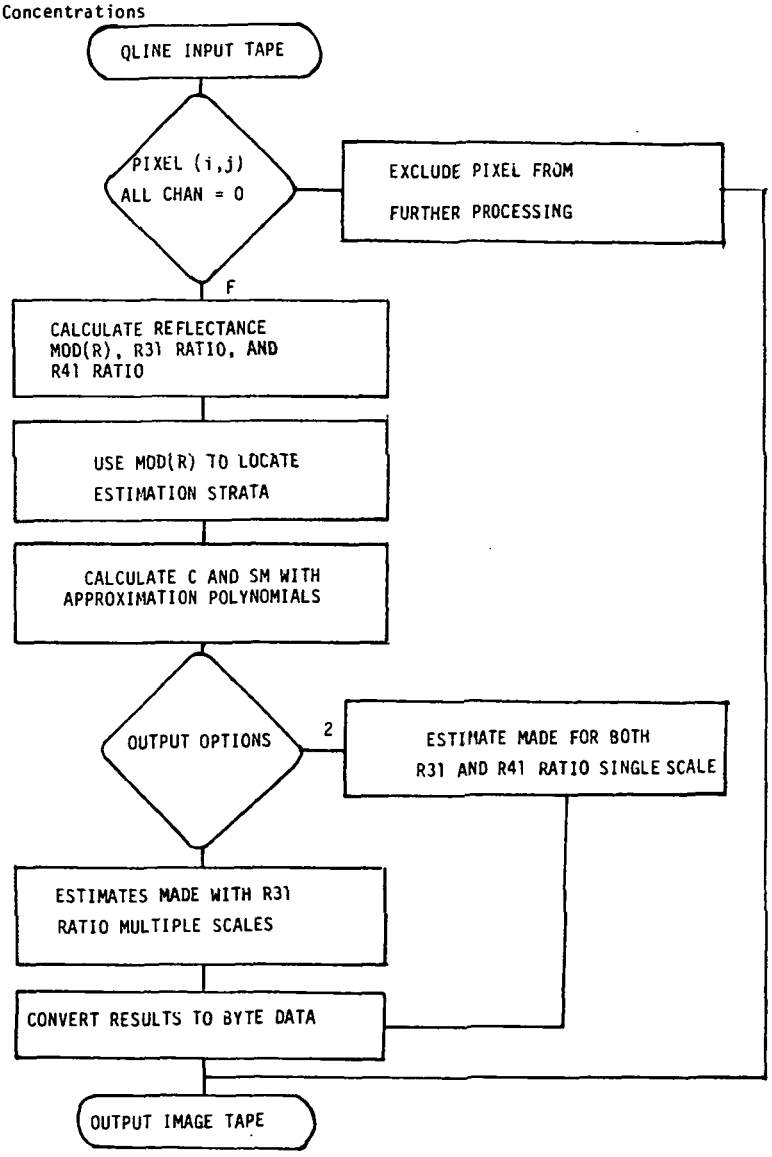

FIGURE 6.8 DIAGRAM OF WATPRM QLINE MODULE

TABLE 6.9

COMPARISON OF MEASURED AND ALGORITHM PREDICTED CONCENTRATIONS FOR CHLOROPHYLL PIGMENTS AND SUSPENDED SEDIMENTS

Date	Stratum	Measured Chlorophyll (µg/ℓ)	Predicted Chloorphyll (µg/ℓ)		Measured Suspended Sediments (mg/ℓ)	Predicted Suspended Sediments (mg/ℓ)	
			R31	R41		R31	R41
June 11 (Lake Michigan)	1	6.91	22.0	7.40	1.09	2.40	1.0
	2	5.24	3.2	3.2	0.40	0.8	0.6
	3	4.55	3.0	3.8	0.45	0.8	0.8
	4	5.99	3.4	4.4	0.41	<0.2	0.8
	5	29.3	30.0	11.0	2.95	5.0	1.4
July 14 (Lake Erie)	1	18.1	18.8	10.8	2.01	4.6	2.2
	2	21.1	22.6	11.2	2.2	6.8	3.0
July 17 (Lake Erie)	1	43.0	Sat & 40		21.7	Sat & 20	
	2	22.9	14.6	5.2	2.73	2.6	1.0
July 23 (Lake Michigan)	4	7.7	1.8	2.0	0.52	0.8	0.4
	5	6.2	1.8	1.8	0.31	0.8	0.4
	6	78.5	2.2	2.0	0.42	0.8	0.4
August 6 (Lake Superior)	1	13.1	6.6	11.2	2.05	0.2	0.6
	2	1.72	3.8	2.6	1.0	<0.2	0.8
	3	7.16	6.8	11.8	0.67	0.2	0.8
	4	3.88	3.8	2.4	0.2	0.2	<0.2
	5	1.43	3.2	4.2	1.0	<0.2	<0.2

R31 = Lu(550/Lu(443) R41 = Lu(670)/Lu(443)

in the immediate area of each sampling site showed both the count values and band to band spectral shape to be consistent with low concentrations of chlorophyll and suspended sediments. The measured concentrations on the other hand were medium to very high. No sizable errors in the image registration and geometry could be established. Spectral shapes of the subsurface radiometer measurements are consistent with the CZCS derived shaped for the upwelling radiance and do not indicate the presence of large chlorophyll or sediment concentrations. Since all of the Grand Haven sampling stations were located in the Grand River plume or in coastal waters influenced by the river it is possible that the optical properties of the river waters substantially between the June 11 and July 23 sampling dates.

Water samples collected at station 1, July 17, 1980, Western Lake Erie showed very high concentrations of chlorophyll-a and suspended sediments. CZCS derived radiances were either saturated or implied spectral brightness values were larger than the upper bounds set in the WATPRM module. As a result no reliable estimate could be extracted from the CZCS data for station 1.

Color coded images for each processed subscene depicting either chlorophyll-a pigment or suspended sediment concentrations are shown in Appendix B. A total of twelve different subscenes were processed using the subscene parameters listed in Table 6.8. A brief description and interpretation of selected concentration maps on a lake by lake basis follows.

Concentration maps are grouped as whole lake and sublake scenes. A total of fifteen colors were used to code a very wide range of CZCS extracted chlorophyll and suspended sediments concentrations. The color codes are graduated to show very small changes at the low end and very large changes at the high end. This scheme was considered consistent with the 0.5 Log(C) errors and brings out both open lake and nearshore features in the concentration of chlorophyll-a pigments and suspended

sediments. These color codes were applied in exactly the same way to the output of the WATPRM module for each of the scene dates.

Lake Superior, August 6, 1980. The Keweenaw current is clearly visible in the whole lake subscene. Also there are subtle differences in the chlorophyll concentration (.1-.2 μg/ℓ) and primary productivity from the western end of the lake as opposed to the central region just north and east of the Keweenaw Peninsula. These waters may be at the center of a large clockwise circulation pattern. The thermal maps consistently show these central lake waters to be cooler. It has been conjectured by some that these waters never stratify throughout the ice free period and, therefore, probably do not mix extensively with the more productive and nutrient rich coastal waters. The western Lake Superior subscene shows a large concentration gradient in the vicinity of the Duluth harbor and river discharge. Also visible are less productive colder waters upwelling along the Minnesota shoreline north of Duluth. Black Bay on the Canadian North Shore stands out as highly productive. Since this bay is very shallow, some of the radiance associated with productivity may in fact, be bottom reflected energy.

Lake Michigan, June 11, 1980. The structure of the nearshore thermal bar system is quite evident in these maps with high concentrations of chlorophyll and suspended sediments essentially ringing the lower basin shoreline. Since each map was generated with processing using a single set of atmospheric and solar geometrical parameters small differences can be observed in the resulting products processed from the same CZCS scene. Case in point are the whole lake and southern Lake Michigan concentration maps, the latter of which shows slightly higher concentrations than the whole lake map for the central lake waters.

Chlorophyll-a pigment concentration values representative of the open lake waters, bays, and other sublake regions are summarized in Table 6.10 along with corresponding values reported in the 1976 Upper Great Lakes Reference Group Study [12].

TABLE 6.10

COMPARISON OF CZCS DERIVED CHLOROPHYLL-A (mg/m^3) PIGMENT CONCENTRATIONS WITH IJC SUMMARY RESULTS

Location	Predicted by CZCS Summer, 1980	IJC/ULRG (12) Circa. 1976
Duluth Area	2.0 - 3.0	2.0
Lake Superior	1.1 - 1.2	0.95
N. Lake Huron	1.2 - 1.4	1.4
North Channel	1.2 - 1.4	1.7
Georgian Bay	1.1	1.2
Saginaw Bay	15.0 -30.0	15.7
S. Lake Huron	1.4	1.4
W. Lake Erie	15.0 -20.0	11.1
C. Lake Erie	1.7 - 3.0	5.5
E. Lake Erie	1.7 - 3.0	4.3
Lake Ontario	5.0	4.8
Lake Michigan	1.4 - 1.7	1.3

IJC ULRG International Joint Commission Upper Lakes Reference Group

These latter values represent summaries of ship gathered chlorophyll data over a several year period of the early seventies. The reported values which can be considered typical of those water bodies are in general remarkably close to the values derived from the CZCS data and especially in the clear low productive waters of the Great Lakes where the summer productivity levels would be expected to change very slowly if at all. In highly productive areas such as Saginaw Bay and the western basin of Lake Erie the reporting of a typical value is more dubious as is the comparison with previous data. The productivity of these latter waters can be expected to change dramatically over a short time.

7.0

CONCLUSIONS

This program to validate the use of CZCS for application to Great Lakes waters has resulted in the development of quantitative algorithms designed to correct the radiometric and geometric distortions which are inherent in the CZCS data sets as made available from NOAA. This study which has been conducted in two separate phases as a data collection and data analysis and algorithm development phase has led to the following set of conclusions and recommendations.

7.1 GENERAL CONCLUSION

The prospects for using satellite data and specifically that from the CZCS to study the Great Lakes ecosystem have been greatly enhanced by the advancements in quantitative methods developed under this study. Changing prospects to realities requires that satellite data be brought to bear on some major problem in the region. The Great Lakes represent large and diverse ecosystems with enormous spatial heterogeneity. Because of the heterogeneity in water and atmospheric optical properties over the Great Lakes, extraction of meaningful chlorophyll and suspended sediment information is considerably more difficult there than in the deep ocean. It is the conclusion of this study that algorithms can be developed to adequately handle the conditions present in the Great Lakes environment although these algorithms will be generally more complex than those which have been developed for the ocean case. Because of limited experimental data the approach taken was to develop a single algorithm for the entire Great Lakes waters. Predicted chlorophyll-a pigment concentrations in the open lake waters of Huron, Michigan, and Superior were comparable to long term average values. On the other hand, concentrations of chlorophyll and suspended mineral were more difficult to predict for the highly turbid and productive waters of Lake Erie, Saginaw Bay, Western Lake Superior. Much of the surface truth data collected on this program was collected in these highly turbid

areas which may have led to large CZCS sampling errors. Most CZCS predicted chlorophyll pigment concentrations were within 0.5 $Log_n[C]$ of the measured values which is consistent with the experience of other investigators [5,6,7]. There are not sufficient data to establish a separate optical model for each lake or sublake region but in situ bio-optical measurements suggested that such a modelling approach would be appropriate. Largest errors in the predicted concentration were found at sampling sites located in or near sediment plumes from tributary discharge. These errors may have resulted from simultaneous sampling of multiple water masses. In this case the CZCS instantaneous field of view is ultimately averaging the upwelling radiance from the plume with that from adjacent waters having less turbidity. Thus inaccuracies in geographical location of any pixel and the large IFOV imply a need for extensive surface sampling where water quality gradients are significant.

7.2 SPECIFIC CONCLUSIONS

1. A geometric correction algorithm was developed based upon a CZCS scanner model and was found to be capable of resampling CZCS pixels to within approximately plus or minus two pixels RMS.

2. A comparison of existing atmospheric correction algorithms with one developed for the Great Lakes showed (a) that significant quantities of radiance are upwelled in the 670 nm band invalidating the possible use of the NOAA algorithms developed for ocean applications, (b) that the residual component method, developed for this project, was able to remove the radiometric effects of haze when those effects are severe. However, under those same severe conditions errors in estimating the upwelling radiance will be larger.

   Under conditions of light haze, Smith and Wilson [5] iterative algorithms, the pseudo optical depth algorithm [6], and the residual component algorithm all appeared capable of removing

haze in CZCS bands 1, 2, and 3. The latter algorithm appears to be able to normalize the severe haze conditions in band 4 as well.

3. A principal component technique was used to extract the necessary scene dependent aerosol optical parameters for each algorithm from the CZCS data minimizing the need for independent ground measurements. The ability of this technique to work is dependent on two basic requirements. First, there must be some water masses in the scene which have low and stable levels of chlorophyll-a pigment concentration. Further, it must be possible to estimate the upwelling radiance for the calibration areas under a variety of illumination conditions. This need can best be satisfied with a combination of upwelling radiance measurements and/or reflectance model calculations. Second, the scene must contain variable concentrations of aerosol haze over the required calibration areas in order to extract the aerosol characteristic vector.

4. Chlorophyll and sediment prediction algorithms were based on a reflectance model developed for the Great Lakes. A two parameter algorithm was found to be necessary to specify both the chlorophyll and suspended mineral concentration from the same extracted upwelling radiance values. These parameters are a CZCS band one to band three ratio and the normalized spectral brightness in bands one and three.

5. Chlorophyll absorption coefficients derived from the NASA/LaRC optical data set were found to be approximately one half of those obtained from the Lake Ontario study. Further, the backscatter coefficients were only about one tenth those obtained by the same study. Chlorophyll absorption and scattering cross sections as obtained by this regression analysis were considerably less than those reported in the

literature [9, 16]. However, most samples included in this analysis were collected from turbid waters where the optical properties are dominated by suspended solids.

6. Simulation studies which described the reflectance space for the Great Lakes optical model suggest that concentrations of chlorophyll-a and suspended sediment are highly correlated to ratios of bands one to four or one to three. A band two to three ratio, on the other hand, offers little sensitivity to the concentration of chlorophyll. This result is somewhat contrary to the marine experiernce where Gordon has suggested that this ratio will prepdict such concentrations in the 1.5 to 20 μg/ℓ range.

Lakes Ontario and Erie as well as Saginaw Bay and Green Bay have high concentrations of dissolved organics (approximate 2.5 mg/ℓ). In these water bodies the influence of dissolved organics on volume reflectance is minimal except for extreme cases. In many parts of Lakes Huron, Superior and Michigan the influence of dissolved organics is pronounced since the concentrations of chlorophyll and suspended sediments are low. For example in central Lake Superior changes in the dissolved organic concentration on the order of 0.2 mg/ℓ would have a very noticeable affect on the upwelling radiance spectra. This conclusion is based upon reflectance model studies and interpretations made of CZCS spectral signatures found in the open clear waters of the upper Great Lakes.

7.3 RECOMMENDATIONS

This study and our assessment of the requirements for Great Lakes monitoring has led to making the following recommendations.

1. In order to refine CZCS algorithms for the Great Lakes a greater body of data are needed on the optical properties of Great Lakes waters. If possible in situ measurements should be

obtained of necessary apparent and inherent absorption and scattering properties. Accuracies of CZCS extracted concentrations may be improved if sub-lake algorithms are implemented.

2. Little is known concerning the spatial and temporal distributions of dissolved organic substance in Great Lakes waters. Since it is known that these substances can influence the upwelling spectra, measurement of dissolved organics should be included in any subsequent investigations which contain a remote sensing element.

3. In the present program the sea truth sampling scheme consisted of detailed sampling at selected points. The scarcity of sea truth values limited our ability to place statistical confidence on much of the results. Future investigations of this type should look at transect and/or array collection schemes.

4. While CZCS appears suitable to monitor whole lake conditions uncertainty remains as to how the CZCS will sample complex coastal waters. The density of supporting sea truth is related to the areal complexity of surface concentrations and the need to describe their spatial relationships. It is difficult, if not impossible, to directly sample complex waters and geographically relate those features to coarse satellite observations. For purposes of understanding more completely how CZCS is averaging these features a study should be made where a high resolution remote sensor (e.g., Landsat-D TM) is used as an immediate stage for sampling.

8.0

REFERENCES

1. Rogers, R., Application of Landsat to the Surveillance of Lake Eutrophication in the Great Lakes Basin, Bendix Aerospace Systems Division, September 1977.

2. Wezernak, C.T., Satellite Remote Sensing Study of the Trans-Boundary Movement of Pollutants, EPA-600/3/-77-056, U.S> Environmental Protection Agency, Duluth, Minnesota, May 1977.

3. Tanis, F.J. and D.R. Lyzenga, Development of Great Lakes Algorithms for the Nimbus-7, Coastal Zone Color Scanner, ERIM Technical Report 150000-11-F, June 1981.

4. Gordon, H.R., J.L. Mueller, andd R.C. Wrigley, Atmospheric Correction of Nimbus-7 Coastal Zone Color Scanner. In Remote Sensing of Atmospheres and Oceans, Deepak, E., Ed., Academic Press, New York, pp. 457-483.

5. Smith, K.C. and W.H. Wilson, Ship and Satellite Bio-Optical Research in the California Bight, Oceanography from Space, J.F.R. Gower, Pleneum Publishing Corporation, 1981, 281-293.

6. Jain, S. An Evaluation of the Atmospheric Correction Algorithms for Nimbus-G Coastal Zone Color Scanner (CZCS), MONITEQ LTD., March 1981.

7. Gordon, H.R., D.K. Clark, J.L. Mueller, and W.A. Hovis, 1980. Phytoplankton Pigments Derived from the Nimbus-7 CZCS: Initial Comparisons with Surface Measurements, Science, 210, 63-66.

8. Gordon, H.R., O.B. Brown, and M.M. Jacobs, Computed Relationships Between Inherent and Apparent Optical Properties of a Flat Homogeneous Ocean, Applied Optics, Vol. 14, p. 417, February 1975.

9. Morel, A.Y. and L. Prieur, Ocean Color Analysis, Limnology and Oceanography, Vol. 22, 709-722, 1977.

10. Whitlock, C. Personal Communication, NASA Langley Research Center, June 1981.

11. Hooke, R. and T. Jeeves, Direct Search Solution of Numerical and Statistical Problems. J. Assoc. Computing Machinery, Vol. 8, 1981, pg. 212.

12. Report to International Joint Commission by the Upper Lakes Reference Group, Waters of Lake Huron and Lake Superior, Vol. 1, Windsor, Ontario, 1976.

13. Sturm, B. Atmospheric Correction of Satellite and Aircraft Remotely Sensed Data in the Visible Spectral Range and Quantitative Determination of Suspended Matter in the Surface Layer of Water Bodies from Remotely Sensed Upwelling Spectral Radiance, JRC, Ispra, Italy, 1980.

14. Hovis, H.R. and K.C. Leung, Optical Engineering, Vol. 16, pg. 157, 1977.

15. Quenzel, H. and M. Kaestner, Optical Properties of the Atmosphere: Calculated Variability and Application to Satellite Remote Sensing of Phytoplankton, Applied Optics, Vol. 19, No. 8, April 1980.

16. Bukata, R.P., et al., Optical Water Quality Model of Lake Ontario 1: Determination of Optical Cross Sections of Organicand Inorganic Particulates in Lake Ontario. Applied Optics, Vol. 20, No. 9, May 1, 1981.

17. Larson, P.L. and C. Jorgensen, Coastal Zone Color Scanner Data Applied for Mapping of the Phytoplankton Pigment Concentration in the North Sea. University of Aalborg Denmark, Technical Report, March 1981.

18. Howarth, R. Personal Communication, U.S. Naval Ocean Systems Center, San Diego, March 1982.

19. Coney, T. Personal Communication, NASA/Lewis Research Center, Cleveland, Ohio, February 1982.

20. Moll, R. Personal Communication, Great Lakes Research, University of Michigan, Ann Arbor, 1983.

21. Turner, R.E. Atmospheric Transformation of Multispectral Remote Sensor Data, ERIM Report NASA CR-135338, November 1977.

22. Elterman, L. Vertical-Attenuation Model with Eight Surface Meteorological Ranges 2 to 13 kilometers, Report No. AFCRL-70-200, Air Force Cambridge Research Laboratories, Office of Aerospace Research, Bedford, Massachusetts, 1970.

23. Lyzenga, D.R. Coastal Remote Sensing Investigations, Vol. 1: Marine Environment, prepared for Office of Naval Research by the Environmental Research Institute of Michigan, Ann Arbor, April 1980.

24. Gordon, H.R. and D.K. Clark, Clear Water Radiances for Correction of Coastal Zone Color Scanner Imagery, Applied Optics, Vol. 20, No. 24, December 1981.

25. Austin, R.W. and T.J. Petzold, The Determination of the Diffuse Attenuation Coefficient of Sea Water Using the Coastal Zone Color Scanner, Paper presented at COSPAR/SCPR/IUCRM Symposium, Oceanography from Space, Venice, Italy 26-29, 1980.

26. Gordon, H.R., Minutes of 19th CZCS NET Meeting, College Station, Texas, May 1982.

27. Gordon, H.R., et al., Phytoplankton Pigment Concentration in the Middle Atlantic Bight: Comparison of Ship Determinations and CZCS Estimates. Applied Optics, Vovl. 22, No. 1, January 1983.

28. Munawar, M. Phytoplankton of Lake Superior - 1973, Journal of Great Lakes Research, Vol. 4, No. 3-4, 1978.

29. Kattawar, G.W., T.J. Humphreys, and G.N. Plass, Radiative Transfer in an Atmosphere-Ocean System: A Matrix Operator Approach, SPIE, Vol. 160, Ocean Optics V, 1978.

30. Smith, R.C. and K.S. Baker, Optical Classification of Natural Waters, Limnology Oceanography, 23, 1978, pp. 260-267.

31. Whitlock, Charles, et al., Comparison of Reflectance with Backscatter and Absorption Parameters for Turbid Waters. Applied Optics, Vol. 20, No. 3, pg. 517, February 1, 1981.

APPENDIX A

MEASURED SEA TRUTH DATA WATER OPTICAL AND QUALITY PARAMETERS

INHERENT WATER OPTICAL PARAMETERS AS MEASURED BY THE NASA LANGLEY MOBILE WATER OPTICAL LABORATORY

This portion of Appendix A contains the NASA Langley Research Center measured optical parameters for eighteen samples as Tables A1 through A28 [10]. Measured optical parameters include:

1. Volume scattering function (theta)
2. Beam attenuation (alpha)
3. Absorption (A)

These measurements were made at eight wavelengths in 50 m increments from 450 nm through 800 nm. The above measurements were made with three separate instruments as described by Whitlock [31]. Three additional samples were collected in Lake Erie for optical analysis, but contained sufficient sediment to make measurement unreliable. Results from Tables A1 through A9, A11, and A18 were used in the regressionn analysis results reported in section 6.1.

TABLE A1

13 July 1980 Lake Erie Rocky River Mouth

THETA	450.	500.	550.	600.	650.	700.	750.	800.
.374	.10631E+04	.92436E+03	.80134E+03	.74986E+03	.69474E+03	.68467E+03	.63945E+03	.60028E+03
.751	.34864E+03	.30170E+03	.27231E+03	.25355E+03	.23646E+03	.22895E+03	.20508E+03	.19609E+03
1.490	.94460E+02	.94242E+02	.35388E+02	.58875E+02	.78649E+02	.72760E+02	.68902E+02	.63061E+02
25.000	.65978E+00	.65779E+00	.62638E+00	.57724E+00	.53343E+00	.54024E+00	.49513E+00	.45741E+00
30.000	.42428E+00	.41434E+00	.37676E+00	.36902E+00	.33291E+00	.34441E+00	.30894E+00	.28668E+00
45.000	.14495E+00	.14066E+00	.12804E+00	.14029E+00	.11129E+00	.11753E+00	.10262E+00	.10016E+00
60.000	.65460E-01	.62503E-01	.59830E-01	.54660E-01	.51746E-01	.52047E-01	.48355E-01	.43204E-01
75.000	.34318E-01	.32632E-01	.31487E-01	.15666E-01	.26807E-01	.28042E-01	.25559E-01	.23005E-01
90.000	.22246E-01	.21814E-01	.19630E-01	.21248E-01	.16737E-01	.17227E-01	.15219E-01	.14467E-01
105.000	.17039E-01	.16746E-01	.15439E-01	.16850E-01	.12921E-01	.13677E-01	.11601E-01	.11569E-01
120.000	.15673E-01	.14968E-01	.13668E-01	.14834E-01	.11607E-01	.12007E-01	.10151E-01	.10710E-01
135.000	.15430E-01	.15067E-01	.13936E-01	.14659E-01	.11782E-01	.12814E-01	.10467E-01	.10379E-01
150.000	.18541E-01	.17774E-01	.16923E-01	.14905E-01	.13957E-01	.14430E-01	.12107E-01	.12465E-01
155.000	.20567E-01	.19939E-01	.17980E-01	.17008E-01	.15842E-01	.16780E-01	.13896E-01	.13336E-01
ALPHA	3.97	3.39	3.07	2.93	2.76	2.83	4.84	4.14
A	.66	.42	.41	.45	.44	.64	2.60	1.95

TABLE A2

14 July 80 Lake Erie West Basin Hydra I, Sample 1

THETA	450.	500.	550.	600.	650.	700.	750.	800.
.374	.84286E+03	.68916E+03	.57597E+03	.48840E+03	.43846E+03	.40974E+03	.36963E+03	.33025E+03
.751	.39291E+03	.32939E+03	.28793E+03	.24181E+03	.21605E+03	.19950E+03	.17695E+03	.16040E+03
1.490	.14126E+03	.13777E+03	.12052E+03	.79363E+02	.10145E+03	.88371E+02	.79488E+02	.71605E+02
25.000	.95193E+00	.95332E+00	.86417E+00	.80714E+00	.72726E+00	.72427E+00	.65819E+00	.58698E+00
30.000	.59165E+00	.59476E+00	.53075E+00	.50418E+00	.44818E+00	.44341E+00	.40249E+00	.38274E+00
45.000	.19528E+00	.19923E+00	.17483E+00	.16775E+00	.15160E+00	.15359E+00	.13904E+00	.13020E+00
60.000	.86911E-01	.85762E-01	.77916E-01	.72861E-01	.65010E-01	.67189E-01	.60323E-01	.54291E-01
75.000	.43697E-01	.43090E-01	.40874E-01	.42811E-01	.34209E-01	.35002E-01	.31334E-01	.29264E-01
90.000	.28202E-01	.27912E-01	.25484E-01	.26758E-01	.21047E-01	.21692E-01	.19038E-01	.19049E-01
105.000	.21691E-01	.21435E-01	.18550E-01	.20351E-01	.16099E-01	.16329E-01	.14529E-01	.14401E-01
120.000	.19374E-01	.19064E-01	.16427E-01	.18523E-01	.14310E-01	.14880E-01	.12901E-01	.12875E-01
135.000	.19580E-01	.18881E-01	.16344E-01	.18903E-01	.14046E-01	.14914E-01	.13340E-01	.12364E-01
150.000	.23691E-01	.22212E-01	.20032E-01	.18872E-01	.16590E-01	.17752E-01	.15584E-01	.14764E-01
155.000	.26010E-01	.24117E-01	.21040E-01	.27527E-01	.18769E-01	.20469E-01	.17547E-01	.18565E-01
ALPHA	5.31	4.67	4.10	3.78	3.51	3.51	5.36	4.49
A	.87	.62	.55	.59	.55	.71	2.65	2.10

TABLE A3

14 July 80 Lake Erie West Basin Hydra I, Sample 2

THETA	450.	500.	550.	600.	650.	700.	750.	800.
.374	.13601E+04	.11673E+04	.10362E+04	.89742E+03	.81562E+03	.80712E+03	.73027E+03	.67879E+03
.751	.50836E+03	.43761E+03	.38099E+03	.33016E+03	.29961E+03	.29382E+03	.26456E+03	.24194E+03
1.490	.15728E+03	.16323E+03	.14560E+03	.98224E+02	.12354E+03	.11397E+03	.10152E+03	.91596E+02
25.000	.71942E+00	.71428E+00	.65451E+00	.61981E+00	.53639E+00	.56257E+00	.49831E+00	.42984E+00
30.000	.46188E+00	.45154E+00	.40225E+00	.38031E+00	.32964E+00	.33490E+00	.31087E+00	.26548E+00
45.000	.16837E+00	.16722E+00	.14362E+00	.15028E+00	.11410E+00	.12237E+00	.11637E+00	.10356E+00
60.000	.71252E-01	.73953E-01	.63920E-01	.59530E-01	.53883E-01	.54504E-01	.47266E-01	.43508E-01
75.000	.37677E-01	.40189E-01	.33313E-01	.40975E-01	.27836E-01	.30262E-01	.26798E-01	.25408E-01
90.000	.24603E-01	.24916E-01	.21463E-01	.22268E-01	.18358E-01	.19436E-01	.17235E-01	.15631E-01
105.000	.18745E-01	.19721E-01	.16603E-01	.19989E-01	.14065E-01	.15656E-01	.12485E-01	.12182E-01
120.000	.17889E-01	.17724E-01	.15341E-01	.16616E-01	.12259E-01	.13305E-01	.12033E-01	.10374E-01
135.000	.17941E-01	.18506E-01	.14782E-01	.16550E-01	.13292E-01	.13289E-01	.13810E-01	.11045E-01
150.000	.22511E-01	.22627E-01	.18682E-01	.18348E-01	.16474E-01	.16807E-01	.15313E-01	.14516E-01
155.000	.25406E-01	.25809E-01	.21549E-01	.25998E-01	.18458E-01	.19417E-01	.16700E-01	.16538E-01
ALPHA	4.95	4.29	3.69	3.55	3.37	3.37	5.27	4.30
A	.73	.51	.44	.53	.45	.68	2.66	2.08

TABLE A4

15 July 80 Lake Erie Cattaraugus Creek Mouth, Sample 1

THETA	450.	500.	550.	600.	650.	700.	750.	800.
.374	.14904E+04	.11816E+04	.97840E+03	.84474E+03	.75714E+03	.76042E+03	.70602E+03	.64614E+03
.751	.69186E+03	.57614E+03	.50081E+03	.44182E+03	.41282E+03	.40498E+03	.36736E+03	.34763E+03
1.490	.22376E+03	.21519E+03	.18963E+03	.13377E+03	.16609E+03	.16000E+03	.14643E+03	.13673E+03
25.000	.19195E+01	.19137E+01	.19031E+01	.17317E+01	.17451E+01	.18793E+01	.16625E+01	.16938E+01
30.000	.12221E+01	.12402E+01	.12056E+01	.10577E+01	.11209E+01	.11311E+01	.10443E+01	.10264E+01
45.000	.43221E+00	.45558E+00	.43669E+00	.42115E+00	.39521E+00	.44337E+00	.36133E+00	.36914E+00
60.000	.20640E+00	.19950E+00	.20033E+00	.17005E+00	.17996E+00	.18512E+00	.15930E+00	.15307E+00
75.000	.10634E+00	.11069E+00	.10284E+00	.10266E+00	.91528E-01	.94658E-01	.88291E-01	.82375E-01
90.000	.69724E-01	.70821E-01	.67639E-01	.65192E-01	.57378E-01	.60793E-01	.53748E-01	.50291E-01
105.000	.53185E-01	.52992E-01	.51487E-01	.47080E-01	.43501E-01	.45100E-01	.40456E-01	.40693E-01
120.000	.47092E-01	.45779E-01	.43054E-01	.42612E-01	.38020E-01	.38689E-01	.34007E-01	.34623E-01
135.000	.45653E-01	.43440E-01	.42888E-01	.40876E-01	.37728E-01	.36706E-01	.33324E-01	.34906E-01
150.000	.52232E-01	.50008E-01	.46516E-01	.39162E-01	.42501E-01	.43251E-01	.37441E-01	.38413E-01
155.000	.59437E-01	.56044E-01	.51522E-01	.42541E-01	.48563E-01	.45309E-01	.41743E-01	.42034E-01
ALPHA	9.76	9.11	7.96	8.07	7.54	7.19	9.10	8.29
A	1.40	1.12	1.04	1.07	1.03	1.22	3.04	2.47

TABLE A5

15 July 80 Lake Erie Cattaraugus Creek, Sample 2

THETA	450.	500.	550.	600.	650.	700.	750.	800.
.374	.10341E+04	.85215E+03	.72409E+03	.62661E+03	.55149E+03	.53595E+03	.50430E+03	.50670E+03
.751	.39347E+03	.33872E+03	.30097E+03	.27461E+03	.25341E+03	.24058E+03	.22208E+03	.21347E+03
1.490	.10907E+03	.10765E+03	.96322E+02	.64644E+02	.87489E+02	.82990E+02	.77824E+02	.74965E+02
25.000	.87863E+00	.90356E+00	.85700E+00	.81420E+00	.75353E+00	.77364E+00	.74174E+00	.67473E+00
30.000	.58427E+00	.54566E+00	.52556E+00	.51159E+00	.48795E+00	.49214E+00	.46866E+00	.42399E+00
45.000	.20574E+00	.20420E+00	.18865E+00	.20696E+00	.16480E+00	.17417E+00	.15751E+00	.14392E+00
60.000	.96029E-01	.95991E-01	.87501E-01	.84970E-01	.77167E-01	.77780E-01	.72054E-01	.70046E-01
75.000	.51807E-01	.48915E-01	.50300E-01	.50312E-01	.40725E-01	.40564E-01	.38092E-01	.35441E-01
90.000	.32572E-01	.33086E-01	.27919E-01	.33676E-01	.25476E-01	.26893E-01	.24344E-01	.22949E-01
105.000	.25320E-01	.26050E-01	.22258E-01	.23811E-01	.20463E-01	.19842E-01	.20164E-01	.18428E-01
120.000	.22231E-01	.21607E-01	.20585E-01	.22069E-01	.16273E-01	.17847E-01	.16019E-01	.14242E-01
135.000	.21757E-01	.20940E-01	.21704E-01	.20619E-01	.16914E-01	.17266E-01	.16534E-01	.15729E-01
150.000	.24105E-01	.24911E-01	.22662E-01	.21260E-01	.19511E-01	.19955E-01	.18408E-01	.19737E-01
155.000	.28061E-01	.27240E-01	.23818E-01	.26432E-01	.22177E-01	.23229E-01	.21059E-01	.20439E-01
ALPHA	4.03	3.38	2.93	2.81	2.79	2.95	5.03	4.02
A	.79	.70	.71	.68	.64	.85	2.83	2.17

TABLE A6

16 July 80 Lake Erie, North Shore, Sample 1

THETA	450.	500.	550.	600.	650.	700.	750.	800.
.374	.62908E+03	.50486E+03	.42355E+03	.36887E+03	.32545E+03	.31823E+03	.28240E+03	.27189E+03
.751	.33454E+03	.27184E+03	.22966E+03	.20041E+03	.18062E+03	.16921E+03	.15355E+03	.14184E+03
1.490	.13819E+03	.12755E+03	.10865E+03	.69634E+02	.88721E+02	.80420E+02	.73144E+02	.67000E+02
25.000	.17968E+01	.17461E+01	.16733E+01	.13834E+01	.14647E+01	.14795E+01	.13038E+01	.11944E+01
30.000	.11458E+01	.10773E+01	.10434E+01	.85150E+00	.90749E+00	.89328E+00	.83131E+00	.74715E+00
45.000	.38841E+00	.36112E+00	.35207E+00	.32529E+00	.30420E+00	.30147E+00	.28155E+00	.25859E+00
60.000	.17347E+00	.16816E+00	.14610E+00	.12315E+00	.12854E+00	.13652E+00	.11898E+00	.11134E+00
75.000	.87231E-01	.84438E-01	.84269E-01	.80924E-01	.67471E-01	.73253E-01	.61073E-01	.58474E-01
90.000	.59533E-01	.55337E-01	.51449E-01	.49589E-01	.42905E-01	.42817E-01	.38940E-01	.37047E-01
105.000	.43983E-01	.39965E-01	.37426E-01	.36807E-01	.33296E-01	.34136E-01	.29226E-01	.27673E-01
120.000	.40227E-01	.36576E-01	.34103E-01	.34200E-01	.28756E-01	.29754E-01	.25111E-01	.25020E-01
135.000	.37560E-01	.36782E-01	.33000E-01	.32162E-01	.28239E-01	.29885E-01	.23874E-01	.24288E-01
150.000	.43226E-01	.39814E-01	.36415E-01	.30123E-01	.30613E-01	.31540E-01	.27151E-01	.27058E-01
155.000	.46819E-01	.42584E-01	.37082E-01	.32538E-01	.32594E-01	.31710E-01	.27961E-01	.28770E-01
ALPHA	7.40	6.71	5.60	5.23	4.89	4.79	6.59	5.71
A	1.10	.86	.88	.93	.85	1.03	2.93	2.22

TABLE A7

16 July 80 Lake Erie, North Shore, Sample 2

THETA	450.	500.	550.	600.	650.	700.	750.	800.
.374	.79786E+03	.64079E+03	.52884E+03	.45708E+03	.40844E+03	.38503E+03	.33993E+03	.32008E+03
.751	.48944E+03	.39697E+03	.33035E+03	.28863E+03	.25870E+03	.24358E+03	.21553E+03	.19468E+03
1.490	.20327E+03	.19366E+03	.16466E+03	.10885E+03	.13333E+03	.12576E+03	.11238E+03	.10122E+03
25.000	.27498E+01	.25530E+01	.24583E+01	.20395E+01	.20921E+01	.20641E+01	.18317E+01	.17105E+01
30.000	.17653E+01	.16823E+01	.15291E+01	.12767E+01	.13103E+01	.12757E+01	.11725E+01	.10726E+01
45.000	.59017E+00	.54699E+00	.50713E+00	.46290E+00	.46375E+00	.43822E+00	.38374E+00	.37257E+00
60.000	.26454E+00	.24927E+00	.22862E+00	.18892E+00	.19661E+00	.19970E+00	.17104E+00	.16581E+00
75.000	.13594E+00	.13111E+00	.11198E+00	.11230E+00	.99788E-01	.10593E+00	.89019E-01	.84375E-01
90.000	.89717E-01	.80542E-01	.77900E-01	.70351E-01	.65744E-01	.64873E-01	.55425E-01	.53191E-01
105.000	.66744E-01	.62425E-01	.54330E-01	.52897E-01	.47669E-01	.48786E-01	.42698E-01	.43366E-01
120.000	.59197E-01	.55100E-01	.50981E-01	.49947E-01	.41113E-01	.44192E-01	.37181E-01	.35933E-01
135.000	.57845E-01	.52221E-01	.48471E-01	.47325E-01	.40664E-01	.42309E-01	.37617E-01	.36088E-01
150.000	.66437E-01	.58313E-01	.54039E-01	.46616E-01	.46270E-01	.48372E-01	.43124E-01	.41605E-01
155.000	.72669E-01	.65480E-01	.56772E-01	.48857E-01	.50060E-01	.51954E-01	.47734E-01	.44415E-01
ALPHA	11.95	10.58	9.12	8.27	7.62	7.16	8.77	7.62
A	1.41	1.22	1.15	1.21	1.12	1.36	3.28	2.56

TABLE A8

17 July 80 Lake Erie, West Basin, Hydra II, Sample 1

THETA	450.	500.	550.	600.	650.	700.	750.	800.
.374	.10653E+04	.93676E+03	.83398E+03	.76660E+03	.72612E+03	.72551E+03	.65740E+03	.64337E+03
.751	.62430E+03	.54740E+03	.49137E+03	.44529E+03	.41519E+03	.41136E+03	.37119E+03	.35470E+03
1.490	.27523E+03	.27689E+03	.24700E+03	.17757E+03	.21884E+03	.20967E+03	.18914E+03	.17757E+03
25.000	.52313E+01	.47662E+01	.51052E+01	.57008E+01	.43552E+01	.45593E+01	.39521E+01	.36413E+01
30.000	.33593E+01	.29618E+01	.31910E+01	.36625E+01	.27765E+01	.28976E+01	.25191E+01	.24301E+01
45.000	.11807E+01	.11142E+01	.11260E+01	.14126E+01	.98604E+00	.10246E+01	.90618E+00	.80768E+00
60.000	.54489E+00	.50012E+00	.49759E+00	.55552E+00	.44015E+00	.45305E+00	.38392E+00	.36274E+00
75.000	.28557E+00	.26425E+00	.26196E+00	.32496E+00	.22188E+00	.24217E+00	.20221E+00	.19086E+00
90.000	.18134E+00	.16732E+00	.16930E+00	.20430E+00	.13569E+00	.14974E+00	.12745E+00	.11761E+00
105.000	.13732E+00	.12752E+00	.12573E+00	.15446E+00	.10364E+00	.11202E+00	.94545E-01	.88172E-01
120.000	.12329E+00	.11084E+00	.11241E+00	.13812E+00	.95373E-01	.99116E-01	.83933E-01	.78016E-01
135.000	.12151E+00	.11115E+00	.11114E+00	.13720E+00	.92855E-01	.10165E+00	.85435E-01	.82360E-01
150.000	.14906E+00	.13496E+00	.13451E+00	.13467E+00	.11674E+00	.12114E+00	.10518E+00	.95493E-01
155.000	.17513E+00	.15429E+00	.15551E+00	.15426E+00	.14279E+00	.14485E+00	.12351E+00	.11718E+00
ALPHA	25.68	23.21	20.84	18.68	17.04	15.13	16.03	14.51
A	2.68	2.12	1.79	1.83	1.75	1.94	3.45	2.87

TABLE A9

17 July 80 Lake Erie, West Basin, Hydra II, Sample 2

THETA	450.	500.	550.	600.	650.	700.	750.	800.
.374	.92783E+03	.78550E+03	.68419E+03	.60534E+03	.54106E+03	.51603E+03	.45759E+03	.41383E+03
.751	.41397E+03	.34273E+03	.29610E+03	.25248E+03	.22596E+03	.21128E+03	.19163E+03	.17407E+03
1.490	.14607E+03	.14157E+03	.12318E+03	.80255E+02	.10130E+03	.91548E+02	.82566E+02	.72998E+02
25.000	.88816E+00	.91494E+00	.83380E+00	.77860E+00	.69573E+00	.69882E+00	.61751E+00	.61903E+00
30.000	.57638E+00	.57713E+00	.52082E+00	.48293E+00	.44665E+00	.44450E+00	.39420E+00	.35606E+00
45.000	.19162E+00	.19413E+00	.17790E+00	.16724E+00	.15389E+00	.15644E+00	.13652E+00	.12906E+00
60.000	.95550E-01	.86588E-01	.78608E-01	.73854E-01	.68280E-01	.66586E-01	.58954E-01	.53961E-01
75.000	.42630E-01	.45386E-01	.41743E-01	.44343E-01	.34867E-01	.35373E-01	.32243E-01	.29573E-01
90.000	.27703E-01	.29336E-01	.25511E-01	.27649E-01	.21861E-01	.22274E-01	.19530E-01	.18559E-01
105.000	.22616E-01	.21944E-01	.19443E-01	.20894E-01	.16315E-01	.17153E-01	.14886E-01	.13725E-01
120.000	.19726E-01	.20018E-01	.17576E-01	.19154E-01	.14758E-01	.15630E-01	.13184E-01	.12701E-01
135.000	.19705E-01	.20214E-01	.17891E-01	.19970E-01	.14769E-01	.15299E-01	.13789E-01	.12616E-01
150.000	.24011E-01	.23694E-01	.21725E-01	.20301E-01	.17324E-01	.19057E-01	.16259E-01	.15780E-01
155.000	.28724E-01	.27733E-01	.25182E-01	.29308E-01	.21067E-01	.22866E-01	.20516E-01	.17193E-01
ALPHA	4.93	4.28	3.76	3.45	3.34	3.28	5.13	4.33
A	.77	.51	.52	.52	.48	.64	2.70	1.97

TABLE A10

21 July 80 Lake Michigan, Green Bay

THETA	450.	500.	550.	600.	650.	700.	750.	800.
.374	.11468E+04	.93445E+03	.97850E+03	.87821E+03	.85903E+03	.79198E+03	.83265E+03	.73316E+03
.751	.41313E+03	.36954E+03	.33265E+03	.29079E+03	.27120E+03	.25932E+03	.24797E+03	.24109E+03
1.490	.10005E+03	.10368E+03	.91170E+02	.60298E+02	.85043E+02	.77635E+02	.74630E+02	.43707E+02
25.000	.39976E+00	.39854E+00	.36454E+00	.36827E+00	.30656E+00	.32961E+00	.29311E+00	.28834E+00
30.000	.24760E+00	.25276E+00	.23430E+00	.21549E+00	.20107E+00	.21372E+00	.18255E+00	.17990E+00
45.000	.83821E-01	.87207E-01	.82193E-01	.86240E-01	.70180E-01	.72275E-01	.73937E-01	.68306E-01
60.000	.37549E-01	.39578E-01	.35535E-01	.31840E-01	.30928E-01	.38219E-01	.31412E-01	.32511E-01
75.000	.19191E-01	.20978E-01	.19943E-01	.22014E-01	.18405E-01	.20544E-01	.18245E-01	.16320E-01
90.000	.13777E-01	.14612E-01	.13403E-01	.13868E-01	.10874E-01	.12263E-01	.10808E-01	.10172E-01
105.000	.11480E-01	.10172E-01	.11065E-01	.98883E-02	.78435E-02	.82285E-02	.85302E-02	.10101E-01
120.000	.96126E-02	.93388E-02	.94868E-02	.10943E-01	.71758E-02	.80313E-02	.65482E-02	.72074E-02
135.000	.93916E-02	.98628E-02	.86898E-02	.88890E-02	.77484E-02	.98866E-02	.67051E-02	.79641E-02
150.000	.11764E-01	.11786E-01	.10843E-01	.10655E-01	.93507E-02	.10094E-01	.97899E-02	.10555E-01
155.000	.13931E-01	.14502E-01	.13717E-01	.11955E-01	.13426E-01	.13038E-01	.11645E-01	.11622E-01
ALPHA	3.93	3.42	2.97	2.80	2.68	2.71	4.84	3.88
A	.71	.33	.29	.29	.26	.41	2.38	1.81

TABLE A11

21 July 80 Lake Michigan, Grand Haven, Sample 1

THETA	450.	500.	550.	600.	650.	700.	750.	800.
.374	.28487E+04	.23548E+04	.20596E+04	.19050E+04	.18473E+04	.17212E+04	.15695E+04	.14407E+04
.751	.10567E+04	.96138E+03	.88238E+03	.85680E+03	.84002E+03	.79393E+03	.75977E+03	.75319E+03
1.490	.27353E+03	.27656E+03	.25361E+03	.18787E+03	.24144E+03	.24046E+03	.23920E+03	.24330E+03
25.000	.16046E+01	.17798E+01	.17767E+01	.16795E+01	.15500E+01	.16526E+01	.14319E+01	.13016E+01
30.000	.10207E+01	.10859E+01	.10954E+01	.10451E+01	.93256E+00	.10105E+01	.91485E+00	.82433E+00
45.000	.33140E+00	.34866E+00	.35147E+00	.38413E+00	.30932E+00	.34427E+00	.31264E+00	.28007E+00
60.000	.14224E+00	.15510E+00	.15557E+00	.15053E+00	.13410E+00	.14711E+00	.13033E+00	.11947E+00
75.000	.75335E-01	.82394E-01	.79596E-01	.87453E-01	.69411E-01	.77885E-01	.68578E-01	.61184E-01
90.000	.48497E-01	.51567E-01	.49524E-01	.56076E-01	.42071E-01	.46157E-01	.41719E-01	.37285E-01
105.000	.36184E-01	.38813E-01	.37059E-01	.41042E-01	.31978E-01	.34408E-01	.30923E-01	.28268E-01
120.000	.32892E-01	.34818E-01	.32829E-01	.36911E-01	.27769E-01	.30427E-01	.27033E-01	.24647E-01
135.000	.32239E-01	.34570E-01	.33302E-01	.35892E-01	.28644E-01	.31572E-01	.27599E-01	.24545E-01
150.000	.42173E-01	.46364E-01	.43059E-01	.41749E-01	.36730E-01	.42181E-01	.37676E-01	.36356E-01
155.000	.51789E-01	.54826E-01	.53593E-01	.65595E-01	.44043E-01	.52846E-01	.48554E-01	.46774E-01
ALPHA	13.66	12.33	10.78	10.00	9.35	9.08	10.90	9.91
A	2.89	2.06	1.46	1.37	1.35	1.47	2.94	2.37

TABLE A12

22 July 80 Lake Michigan, Grand Haven, Sample 2

THETA	450.	500.	550.	600.	650.	700.	750.	800.
.374	.76155E+03	.63912E+03	.55004E+03	.50416E+03	.45950E+03	.44526E+03	.42965E+03	.40854E+03
.751	.27900E+03	.24269E+03	.21808E+03	.19987E+03	.18331E+03	.17575E+03	.16537E+03	.15413E+03
1.490	.73513E+02	.74561E+02	.67882E+02	.45988E+02	.65213E+02	.58150E+02	.56277E+02	.52024E+02
25.000	.26787E+00	.26440E+00	.24653E+00	.23981E+00	.21704E+00	.22895E+00	.20132E+00	.19717E+00
30.000	.17052E+00	.16185E+00	.15344E+00	.14070E+00	.12782E+00	.13199E+00	.11803E+00	.11282E+00
45.000	.51244E-01	.52323E-01	.46725E-01	.54094E-01	.42781E-01	.44631E-01	.37663E-01	.38149E-01
60.000	.21574E-01	.21659E-01	.20003E-01	.19511E-01	.17735E-01	.19083E-01	.16389E-01	.14979E-01
75.000	.11249E-01	.11110E-01	.10492E-01	.11730E-01	.90298E-02	.94405E-02	.79551E-02	.79363E-02
90.000	.77595E-02	.73056E-02	.65056E-02	.69956E-02	.56550E-02	.58358E-02	.50131E-02	.47326E-02
105.000	.59337E-02	.56040E-02	.49427E-02	.52413E-02	.41974E-02	.42012E-02	.38490E-02	.38844E-02
120.000	.54526E-02	.50345E-02	.44021E-02	.49887E-02	.42978E-02	.38935E-02	.35849E-02	.34426E-02
135.000	.55300E-02	.52468E-02	.48388E-02	.51740E-02	.40648E-02	.41894E-02	.36529E-02	.36098E-02
150.000	.81557E-02	.77926E-02	.73216E-02	.68568E-02	.66714E-02	.64169E-02	.58475E-02	.58356E-02
155.000	.10660E-01	.10317E-01	.98170E-02	.11345E-01	.82566E-02	.85604E-02	.73838E-02	.77796E-02
ALPHA	2.37	2.01	1.83	1.80	1.90	1.94	3.98	3.58
A	.11	.07	.11	.22	.15	.38	2.38	1.74

TABLE A13

22 July 80 Lake Michigan, Grand Haven, Sample 3

THETA	450.	500.	550.	600.	650.	700.	750.	800.
.374	.47144E+03	.39608E+03	.34492E+03	.31732E+03	.27966E+03	.27103E+03	.24921E+03	.25640E+03
.751	.17451E+03	.15299E+03	.13888E+03	.12830E+03	.12193E+03	.11542E+03	.10773E+03	.10175E+03
1.490	.42869E+02	.44359E+02	.40376E+02	.26221E+02	.42270E+02	.35902E+02	.34975E+02	.32791E+02
25.000	.14120E+00	.13567E+00	.12321E+00	.10735E+00	.10867E+00	.11749E+00	.97153E-01	.10478E+00
30.000	.84576E-01	.80417E-01	.80038E-01	.64862E-01	.67552E-01	.69284E-01	.60261E-01	.60425E-01
45.000	.26736E-01	.27863E-01	.24402E-01	.21678E-01	.22586E-01	.22720E-01	.19844E-01	.19025E-01
60.000	.12041E-01	.10980E-01	.10811E-01	.91009E-02	.91188E-02	.11089E-01	.78746E-02	.98865E-02
75.000	.63186E-02	.60905E-02	.57238E-02	.49583E-02	.46774E-02	.50865E-02	.42792E-02	.47696E-02
90.000	.40203E-02	.38361E-02	.36339E-02	.33819E-02	.29912E-02	.29246E-02	.25993E-02	.28790E-02
105.000	.33538E-02	.29987E-02	.26960E-02	.24261E-02	.25402E-02	.22728E-02	.19997E-02	.21144E-02
120.000	.35470E-02	.29192E-02	.26971E-02	.23854E-02	.23363E-02	.21824E-02	.17628E-02	.21041E-02
135.000	.37215E-02	.32907E-02	.30191E-02	.26705E-02	.23981E-02	.25992E-02	.23282E-02	.23929E-02
150.000	.57833E-02	.51445E-02	.47985E-02	.36875E-02	.38261E-02	.38389E-02	.34068E-02	.38674E-02
155.000	.73600E-02	.68552E-02	.65961E-02	.63296E-02	.54646E-02	.55489E-02	.50947E-02	.53968E-02
ALPHA	1.29	1.10	.98	1.07	1.11	1.31	3.36	2.37
A	.01	.01	.03	.11	.07	.31	2.33	1.77

TABLE A14

July 80 Lake Michigan, Grand Haven, Sample 4

THETA	450.	500.	550.	600.	650.	700.	750.	800.
.374	.59069E+03	.46033E+03	.41888E+03	.39652E+03	.35222E+03	.32521E+03	.29248E+03	.28800E+03
.751	.19853E+03	.16760E+03	.16094E+03	.15008E+03	.14593E+03	.13767E+03	.12236E+03	.11523E+03
1.490	.47608E+02	.48884E+02	.44825E+02	.29303E+02	.44590E+02	.39497E+02	.40692E+02	.37379E+02
25.000	.24039E+00	.24463E+00	.23214E+00	.18155E+00	.19505E+00	.20785E+00	.18098E+00	.16995E+00
30.000	.14631E+00	.14784E+00	.13537E+00	.11413E+00	.11914E+00	.12389E+00	.11453E+00	.10543E+00
45.000	.45103E-01	.46211E-01	.43762E-01	.40876E-01	.37943E-01	.38243E-01	.36292E-01	.34572E-01
60.000	.18959E-01	.18616E-01	.17416E-01	.14509E-01	.15299E-01	.17382E-01	.14458E-01	.15497E-01
75.000	.97918E-02	.96664E-02	.91571E-02	.84257E-02	.76061E-02	.82411E-02	.73759E-02	.83961E-02
90.000	.60440E-02	.60921E-02	.55314E-02	.50982E-02	.47274E-02	.49941E-02	.46420E-02	.55972E-02
105.000	.48575E-02	.47550E-02	.41231E-02	.38731E-02	.36569E-02	.40932E-02	.37223E-02	.48355E-02
120.000	.44966E-02	.44296E-02	.38497E-02	.37065E-02	.33408E-02	.35642E-02	.34140E-02	.46756E-02
135.000	.50694E-02	.49688E-02	.41736E-02	.37573E-02	.35646E-02	.38221E-02	.33213E-02	.42062E-02
150.000	.70822E-02	.66554E-02	.55838E-02	.36447E-02	.52344E-02	.54830E-02	.47207E-02	.51144E-02
155.000	.91054E-02	.88841E-02	.74272E-02	.88773E-02	.72318E-02	.75743E-02	.67671E-02	.70631E-02
ALPHA	2.06	1.82	1.60	1.61	1.64	1.79	3.78	3.21
A	.03	.00	.03	.15	.07	.30	2.26	1.87

TABLE A15

23 July 80 Lake Michigan, Grand Haven, Sample 5

THETA	450.	500.	550.	600.	650.	700.	750.	800.
.374	.22027E+04	.18708E+04	.16868E+04	.14522E+04	.13403E+04	.12887E+04	.11779E+04	.11467E+04
.751	.76332E+03	.68133E+03	.64823E+03	.62705E+03	.60331E+03	.59043E+03	.55546E+03	.54680E+03
1.490	.18234E+03	.16731E+03	.17293E+03	.12613E+03	.16544E+03	.16597E+03	.16005E+03	.15785E+03
25.000	.90060E+00	.98547E+00	.97707E+00	.93070E+00	.83820E+00	.88015E+00	.85099E+00	.78598E+00
30.000	.57137E+00	.60474E+00	.58990E+00	.55579E+00	.51276E+00	.55633E+00	.51650E+00	.51704E+00
45.000	.17852E+00	.19744E+00	.19167E+00	.20428E+00	.16569E+00	.17551E+00	.16564E+00	.15363E+00
60.000	.77035E-01	.83946E-01	.79580E-01	.78531E-01	.69934E-01	.74223E-01	.69869E-01	.69346E-01
75.000	.40508E-01	.43687E-01	.40289E-01	.44812E-01	.34941E-01	.38698E-01	.17940E-01	.32870E-01
90.000	.24795E-01	.26473E-01	.24877E-01	.26583E-01	.21626E-01	.23568E-01	.20143E-01	.20266E-01
105.000	.19019E-01	.19780E-01	.18240E-01	.20419E-01	.15942E-01	.16522E-01	.15408E-01	.15631E-01
120.000	.16672E-01	.17696E-01	.15740E-01	.18226E-01	.13911E-01	.14674E-01	.13130E-01	.13438E-01
135.000	.17762E-01	.18426E-01	.17970E-01	.19028E-01	.14725E-01	.15681E-01	.14221E-01	.14104E-01
150.000	.23033E-01	.24839E-01	.22979E-01	.22623E-01	.19622E-01	.20706E-01	.18072E-01	.16744E-01
155.000	.32259E-01	.31324E-01	.29704E-01	.38151E-01	.26430E-01	.29102E-01	.25336E-01	.24933E-01
ALPHA	7.35	6.75	6.35	5.95	5.80	5.74	7.52	6.79
A	1.46	.97	.75	.76	.73	.88	2.66	2.16

TABLE A16

24 July 80 Lake Superior, Duluth, Sample 1

THETA	450.	500.	550.	600.	650.	700.	750.	800.
.374	.70926E+03	.56742E+03	.46247E+03	.40671E+03	.36041E+03	.34623E+03	.30575E+03	.27[illegible]E+03
.751	.32187E+03	.26361E+03	.22217E+03	.19209E+03	.17419E+03	.16363E+03	.14503E+03	.13[illegible]E+03
1.490	.11302E+03	.10362E+03	.87252E+02	.57000E+02	.74361E+02	.66P93E+02	.61239E+02	.5[illegible]E+02
25.000	.16626E+01	.16342E+01	.14440E+01	.11647E+01	.12225E+01	.11546E+01	.99010E+00	.9[illegible]E+00
30.000	.11369E+01	.10419E+01	.99040E+00	.79037E+00	.81485E+00	.77051E+00	.64386E+00	.61[illegible]E+00
45.000	.43268E+00	.39841E+00	.37670E+00	.35738E+00	.31465E+00	.30236E+00	.25866E+00	.24901E+00
60.000	.19708E+00	.19717E+00	.18351E+00	.15456E+00	.14930E+00	.14110E+00	.12295E+00	.12[illegible]E+00
75.000	.10705E+00	.10495E+00	.10085E+00	.97015E-01	.86201E-01	.79959E-01	.71166E-01	.66[illegible]E-01
90.000	.72026E-01	.68559E-01	.65361E-01	.65291E-01	.55604E-01	.53924E-01	.45189E-01	.42[illegible]E-01
105.000	.55193E-01	.55235E-01	.53260E-01	.50129E-01	.42438E-01	.42653E-01	.35160E-01	.3[illegible]E-01
120.000	.50407E-01	.49095E-01	.45733E-01	.44632E-01	.39865E-01	.38323E-01	.31405E-01	.29777E-01
135.000	.48584E-01	.48376E-01	.45764E-01	.43445E-01	.38554E-01	.36560E-01	.30772E-01	.28013E-01
150.000	.57928E-01	.55675E-01	.50330E-01	.42213E-01	.42191E-01	.40837E-01	.34947E-01	.32712E-01
155.000	.68334E-01	.60870E-01	.57753E-01	.49242E-01	.48352E-01	.46165E-01	.39099E-01	.37[illegible]E-01
ALPHA	7.98	6.34	5.14	4.47	4.09	4.03	5.79	[illegible]
A	2.44	1.66	1.31	1.11	1.01	1.09	2.87	2.43

TABLE A17

24 July 80 Lake Superior, Duluth, Sample 2

THETA	450.	500.	550.	600.	650.	700.	750.	800.
.374	.49825E+03	.40526E+03	.31356E+03	.26430E+03	.22713E+03	.21234E+03	.18909E+03	.17932E+03
.751	.23959E+03	.18711E+03	.15367E+03	.13802E+03	.12188E+03	.11474E+03	.10666E+03	.95282E+02
1.490	.79435E+02	.72533E+02	.59921E+02	.36478E+02	.50500E+02	.44637E+02	.42769E+02	.38900E+02
25.000	.10153E+01	.98686E+00	.88417E+00	.78455E+00	.70084E+00	.67888E+00	.59195E+00	.53175E+00
30.000	.66156E+00	.65393E+00	.58921E+00	.53847E+00	.48541E+00	.45635E+00	.39700E+00	.35642E+00
45.000	.24795E+00	.24168E+00	.22297E+00	.24054E+00	.18436E+00	.17565E+00	.15455E+00	.13752E+00
60.000	.11200E+00	.11684E+00	.10328E+00	.99449E-01	.88046E-01	.83053E-01	.71419E-01	.68165E-01
75.000	.61546E-01	.63468E-01	.58669E-01	.63804E-01	.47234E-01	.49161E-01	.41272E-01	.35545E-01
90.000	.40937E-01	.42587E-01	.38526E-01	.41263E-01	.31196E-01	.30863E-01	.26747E-01	.24065E-01
105.000	.31644E-01	.33091E-01	.30744E-01	.33098E-01	.24990E-01	.23865E-01	.20489E-01	.19416E-01
120.000	.29028E-01	.29569E-01	.27331E-01	.29772E-01	.22805E-01	.22158E-01	.18578E-01	.17127E-01
135.000	.28732E-01	.29791E-01	.26794E-01	.28714E-01	.22055E-01	.21965E-01	.18422E-01	.17495E-01
150.000	.34432E-01	.34412E-01	.30017E-01	.28922E-01	.24833E-01	.25360E-01	.22176E-01	.21484E-01
155.000	.41570E-01	.40852E-01	.35754E-01	.35510E-01	.30852E-01	.29641E-01	.26579E-01	.25120E-01
ALPHA	4.95	4.14	3.50	3.18	2.95	2.80	4.68	3.91
A	1.23	.81	.68	.65	.55	.74	2.67	1.99

TALBE A18

25 July 80 Lake Michigan, Grand Haven, Sample 6

THETA	450.	500.	550.	600.	650.	700.	750.	800.
.374	.26799E+04	.22461E+04	.19285E+04	.16363E+04	.14481E+04	.13514E+04	.12137E+04	.12100E+04
.751	.81170E+03	.75821E+03	.73531E+03	.70413E+03	.67464E+03	.64671E+03	.62882E+03	.64378E+03
1.490	.19012E+03	.19646E+03	.18411E+03	.13448E+03	.17529E+03	.17269E+03	.17243E+03	.17736E+03
25.000	.85222E+00	.96765E+00	.94888E+00	.88515E+00	.82631E+00	.90911E+00	.80790E+00	.79016E+00
30.000	.52773E+00	.58723E+00	.57403E+00	.53036E+00	.50680E+00	.55230E+00	.50784E+00	.50286E+00
45.000	.16151E+00	.18802E+00	.18361E+00	.19318E+00	.16039E+00	.17843E+00	.16085E+00	.15557E+00
60.000	.69744E-01	.80483E-01	.75782E-01	.71223E-01	.67263E-01	.71795E-01	.67904E-01	.67768E-01
75.000	.36318E-01	.40019E-01	.38288E-01	.41853E-01	.33791E-01	.37217E-01	.33416E-01	.33137E-01
90.000	.22869E-01	.24612E-01	.24123E-01	.24755E-01	.20108E-01	.22166E-01	.20398E-01	.19688E-01
105.000	.17993E-01	.18345E-01	.17251E-01	.18227E-01	.14829E-01	.16668E-01	.14621E-01	.14943E-01
120.000	.15548E-01	.16209E-01	.17576E-01	.17102E-01	.13114E-01	.14489E-01	.12680E-01	.12771E-01
135.000	.16460E-01	.16880E-01	.16016E-01	.17238E-01	.13805E-01	.15177E-01	.13805E-01	.13394E-01
150.000	.21375E-01	.22069E-01	.21392E-01	.20826E-01	.17700E-01	.19997E-01	.17439E-01	.17380E-01
155.000	.28562E-01	.27026E-01	.27069E-01	.35789E-01	.23180E-01	.25912E-01	.21409E-01	.23817E-01
ALPHA	8.28	7.50	6.90	6.50	6.33	6.36	8.27	7.58
A	1.80	1.17	.80	.80	.80	.92	2.59	2.21

NASA SEA TRUTH SAMPLING DATA

This portion of Appendix A contains sea truth sampling data as collected and analyzed by the University of Michigan Research Center for the Great Lakes [20]. Parameters measured include:

Physical: Secchi depth, sample temperature, wave height, wind speed, wind direction, water color, sky color, and cloud cover.

Biochemical: Chlorophyll pigments (A, A2, B, and C), Phaeophytins, filter residue (total, ashed, volatile), and particulate organics as carbon, hydrogen and nitrogen fractions.

These data are reported in Tables A19 through A32.

TABLE A19

NASA SEA TRUTH SAMPLING DATA																
SAMPLE NUMBER	DATE	SECCHI DEPTH	SURFACE TEMP. (°C)	SAMPLE DEPTH (m)	TEMP @ SAMPLE DEPTH	CHLOROPHYLL (mg/m³) A	A2	B	C	PHAEOPH (mg/m³)	RESIDUE (mg/l) TOTAL	ASHED	VOLAT	CHN DATA (mg/l) C	H	N
1001	MAY 22	1.3	17.8	0.5	17.8	8.88	5.13	0.00	1.70	2.32	3.62	2.03	1.59	0.61	0.14	0.07
1002				1.0	18.0	10.51	6.47	0.31	2.92	2.14	3.32	1.92	1.40	0.62	0.12	0.07
1003				2.0	17.2	14.07	9.87	1.13	5.44	0.90	4.62	2.87	1.75	0.64	0.13	0.08
1004				0.5	17.8	11.58	7.82	0.34	4.59	1.20	3.94	2.37	1.57	0.62	0.12	0.09
1005				1.0	18.0	11.22	7.43	0.31	4.54	1.40	3.89	2.35	1.54	0.58	0.11	0.15
1006				2.0	17.2	14.74	9.68	0.71	6.46	2.03	4.74	2.81	1.93	0.54	0.10	0.14
1007				0.5	17.9	11.37	7.56	0.31	3.78	1.36	4.04	2.49	1.55	0.47	0.09	0.14
1008				1.0	18.0	9.68	6.92	0.31	3.34	0.35	3.80	2.32	1.48	0.44	0.08	0.14
1009				2.0	17.2	14.02	9.16	0.08	3.07	1.92	1.40	0.63	0.77	0.45	0.09	0.14
1010		3.0	18.0	1.0	18.0	11.16	8.46	0.56	5.53	0.00	2.72	1.17	1.55	0.43	0.09	0.14
1011						10.99	7.75	0.21	2.50	0.54	3.29	1.61	1.64	0.44	0.09	0.14
1012						9.90	6.60	0.67	4.53	1.20	2.25	0.96	1.29	0.40	0.07	0.13
1013				2.0	17.2	13.88	6.73	2.42	13.52	6.19	3.08	1.31	1.77	0.84	0.17	0.09
1014						11.87	8.27	0.00	4.32	0.75	2.82	1.24	1.58	0.92	0.18	0.10
1015						12.41	8.59	0.30	4.69	0.92	2.52	0.95	1.57	0.97	0.16	0.10
1016				3.0	16.8	12.90	9.04	0.10	3.19	0.74	2.74	1.17	1.57	0.67	0.14	0.08
1017						13.27	9.42	0.51	3.74	0.58	2.38	0.71	1.67	1.10	0.20	0.15
1018						13.49	8.97	0.00	3.43	1.57	2.74	1.24	1.50	0.90	0.22	0.12
1019		3.9		1.0	18.0	5.06	3.59	0.04	2.44	0.22	1.14	0.10	1.04	2.34	0.53	0.27
1020						5.68	4.29	0.74	4.03	0.00	1.27	0.35	0.92	2.36	0.54	0.25
1021						4.67	2.95	0.09	1.52	0.92	1.16	0.13	1.03	1.73	0.41	0.21
1022				2.0	17.4	5.95	3.59	0.18	2.18	1.35	1.45	0.43	1.02	0.84	0.15	0.09
1023						5.50	3.97	0.43	2.78	0.15	0.99	0.32	0.67	0.80	0.17	0.07
1024						6.49	4.42	0.88	5.63	0.69	1.25	0.07	1.18	0.84	0.17	0.08
1025				3.8	16.9	9.90	5.90	0.59	4.76	2.40	2.26	0.66	1.60	---	---	---
1026						9.82	6.79	0.74	4.86	0.79	1.56	0.51	1.05	---	---	---
1027						10.25	7.24	0.29	4.43	0.52	2.05	0.61	1.44	---	---	---
1028		2.3	20.4	0.5	20.4	3.59	2.11	0.41	3.01	0.94	2.07	0.97	1.10	---	---	---
1029						3.51	2.24	0.33	3.62	0.63	1.18	0.19	0.99	---	---	---
1030						6.80	4.49	0.70	4.09	0.94	2.17	1.14	1.03	1.57	0.32	0.30
1031				1.0	18.9	8.99	6.28	0.27	4.36	0.58	3.54	1.85	1.69	1.74	0.32	0.31
1032						9.85	7.24	0.29	5.35	0.03	3.00	1.66	1.34	1.92	0.35	0.35
1033						6.48	4.23	0.25	3.05	0.93	2.96	1.67	1.29	---	---	---
1034				2.3	18.4	13.06	9.55	0.90	7.33	0.19	4.15	2.24	1.91	---	---	---
1035						12.63	9.59	0.23	4.43	1.19	3.61	1.98	1.63	---	---	---
1036						6.98	4.17	1.36	5.46	1.76	4.13	2.30	1.83	---	---	---
1037	JULY 18	2.0	24.1	0.5	24.1	15.95	10.32	0.00	1.94	2.33	3.93	1.80	2.13	---	---	---
1038				1.0	24.2	13.82	8.91	0.41	2.94	2.13	3.99	1.97	2.02	---	---	---
1039				2.0	24.0	21.59	14.87	1.24	2.13	1.73	4.40	2.03	2.37	---	---	---
1040				0.5	24.1	16.17	10.64	0.77	3.10	2.15	4.60	2.27	2.33	---	---	---
1041				1.0	24.2	13.96	9.29	0.11	1.45	1.61	4.15	2.06	2.09	---	---	---
1042				2.0	24.0	20.18	13.58	0.13	3.57	2.07	4.74	2.14	2.60	---	---	---
1043				0.5	24.1	15.92	10.57	0.18	3.48	1.90	4.09	1.96	2.13	---	---	---
1044				1.0	24.2	14.64	9.61	0.18	1.73	1.92	4.05	2.07	1.98	---	---	---
1045				2.0	24.0	16.18	10.64	0.84	1.39	2.15	4.89	2.21	2.68	---	---	---
1046		2.3	24.6	0.5	24.6	17.48	10.25	0.06	3.74	4.37	3.72	1.56	2.15	---	---	---
1047				1.0		21.57	15.64	0.35	3.55	0.33	4.17	1.63	2.54	---	---	---
1048				2.0	24.3	21.59	14.93	0.00	4.04	1.53	3.82	1.33	2.49	---	---	---
1049				0.5	24.6	19.46	13.52	0.11	7.37	1.33	3.63	1.65	1.98	---	---	---
1050				1.0		21.58	15.38	0.00	5.78	0.68	4.05	1.70	2.35	---	---	---
1051				2.0	24.3	21.75	15.83	0.31	3.77	0.23	2.72	0.51	2.21	---	---	---

TABLE A20

| NASA SEA TRUTH SAMPLING SITE PARAMETERS |

SSPL NO	JUL DATE	DATE	LAT	LONG	LAKE	RESEARCH VESSEL	STA. ON	TIME OFF	WAVE HGT FT.	WIND SP (MPH)	WIND DIR	WATER COLOR	SKY COLOR	CLOUD COVER
1001	143	MAY 22	413420	825420	ERIE	HYDRA	1025	1058	0.5	7	0	GREEN-CLDY	BLUE	CLEAR OVER LAKE
1002														
1003														
1004														
1005														
1006														
1007														
1008														
1009														
1010			414036	825520			1133	1145		3	270	GREEN		CLEAR-HAZY
1011														
1012														
1013														
1014														
1015														
1016														
1017														
1018														
1019			414236	825555			1228	1240		7	225	---		
1020														
1021														
1022														
1023														
1024														
1025														
1026														
1027														
1028			413420	825420			1404	1420	0.0	3	45	GREEN		CLEAR-LT HAZE
1029														
1030														
1031														
1032														
1033														
1034														
1035														
1036														
1037	196	JULY 14	413454	825306			1000	1200	0.5	8	203	GREEN-CLDY	LT BLUE	95% CLEAR
1038														
1039														
1040														
1041														
1042														
1043														
1044														
1045														
1046			414012	825710			1230	1400		9	158			CLEAR OVERHEAD
1047														
1048														
1049														
1050														
1051														

TABLE A21

NASA SEA TRUTH SAMPLING DATA

SAMPLE NUMBER	DATE	SECCHI DEPTH	SURFACE TEMP. (°C)	SAMPLE DEPTH (m)	TEMP @ SAMPLE DEPTH	CHLOROPHYLL (mg/m³) A	A2	B	C	PHAEOPH (mg/m³)	RESIDUE (mg/l) TOTAL	ASHED	VOLAT	CHN DATA (mg/l) C	H	N
1052	JULY 14	2.3	24.6	0.5	24.6	18.52	12.43	0.00	4.23	1.97	6.82	3.40	3.42	---	---	---
1053				1.0		19.71	13.65	0.15	2.57	1.38	4.28	1.50	2.74	---	---	---
1054				2.1	24.3	22.25	15.70	0.11	5.22	1.08	4.90	2.05	2.85	---	---	---
1055	JULY 17	0.5	25.4	0.5	25.7	33.09	19.70	0.00	6.97	7.66	26.70	20.75	5.95	---	---	---
1056				1.0		29.02	17.94	0.96	6.19	5.77	30.34	23.23	7.11	---	---	---
1057				2.0	25.6	29.16	18.80	0.00	5.11	4.38	25.11	19.49	5.63	---	---	---
1058				0.5	25.7	27.63	13.46	1.06	4.45	11.66	28.60	22.09	6.51	---	---	---
1059				1.0		27.81	12.82	0.00	3.65	12.82	28.57	22.29	6.29	---	---	---
1060				2.0	25.6	50.52	30.76	0.45	16.13	10.81	27.97	21.66	6.31	1.11	0.20	0.20
1061				0.5	25.7	41.76	26.43	0.00	6.06	7.19	28.43	22.26	6.17	1.19	0.27	0.24
1062				1.0		31.70	19.04	1.02	4.69	7.23	29.14	22.57	6.57	1.05	0.19	0.19
1063				2.0	25.6	32.66	21.79	0.92	8.24	3.78	28.97	22.57	6.40	0.88	0.15	0.15
1064		2.0	24.6	0.5	25.3	16.91	8.65	0.00	3.67	6.33	5.42	2.99	2.43	0.83	0.13	0.14
1065				1.0		15.46	10.51	0.03	3.89	1.42	5.21	2.83	2.38	0.85	0.15	0.16
1066				2.0		16.11	10.70	0.00	4.83	1.90	4.73	2.52	2.21	0.34	0.05	1.59
1067				0.5		20.94	14.16	0.00	6.85	2.03	5.01	2.58	2.43	0.54	0.11	0.08
1068				1.0		19.19	11.34	0.00	3.79	4.63	5.24	2.85	2.39	0.59	0.11	0.09
1069				2.0		22.96	15.38	0.00	4.29	2.47	4.99	2.75	2.24	1.74	0.33	0.31
1070				0.5		21.22	14.80	0.00	5.42	1.26	4.97	2.63	2.34	1.87	0.36	0.32
1071				1.0		23.10	15.70	0.00	4.61	2.06	5.19	2.92	2.27	2.37	0.42	0.39
1072				2.0		20.17	13.71	0.00	6.52	1.81	5.48	3.16	2.32	1.62	0.35	0.29
1073	SEPT 08	1.0	23.4	0.5	23.7	51.69	34.44	1.32	12.53	6.04	10.11	5.17	4.94	1.98	0.39	0.32
1074						55.23	36.05	0.91	12.81	7.69	10.23	5.06	5.17	2.12	0.42	0.33
1075						49.63	30.76	1.44	10.20	9.72	8.20	3.83	4.37	---	---	---
1076				1.0	23.9	50.69	32.96	2.65	10.43	7.41	9.94	4.94	5.00	---	---	---
1077						64.15	43.03	1.50	10.24	6.96	10.51	5.23	5.29	---	---	---
1078						46.45	29.11	3.21	7.83	8.70	9.11	4.63	4.49	---	---	---
1079			23.6	0.5	24.8	23.98	14.87	1.20	9.15	4.78	8.40	5.36	3.04	---	---	---
1080						25.03	16.15	2.65	9.82	4.04	7.74	4.54	3.20	---	---	---
1081						25.46	17.69	1.64	9.70	1.87	7.88	4.62	3.26	---	---	---
1082				1.0	24.4	29.73	18.46	1.28	10.57	5.86	7.94	4.44	3.50	---	---	---
1083						29.27	18.20	1.46	12.05	5.75	8.70	5.12	3.58	---	---	---
1084						27.92	18.46	0.37	9.98	3.52	8.00	4.68	3.32	---	---	---
1085		1.8	24.0	0.5	24.6	24.38	15.76	0.95	7.27	3.70	2.17	0.00	2.17	---	---	---
1086				1.0		16.18	10.25	0.02	4.04	2.76	1.97	0.05	1.92	---	---	---
1087				0.5		23.05	15.83	0.08	5.34	1.85	2.07	0.00	2.07	---	---	---
1088				1.1		15.53	9.78	0.43	4.49	4.50	2.03	0.23	1.80	---	---	---
1089				2.1		17.14	11.02	0.70	4.27	2.70	1.73	0.07	1.66	---	---	---
1090						15.31	10.00	0.58	4.52	2.16	1.78	0.06	1.72	---	---	---
1091				0.5		20.59	13.20	0.00	4.52	3.22	2.16	0.11	2.05	---	---	---
1092				1.0		16.96	11.66	0.15	4.53	1.35	2.27	0.23	2.04	---	---	---
1093				2.0		15.78	10.06	0.17	3.55	2.59	1.72	0.00	1.72	---	---	---
1094	SEPT 11	1.0	20.2	0.5	20.4	3.59	2.24	0.87	4.71	0.78	9.95	8.04	1.91	---	---	---
1095				1.0	20.6	3.30	2.00	0.68	3.85	0.80	9.49	7.64	1.85	---	---	---
1096				0.5	20.4	3.31	1.76	0.59	3.10	1.21	9.01	7.25	1.76	---	---	---
1097				1.0	20.6	4.20	2.72	1.76	5.59	0.81	9.74	8.01	1.73	---	---	---
1098				0.5	20.4	3.64	1.84	0.85	4.69	1.52	7.53	5.94	1.59	---	---	---
1099				1.0	20.6	3.31	1.92	0.63	3.47	0.94	7.69	6.19	1.50	---	---	---
1100	SEPT 19		19.7	0.5	19.7	52.86	34.97	2.45	10.46	6.68	15.31	10.29	5.03	---	---	---
1101				1.1	19.8	48.57	27.83	1.74	13.17	13.44	16.23	11.49	4.74	---	---	---
1102				0.5	19.7	59.02	39.00	1.87	13.95	7.49	16.89	11.89	5.00	---	---	---

TABLE A22

NASA SRA TRUTH SAMPLING SITE PARAMETERS														
SMPL NO	JDT DATE	DATE	LAT	LONG	LAKE	RESEARCH VESSEL	STA. ON	TIME OFF	WAVE HGT FT.	WIND SP (MPH)	WIND DIR	WATER COLOR	SKY COLOR	CLOUD COVER	RFS. SMPL NO.
1152	196	JULY 14	414012	825710	ERIE	HYDRA	1230	1400	0.5	9	158	GREEN-CLDY	LT BLUE	CLEAR OVERHEAD	---
1153															
1154															
1155	199	JULY 17	413147	825500			920	---		10	248	BROWN-CLDY	BLUE	CLEAR	
1156															
1157															
1158															
1159															
1160															
1161															
1162															
1163															
1164			413406				1210		2.0	15	293	---		80% CLEAR	
1165															
1166															
1167															
1168															
1169															
1170															
1171															
1172															
1173	252	SEPT 08	413030	824124			945	1015	0.8	8	158	BRN-GRN-CL	LT BLUE	CLEAR OVERHEAD	
1174															1075
1175															1077
1176															1074
1177															1076
1178															---
1179			413024	824348			1045	1115	0.5		113				
1180															1093
1181															---
1182															
1183															1091
1184															---
1185				823806			1145	1210		10	158	GREEN			
1186															
1187															
1188															
1189															
1190															
1191															
1192															
1193															
1194	255	SEPT 11	420019	830636			955	---	6.0	17	248	LT GRN-CL		40% CLEAR	
1195															
1196															
1197															
1198															
1199															
1200	262	SEPT 18	414500	832100			1055	1135	0.5	11	203	BROWN-CLDY	BL-GRAY	CLEAR OVER LAKE	
1201															
1202															

TABLE A23

NASA SEA TRUTH SAMPLING DATA																	
SAMPLE NUMBER	DATE	SECCHI DEPTH	SURFACE TEMP. (°C)	SAMPLE DEPTH (m)	TEMP @ SAMPLE DEPTH	CHLOROPHYLL (mg/m³) A	A2	B	C	PHAEOPH (mg/m³)	RESIDUE (mg/l) TOTAL	ASHED	VOLAT	CHN DATA (mg/l) C	H	N
1103	SEPT 18	1.0	19.7	1.0	19.8	51.40	33.69	2.51	12.86	7.07	16.57	11.43	5.14	---	---	---
1104				0.5	19.7	54.96	33.50	3.59	22.07	11.99	18.00	12.31	5.69	---	---	---
1105				1.0	19.8	56.61	37.53	1.49	14.22	6.94	16.40	11.23	5.17	---	---	---
1106			19.5	0.5	19.5	46.79	29.48	2.08	13.69	8.46	20.83	14.97	5.86	---	---	---
1107				1.0	20.0	42.98	27.10	2.08	13.58	7.76	20.14	14.71	5.43	---	---	---
1108				0.5	19.5	45.64	29.11	2.49	12.29	7.67	20.23	14.89	5.34	---	---	---
1109				1.0	20.0	46.06	30.21	2.17	14.13	6.32	21.11	15.54	5.57	---	---	---
1110				0.5	19.5	48.81	32.04	2.76	12.15	6.66	24.31	17.94	6.37	---	---	---
1111				1.0	20.0	48.83	32.04	2.22	14.46	6.66	21.86	16.20	5.66	---	---	---
2001	JULY 17		25.0	0.5	25.0	74.97	52.80	0.00	23.86	3.63	10.96	4.30	6.66	3.00	0.47	0.58
2002				1.0	---	74.50	52.29	0.00	15.04	3.78	11.02	4.42	6.60	---	---	---
2004				0.5	25.0	73.70	51.14	0.00	16.28	4.75	10.86	4.42	6.44	3.00	0.47	0.51
2005				1.0	---	75.16	52.93	0.00	13.35	3.59	10.60	4.22	6.38	---	---	---
2007				0.5	25.0	69.75	49.09	0.00	14.28	3.40	10.20	4.06	6.14	2.86	0.45	0.49
2008				1.0	---	73.08	51.65	0.00	14.53	3.26	10.52	3.82	6.70	---	---	---
2009		3.0	24.5		24.5	19.74	12.50	0.41	5.01	2.17	3.27	0.85	2.42	0.98	0.15	0.12
2010				3.0	---	18.60	12.75	0.00	5.31	1.51	2.78	0.71	2.07	---	---	---
2011				1.0	24.5	18.14	12.94	0.72	5.67	0.69	3.16	0.85	2.31	0.86	0.15	0.14
2012				3.0	---	20.55	10.96	2.07	11.85	7.25	2.69	0.56	2.13	---	---	---
2013				1.0	24.5	18.61	12.37	0.00	3.25	2.17	2.75	0.62	2.13	0.89	0.16	0.13
2014				3.0	---	19.09	13.14	0.00	3.71	1.44	2.79	0.61	2.18	---	---	---
2015			---	1.0		18.88	13.46	0.32	6.13	0.72	3.30	0.86	2.44	1.02	0.18	0.11
2016				3.0		19.70	13.65	0.02	5.80	1.38	3.11	0.48	2.63	---	---	---
2017				1.0		16.57	10.96	0.00	4.80	2.01	2.66	0.34	2.32	1.00	0.17	0.14
2018				3.0		20.33	14.61	0.31	5.77	0.55	2.82	0.33	2.49	---	---	---
2019				1.0		16.20	10.83	0.00	4.25	1.78	2.71	0.30	2.41	1.11	0.20	0.12
2020				3.0		19.10	12.82	1.67	12.23	2.26	2.65	0.31	2.34	---	---	---
2050	JULY 13	---		0.5		14.67	9.74	0.93	8.62	1.88	3.62	1.70	1.92	1.10	0.22	0.35
2051						13.54	8.78	0.52	5.17	2.03	3.54	1.06	2.48	1.06	0.21	0.35
2052						14.64	9.87	1.20	6.12	1.61	3.18	1.00	2.18	1.01	0.19	0.33
2053	JULY 15					12.89	7.60	1.83	5.91	3.34	18.04	15.34	2.70	1.31	0.33	0.36
2054						11.89	7.95	1.30	3.57	1.44	18.40	15.24	3.16	1.19	0.26	0.35
2055						11.99	7.01	1.21	4.23	3.16	17.80	14.66	3.14	1.30	0.26	0.34
2056						9.79	6.47	0.40	1.71	1.24	12.10	9.54	2.56	0.83	0.14	0.31
2057						9.63	6.54	0.65	1.62	0.95	11.52	9.09	2.44	0.78	0.14	0.32
2058						9.90	6.09	0.84	3.25	2.08	11.76	9.24	2.52	0.97	0.22	0.09
2059	JULY 16					8.79	4.55	1.37	6.71	3.39	6.98	5.26	1.72	0.63	0.14	0.07
2060						8.31	5.83	1.14	5.27	0.58	8.15	5.93	2.22	0.79	0.17	0.08
2061						5.77	3.14	0.53	3.98	1.93	10.17	7.56	2.61	0.69	0.15	0.07
2062						7.84	4.61	1.12	5.62	2.07	11.38	9.49	1.89	0.78	0.15	0.09
[illegible]						5.10	3.52	0.12	1.19	0.38	11.91	9.79	2.12	0.64	0.15	0.07
2064						6.15	3.20	1.48	6.69	2.40	13.60	11.26	2.34	0.84	0.15	0.10
2065	JULY 19					53.29	31.08	1.82	11.39	13.78	52.55	41.50	11.05	3.02	0.66	0.40
2066						56.73	37.17	4.74	28.63	8.14	58.05	46.60	11.45	3.02	0.18	0.42
2067						53.85	32.04	1.68	10.28	12.82	56.60	45.55	11.05	2.97	0.66	0.40
2068						72.87	41.65	0.00	23.95	20.02	56.45	45.45	11.00	3.28	0.79	0.46
2069						74.00	46.78	0.87	19.57	12.88	57.55	46.15	11.40	3.48	0.76	0.45
2070						73.20	45.18	2.14	19.08	14.71	57.70	46.50	11.20	3.41	0.85	0.45
2071	JULY 21					13.12	2.40	1.73	11.36	12.51	2.75	0.00	2.75	1.14	0.21	0.19
2072						13.99	0.00	2.97	16.31	18.81	3.45	0.00	3.45	1.16	0.23	0.15
2073						13.83	5.93	3.58	18.32	7.64	3.17	0.00	3.17	1.20	0.25	0.15

TABLE A24

NASA SEA TRUTH SAMPLING SITE PARAMETERS														
SMPL NO	JUL DATE	DATE	LAT	LONG	LAKE	RESEARCH VESSEL	STA. ON	TIME OFF	WAVE HGT FT.	WIND SP MPH	WIND DIR	WATER COLOR	SKY COLOR	CLOUD COVER	RES. SMPL NO.
1103	262	SEPT 18	414500	832100	ERIE	HYDRA	1055	1135	0.5	11	203	BROWN-CLDY	BL-GRAY	CLEAR OVER LAKE	---
1104															
1105															
1106			414400	832040			1150	1210							
1107															
1108															
1109															
1110															
1111															
2001	199	JULY 17	---	---		GS-1	1045	1110	2.0	10	225	BROWN-GRN	BLUE		
2002															
2004															
2005															
2007															
2008															
2009							1210	1216	2.5	12	315	GREEN		CLEAR OVERHEAD	2904
2010															2905
2011															---
2012															
2013															
2014															
2015							1240	1250	4.0	--	---				
2016															
2017															
2018															
2019															
2020															
2050	195	JULY 13				PRVTBT	1315	1325	---			---	---	---	
2051															
2052															
2053	197	JULY 15				CG BYP	---	---							2901
2054															---
2055															
2056															
2057															
2058															
2059	199	JULY 16				CG MRB									
2060															
2061															
2062															
2063															
2064															
2065	2[illegible]	JULY 18				CG TLD									
2066															
2067															
2068															
2069															
2070															
2071	203	JULY 21			MICH	MSNF									
2072															
2073															

TABLE A25

NASA SEA TRUTH SAMPLING DATA																	
SAMPLE NUMBERS	DATE	SECCHI DEPTH	SURFACE TEMP. (°C)	SAMPLE DEPTH (m)	TEMP @ SAMPLE DEPTH	CHLOROPHYLL (mg/m³) A	A2	B	C	PHAEOPH (mg/m³)	RESIDUE (mg/l) TOTAL	ASHED	VOLAT	CHN DATA (mg/l) C	H	N
3074	JULY 23	---	---	0.5	---	62.75	37.49	2.38	16.48	14.77	18.80	11.40	7.40	2.67	0.61	0.39
3075						63.86	40.05	3.62	25.31	11.98	19.15	11.70	7.45	2.73	0.55	0.39
3076						67.44	41.01	8.18	32.90	15.28	19.10	12.00	7.10	2.66	0.61	0.35
3077						10.77	5.90	0.42	1.83	3.43	7.98	4.56	3.42	---	---	---
3078						15.02	8.61	2.46	10.21	11.18	4.52	2.00	2.52	---	---	---
3001	MAY 28	8.0	3.9	1.0	4.0	3.74	0.90	1.45	6.46	3.32	0.99	0.30	0.69	0.27	0.06	0.05
3002				4.5	3.9	3.03	1.35	0.63	3.06	1.57	0.89	0.25	0.64	---	---	---
3003				8.0	3.7	2.97	1.86	0.06	1.44	0.56	0.69	0.20	0.49	---	---	---
3004	MAY 31	5.5	13.6	1.1	13.6	3.97	1.99	0.52	4.12	1.65	1.40	0.00	1.40	0.39	0.06	0.06
3005				3.3	13.0	5.73	3.65	0.16	2.67	0.97	1.65	0.00	1.65	---	---	---
3006				5.5	12.0	6.02	4.36	0.45	4.35	0.17	1.54	0.00	1.54	---	---	---
3007	JUNE 11	1.3	12.0	0.5	12.5	25.34	17.17	0.00	6.48	2.34	5.61	3.00	2.61	0.84	0.16	0.14
3008						28.58	19.99	0.00	8.84	1.63	5.54	2.87	2.67	0.87	0.16	0.15
3009						28.33	19.80	0.00	7.54	1.60	5.67	2.98	2.69	0.90	0.17	0.14
3011		6.0	5.9		5.8	4.36	3.14	0.23	2.77	0.13	1.15	0.42	0.74	0.30	0.04	0.06
3012				3.0	5.6	4.58	3.20	0.46	4.06	0.34	1.01	0.29	0.72	---	---	---
3013				6.0	5.2	5.09	2.18	1.89	9.06	2.89	0.98	0.35	0.63	---	---	---
3014				0.5	5.8	4.21	2.63	0.63	3.86	0.87	0.91	0.23	0.67	0.40	0.07	0.11
3015				3.0	5.6	3.92	2.50	0.75	3.80	0.73	0.95	0.31	0.64	---	---	---
3016				6.0	5.2	3.49	2.16	0.30	2.27	0.72	1.43	0.80	0.63	---	---	---
3017				0.5	5.8	3.49	2.24	0.31	2.51	0.58	1.31	0.71	0.61	0.37	0.07	0.10
3018				3.0	5.6	3.54	2.44	0.44	3.50	0.35	1.32	0.64	0.68	---	---	---
3019				6.0	5.2	3.62	2.63	0.46	2.94	0.11	1.28	0.58	0.71	---	---	---
3021		4.5	7.9	0.5	7.9	4.52	3.09	0.75	4.52	0.51	1.22	0.36	0.86	0.40	0.08	0.10
3022				2.0	7.5	4.79	3.20	0.14	3.19	0.56	1.30	0.45	0.85	---	---	---
3023				4.0	6.9	6.64	4.36	0.01	2.97	0.89	1.55	0.56	0.98	---	---	---
3024				0.5	7.9	4.52	3.14	0.00	1.86	0.31	1.16	0.42	0.74	0.38	0.07	0.10
3025				2.0	7.5	5.32	3.40	0.34	3.31	0.91	1.23	0.38	0.85	---	---	---
3026				4.0	6.9	6.46	4.04	0.00	2.80	1.21	1.51	0.54	0.96	---	---	---
3027				0.5	7.9	4.99	3.14	0.00	2.52	0.90	1.24	0.39	0.85	0.35	0.07	0.05
3028				2.0	7.5	4.98	3.46	0.14	2.24	0.35	1.22	0.34	0.88	---	---	---
3029				4.0	6.9	6.80	3.84	1.06	5.59	2.08	1.40	0.41	1.00	---	---	---
3031		3.0	8.3	0.5	8.2	5.80	3.65	0.17	2.94	1.06	2.10	1.08	1.02	0.43	0.08	0.06
3032				1.5	8.0	6.23	4.36	0.23	3.08	0.40	2.08	1.16	0.92	---	---	---
3033				3.0	7.7	8.14	5.38	1.60	9.27	1.21	2.43	1.23	1.20	---	---	---
3034				0.5	8.2	5.93	3.72	0.34	3.20	1.13	2.18	1.08	1.10	0.36	0.08	0.05
3035				1.5	8.0	6.07	4.04	0.03	2.71	0.72	2.46	1.45	1.01	---	---	---
3036				3.0	7.7	6.97	4.74	0.34	3.94	0.69	2.27	1.20	1.07	---	---	---
3037				0.5	8.2	6.14	4.17	0.75	4.51	0.68	2.08	1.11	0.98	0.41	0.09	0.05
3038				1.5	8.0	6.07	4.23	0.73	4.42	0.48	2.05	1.00	1.05	---	---	---
3039				3.0	7.7	6.80	3.97	1.45	5.91	1.90	2.10	1.06	1.04	---	---	---
3041		4.3	9.6	0.5	9.5	5.02	3.52	0.00	1.25	0.24	1.33	0.43	0.91	0.45	0.08	0.05
3042				2.0	8.1	5.73	4.36	0.26	2.26	0.00	1.26	0.39	0.87	---	---	---
3043				4.0	6.9	6.14	4.23	0.11	1.27	0.48	1.40	0.42	0.98	---	---	---
3044				0.5	9.5	4.32	3.33	0.00	1.93	0.00	1.24	0.48	0.76	0.38	0.08	0.05
3045				2.0	8.1	---	---	---	---	---	1.31	0.44	0.88	---	---	---
3046				4.0	6.9	6.33	4.61	0.00	2.43	0.05	1.43	0.45	0.98	---	---	---
3047				0.5	9.5	5.68	2.63	1.69	5.89	2.76	1.09	0.31	0.78	0.37	0.09	0.05
3048				2.0	8.1	6.49	4.42	0.00	2.18	0.56	1.11	0.27	0.85	---	---	---
3049				4.0	6.9	6.22	4.42	0.00	2.35	0.24	1.52	0.29	1.23	---	---	---
3051	JULY 21	1.5	24.2	1.0	24.2	17.70	39.22	4.09	13.07	67.90	13.57	7.20	6.37	2.54	0.38	0.41

TABLE A26

| NASA SEA TRUTH SAMPLING SITE PARAMETERS |

SMPL NO	JUL DATE	DATE	LAT	LONG	LAKE	RESEARCH VESSEL	STA. ON	TIME OFF	WAVE HGT FT.	WIND SP (MPH)	WIND DIR	WATER COLOR	SKY COLOR	CLOUD COVER	PRS. SMPL NO.
2974	205	JULY 23	---	---	ERIE	CG TLO	---	---	---	--	---	---	---	---	---
2975															
2976															
2977															
2978															
3001	149	MAY 29	424910	862925	MICH	SHERSH	1258	1330	2.0	10	135	BLUE-GREEN	LT BLUE	70% CLEAR	
3002															
3003															
3004	152	MAY 31	414550	872319			1154	1219	1.0	--	293	DK GREEN		CLEAR OVERHEAD	
3005															
3006															
3007	163	JUNE 11	430401	861601			1314	1330	0.5		200	BROWN-GRN		CLEAR-LT HAZE	
3008															
3009															
3011			430419	863238			952	1055	0.0		190	BLUE-GREEN			
3012															
3013															
3014															
3015															
3016															
3017															
3018															
3019															
3021				862530			1128	1152				LT GREEN			
3022															
3023															
3024															
3025															
3026															
3027															
3028															
3029															
3031				861825			1218	1314	0.5		180				
3032															
3033															
3034															
3035															
3036															
3037															
3038															
3039															
3041			430206	862530			1446	1512			210	GREEN			
3042															
3043															
3044															
3045															
3046															
3047															
3048															
3049															
3050	203	JULY 21	433339	861532			803	826	2.0	6	242	BROWN	---	OVCST-LT GY CLDS	

TABLE A27

NASA SEA TRUTH SAMPLING DATA																	
SAMPLE NUMBER	DATE	SECCHI DEPTH	SURFACE TEMP. (°C)	SAMPLE DEPTH (m)	TEMP @ SAMPLE DEPTH	CHLOROPHYLL (mg/m³) A	A2	B	C	PHAEOPH (mg/m³)	RESIDUE (mg/l) TOTAL	ASHED	VOLAT	CHN DATA (mg/l) C	H	N
3051	JULY 21	1.1	24.2	1.0	24.2	118.72	69.85	1.25	21.04	29.37	15.36	7.80	7.56	3.19	0.50	0.49
3052						108.56	28.07	3.15	12.91	87.84	15.48	7.58	7.90	2.82	0.47	0.41
3053	JULY 22	3.9	22.3		22.3	8.30	4.55	0.13	2.19	2.63	2.05	0.31	1.74	0.56	0.09	0.23
3054						7.61	4.42	0.23	2.10	1.99	1.75	0.14	1.61	0.57	0.09	0.23
3055						7.92	4.36	0.38	2.41	2.51	1.71	0.00	1.71	0.54	0.07	0.23
3056		7.5	20.0		20.0	4.79	3.14	0.24	2.79	0.67	1.12	0.00	1.12	0.35	0.07	0.23
3057						5.23	3.40	0.94	4.51	0.87	1.32	0.00	1.32	0.00	0.07	0.23
3058						6.64	3.59	2.79	10.33	2.51	1.03	0.00	1.03	0.36	0.09	0.23
3059	JULY 23	1.3	16.1		16.1	68.53	44.47	1.56	13.21	9.98	5.52	0.42	5.10	2.03	0.33	0.44
3060						54.58	34.73	3.23	13.56	9.32	4.26	0.00	4.26	1.91	0.33	0.46
3061		4.3	20.8	0.5	20.9	5.74	3.33	0.17	1.84	1.51	1.09	0.00	1.09	0.45	0.08	0.05
3062				2.0	20.6	6.09	4.23	0.72	2.94	0.48	1.18	0.00	1.18	---	---	---
3063				4.1	20.0	6.20	3.72	0.62	3.60	1.49	1.22	0.00	1.22	---	---	---
3064				0.5	20.8	6.00	3.72	0.45	3.07	1.22	1.13	0.00	1.13	0.45	0.09	0.05
3065				2.0	20.6	6.22	3.97	0.75	4.13	1.10	1.13	0.00	1.13	---	---	---
3066				4.0	20.0	6.58	4.17	0.72	4.23	1.22	1.24	0.00	1.24	---	---	---
3067				0.5	20.8	5.93	2.76	0.45	2.62	2.76	1.15	0.00	1.15	0.44	0.09	0.05
3068				2.0	20.6	5.98	3.78	0.62	3.26	1.11	1.03	0.00	1.03	---	---	---
3069				4.0	20.0	6.66	4.17	0.75	3.49	1.31	1.05	0.00	1.05	---	---	---
3070		1.0	16.1	1.0	16.1	53.35	32.81	2.56	10.06	10.97	5.04	0.52	4.52	1.73	0.26	0.24
3071		6.0	19.9	0.5	19.9	4.96	3.20	0.74	3.89	0.83	0.86	0.00	0.86	0.38	0.07	0.04
3072				3.0	19.8	4.86	2.95	0.76	3.45	1.13	0.97	0.00	0.97	---	---	---
3073				6.0	18.1	4.63	3.01	0.42	3.57	0.71	1.03	0.00	1.03	---	---	---
3074				0.5	19.9	4.75	3.08	0.65	3.78	0.78	0.98	0.00	0.98	0.40	0.09	0.05
3075				3.0	19.8	4.65	3.14	0.62	3.22	0.54	0.84	0.00	0.84	---	---	---
3076				6.0	18.1	4.56	3.27	0.82	3.45	0.23	0.91	0.00	0.91	---	---	---
3077				0.5	19.9	5.06	2.63	2.62	2.58	2.08	0.91	0.00	0.91	0.40	0.08	0.05
3078				3.0	19.8	4.62	3.01	0.57	3.29	0.71	0.91	0.00	0.91	---	---	---
3079				6.0	18.1	4.62	2.88	0.53	2.99	0.93	0.91	0.00	0.91	---	---	---
3080	JULY 24	1.7	---	1.0	---	97.55	66.26	0.00	15.88	8.92	8.00	1.44	6.56	1.55	0.37	0.27
3081						98.28	58.06	0.00	25.38	23.85	8.00	1.78	6.22	1.40	0.35	0.27
3082						101.86	68.05	2.52	18.53	11.52	8.20	2.18	6.02	1.50	0.46	0.27
3083				1.7		82.54	55.62	0.00	15.55	8.34	5.80	0.88	4.92	1.34	0.47	0.27
3084						81.81	55.37	0.72	17.90	7.97	6.12	1.20	4.92	0.94	0.20	0.18
3085						83.10	54.34	1.55	20.56	11.42	6.54	1.78	4.76	0.93	0.16	0.18
4001		1.0	18.0	1.0	18.0	10.08	4.87	1.27	8.17	4.46	4.80	3.03	1.77	0.72	0.16	0.11
4002						10.73	5.13	2.14	8.94	4.92	5.09	3.27	1.83	0.74	0.15	0.15
4003						11.09	7.18	1.18	10.15	1.79	4.91	3.04	1.87	0.67	0.16	0.11
4004		2.0	19.1		19.1	7.00	4.19	0.55	2.76	1.82	3.25	1.87	1.38	0.54	0.11	0.10
4005						7.14	4.10	1.13	6.76	2.09	1.18	0.00	1.18	0.44	0.10	0.07
4006						7.14	4.36	1.23	7.01	1.65	3.21	1.81	1.40	0.52	0.12	0.09
4010	AUG 01	4.5	19.8		19.2	2.66	1.73	0.00	1.08	0.38	1.24	0.49	0.75	0.30	0.07	0.04
4011						2.82	1.99	0.22	1.75	0.17	1.12	0.47	0.65	0.28	0.07	0.04
4012						2.99	2.18	0.26	2.57	0.06	1.22	0.51	0.71	0.30	0.07	0.05
4013				2.5	19.1	3.31	2.37	0.20	3.21	0.14	1.31	0.58	0.73	---	---	---
4014						3.14	2.11	0.24	2.16	0.35	0.90	0.25	0.65	---	---	---
4015						3.21	1.67	0.53	3.34	1.25	0.55	0.03	0.52	---	---	---
4016				4.5		3.53	1.86	0.70	3.47	1.33	1.29	0.43	0.85	---	---	---
4017						3.39	2.24	0.27	1.95	0.45	1.38	0.48	0.90	---	---	---
4018						2.92	1.86	0.00	0.97	0.47	1.19	0.49	0.70	---	---	---
4019		7.0	20.1	1.0	20.1	1.59	0.90	0.10	1.19	0.48	0.66	0.11	0.55	0.20	0.04	0.03

TABLE A28

NASA SEA TRUTH SAMPLING SITE PARAMETERS

SMPL NO	JUL DATE	DATE	LAT	LONG	LAKE	RESEARCH VESSEL	STA. ON	TIME OFF	WAVE HGT FT.	WIND SP MPH	WIND DIR	WATER COLOR	SKY COLOR	CLOUD COVER	RES. SMPL NO.
3051	203	JULY 21	430338	861532	MICH	SHENEH	803	826	2.0	6	242	BROWN	---	OVCST-LT GR CLDS	---
3052															
3053	204	JULY 22	430307	861508			712	732	0.0		45	GREEN	LT BLUE	80% CLEAR-HAZY	
3054															
3055															
3056			430318	861850			746	803		2	30				
3057															
3058															
3059	205	JULY 23	430243	861516			1530	1615	3.0	6	338	YELLOW-GRN	PALE BL	CLEAR	
3060															
3061			430177	861740			1057	1223	1.0	5		GREEN	LT BLUE	CLEAR OVER LAKE	
3062															
3063															
3064															
3065															
3066															
3067															
3068															
3069															
3070			430243	861516			1530	1615	3.0	6		YELLOW-GRN	PALE BL	CLEAR	
3071			430114	862604			1305	1402				GREEN	BLUE	CLEAR OVER LAKE	
3072															
3073															
3074															
3075															
3076															
3077															
3078															
3079															
3081	206	JULY 24	430329	861548			910	1000	4.0	4	158	BROWN	LT BLUE	CLEAR OVERHEAD	
3081															
3082															
3083															
3084															
3085															
4001			464403	915703	SUP	LEPTO	940	955	2.0	12	248	RED-BROWN	---	---	
4002															
4003															
4004			464300	915200			1000	1014				LT BROWN			
4005															
4006															
4010	214	AUG 01	464403	915700				1030	1.0	10	225	BROWN-GRN	BLUE	CLEAR	
4011															
4012															
4013															
4014															
4015															
4016															
4017															
4018															
4019			464300	915700			1110	1128	2.0	12		BLUE-GREEN			

TABLE A29

NASA SEA TRUTH SAMPLING SITE PARAMETERS

SMPL NO	JUL DATE	DATE	LAT	LONG	LAKE	RESEARCH VESSEL	STA. ON	TIME OFF	WAVE HGT FT.	WIND SP (MPH)	WIND DIR	WATER COLOR	SKY COLOR	CLOUD COVER	RES. SMPL NO.
4020	214	AUG 01	464300	915200	SUP	LEPTO	1110	1128	2.0	12	225	BLUE-GREEN	BLUE	CLEAR	4920
4021															---
4022															
4023															
4024															
4025															
4026															
4027															
4028			464330	915900			1215	1300		15	293	BROWN		60% CLEAR	
4029															
4030															
4034															
4035															
4036															
4037	219	AUG 06	464307	915936			950	1026	0.0	0	---	BROWN-GRN		CLEAR-LT HAZE	
4038															
4039															
4040															
4041															
4042															
4043															
4044															
4045															
4046			464252	915046			1101	1117			135	GREEN	BL-GRAY		
4047															
4048															
4049															
4050															
4051															
4052															
4053															
4054															
4055			464301	920007			1220	1242	0.5	7	158	BROWN-GRN	BLUE	CLEAR	
4056															
4057															
4058															
4059															
4060															
4061															
4062															
4063															
4064			464403	915652			1309	1325	1.0	3	---	GREEN		CLEAR-LT HAZE	
4065															
4066															
4067															
4068															
4069															
4070															
4071															
4072															
4073			465004	915061			1405	1416		5	135	DK GREEN			

TABLE A30

NASA SEA TRUTH SAMPLING DATA

SAMPLE NUMBER	DATE	SECCHI DEPTH	SURFACE TEMP. (°C)	SAMPLE DEPTH (m)	TEMP @ SAMPLE DEPTH	CHLOROPHYLL (mg/m³) A	A2	B	C	PHAEOPH (mg/m³)	RESIDUE (mg/l) TOTAL	ASHED	VOLAT	CHN DATA (mg/l) C	H	N
4020	AUG 01	7.0	20.1	1.0	20.1	1.65	0.90	0.19	1.72	0.57	0.79	0.32	0.47	0.19	0.04	0.03
4021						1.59	1.11	0.12	1.51	0.12	0.69	0.17	0.52	0.21	0.05	0.03
4022				3.5	20.0	1.67	0.90	0.06	1.28	0.57	0.63	0.05	0.59	---	---	---
4023						1.93	1.24	0.31	2.30	0.35	0.65	0.05	0.60	---	---	---
4024						1.89	1.20	0.28	1.92	0.36	0.62	0.05	0.57	---	---	---
4025				7.0	19.8	2.07	1.11	0.08	1.52	0.71	1.02	0.37	0.65	---	---	---
4026						2.08	0.98	0.04	1.44	0.93	1.12	0.43	0.69	---	---	---
4027						2.27	1.62	0.28	1.97	0.11	1.02	0.40	0.62	---	---	---
4028		2.0	20.0	1.0	20.0	15.18	10.38	0.72	5.64	1.37	3.49	1.50	1.99	0.88	0.18	0.14
4029						16.74	11.28	0.97	6.62	1.82	3.76	1.53	2.23	0.83	0.17	0.13
4030						15.23	10.38	0.23	4.05	1.37	3.58	1.25	2.33	0.94	0.19	0.14
4034				2.0		16.43	11.02	0.13	3.78	1.76	1.84	0.00	1.84	---	---	---
4035						16.25	10.96	0.16	3.55	1.65	3.38	1.22	2.16	---	---	---
4036						16.48	11.60	1.13	2.25	0.92	2.77	0.51	2.26	---	---	---
4037	AUG 06	4.0	14.0	1.0	14.0	12.09	7.88	0.24	3.98	1.72	3.23	1.68	1.55	0.63	0.13	0.11
4038						12.12	8.33	0.00	3.53	0.95	4.81	3.22	1.59	0.59	0.12	0.11
4039						11.26	7.63	0.28	4.05	1.12	2.78	1.25	1.53	---	---	---
4040				2.0	13.2	7.45	4.55	0.23	2.86	1.60	4.79	3.42	1.37	---	---	---
4041						6.65	4.17	0.02	2.14	1.22	1.55	0.31	1.24	---	---	---
4042						6.67	4.29	0.47	3.88	1.09	1.25	0.00	1.25	---	---	---
4043				4.0	12.3	2.59	1.22	0.29	2.01	1.20	0.93	0.00	0.93	---	---	---
4044						2.42	1.67	0.27	1.66	0.22	1.02	0.00	1.02	---	---	---
4045						2.67	1.47	0.25	2.16	0.86	1.08	0.00	1.08	---	---	---
4046		8.0	16.6	1.0	16.6	1.24	0.64	0.25	1.53	0.50	0.52	0.00	0.52	0.17	0.05	0.05
4047						1.16	0.68	0.16	1.12	0.30	0.40	0.00	0.40	0.14	0.02	0.04
4048						1.36	0.68	0.55	2.29	0.60	0.43	0.00	0.43	0.17	0.05	0.05
4049				4.0	16.2	1.98	1.11	0.07	1.16	0.59	0.60	0.00	0.60	---	---	---
4050						1.98	0.94	0.00	0.59	0.85	0.60	0.00	0.60	---	---	---
4051						2.34	1.45	0.29	2.03	0.49	0.65	0.00	0.65	---	---	---
4052				8.0	12.0	3.26	2.01	0.00	1.14	0.65	0.74	0.00	0.74	---	---	---
4053						3.12	1.92	0.00	1.09	0.62	0.96	0.23	0.73	---	---	---
4054						3.44	2.26	0.34	1.86	0.49	0.80	0.01	0.78	---	---	---
4055		4.0	13.2	1.0	13.2	6.42	4.29	0.50	4.03	0.78	1.74	0.55	1.19	0.47	0.11	0.12
4056						6.82	4.87	0.06	2.97	0.24	2.18	0.84	1.34	0.46	0.12	0.11
4057						6.50	4.36	0.30	2.43	0.71	1.92	0.61	1.31	0.45	0.11	0.11
4058				2.0	12.2	6.28	4.17	0.01	2.57	0.77	1.63	0.23	1.40	---	---	---
4059						5.58	3.40	0.00	2.58	1.18	1.42	0.19	1.24	---	---	---
4060						4.95	3.40	0.13	1.78	0.42	1.28	0.07	1.21	---	---	---
4061				4.0	11.2	6.05	4.17	0.07	3.66	0.50	2.10	0.72	1.38	---	---	---
4062						5.71	3.59	0.04	2.14	1.03	1.92	0.59	1.33	---	---	---
4063						5.24	3.33	0.00	2.19	0.88	1.57	0.31	1.26	---	---	---
4064		6.0	17.3	1.0	17.3	5.19	6.92	4.90	19.76	0.90	1.35	0.58	0.77	0.38	0.11	0.10
4065						2.36	1.03	0.11	1.67	1.22	0.79	0.00	0.79	0.24	0.05	0.05
4066						2.38	1.47	0.19	2.08	0.50	0.74	0.00	0.74	0.21	0.04	0.04
4067				3.0	15.9	2.69	1.73	0.31	2.74	0.47	0.73	0.00	0.73	---	---	---
4068						2.71	1.73	0.09	2.42	0.47	0.83	0.05	0.77	---	---	---
4069						2.61	1.35	0.08	1.52	0.99	0.77	0.00	0.77	---	---	---
4070				6.0	14.4	2.69	1.73	0.43	2.81	0.47	1.03	0.11	0.91	---	---	---
4071						2.67	1.86	0.25	2.16	0.21	0.79	0.05	0.74	---	---	---
4072						2.51	1.86	0.46	2.59	0.03	0.85	0.00	0.85	---	---	---
4073		10.0	14.1	1.0	14.0	1.15	0.73	0.19	1.32	0.23	0.43	0.00	0.43	0.15	0.03	0.03

TABLE A31

NASA SEA TRUTH SAMPLING DATA																
SAMPLE NUMBER	DATE	SECCHI DEPTH	SURFACE TEMP. (°C)	SAMPLE DEPTH (m)	TEMP @ SAMPLE DEPTH	CHLOROPHYLL (mg/m³) A	A2	B	C	PHAEOPH (mg/m³)	RESIDUE (mg/l) TOTAL	ASHED	VOLAT	CHN DATA (mg/l) C	H	N
4074	AUG 86	10.0	14.0	1.0	14.0	1.30	0.85	0.43	2.11	0.22	0.44	0.00	0.44	0.14	0.03	0.03
4075						1.22	0.81	0.30	1.62	0.18	0.41	0.00	0.41	0.14	0.03	0.03
4076				5.0	11.8	2.04	1.50	0.25	1.63	0.03	0.59	0.00	0.59	---	---	---
4077						2.08	1.37	0.22	1.72	0.31	0.53	0.00	0.53	---	---	---
4078						2.46	1.71	0.82	3.24	0.26	0.62	0.08	0.53	---	---	---
4079				10.0	6.9	3.74	2.52	0.46	2.31	0.44	0.67	0.00	0.67	---	---	---
4080						3.66	2.52	0.33	2.37	0.32	0.61	0.00	0.61	---	---	---
4081						3.51	2.35	0.32	2.26	0.43	0.61	0.00	0.61	---	---	---

*** END OF FILE ON INPUT
TOTAL CPU TIME: 1.815 SEC.
EXECUTION TERMINATED 09:28:33 T=1.926 RC=0 $1.10

TABLE 32

| NASA SEA TRUTH SAMPLING SITE PARAMETERS |

SMPL NO	JUL DAY	DATE	LAT LONG	LAKE	RESEARCH VESSEL	STA. ON	TIME OFF	WAVE HGT FT.	WIND SP (MPH)	WIND DIR	WATER COLOR	SKY COLOR	CLOUD COVER	RES. SMPL NO.
4074	219	AUG 06	465004 915001	SUP	LEPTO	1405	1416	1.0	5	135	DK GREEN	BLUE	CLEAR-LT HAZE	---
4075														
4076														
4077														
4078														
4079														
4080														
4081														

*** END OF FILE ON INPUT

APPENDIX B

CZCS COLOR CODED RADIANCE, CHLOROPHYLL-A PIGMENT, SUSPENDED SEDIMENT, AND SURFACE TEMPERATURE MAPS

TABLE OF COLOR PLATES

PLATE I

SPATIAL COMPARISON OF ATMOSPHERIC CORRECTION ALGORITHMS FOR THE LAKE SUPERIOR SUBSCENE

This plate shows a series of color coded radiance maps ($mw/cm^2.sr.\mu$) for each of the first four CZCS channels as collected on June 11, 1980. Shown are the original uncorrected radiance image which does not include any adjustment for sensor deterioration, and the corrected radiance map for each of the following three algorithms: Smith and Wilson [5] (Algorithm 2), Jain's pseudo optical depth algorithm [6] (Algorithm 3), and the residual component algorithm (Algorithm 4). The corrected radiances are shown as transformed to a nadir view geometry and a Rayleigh atmosphere.

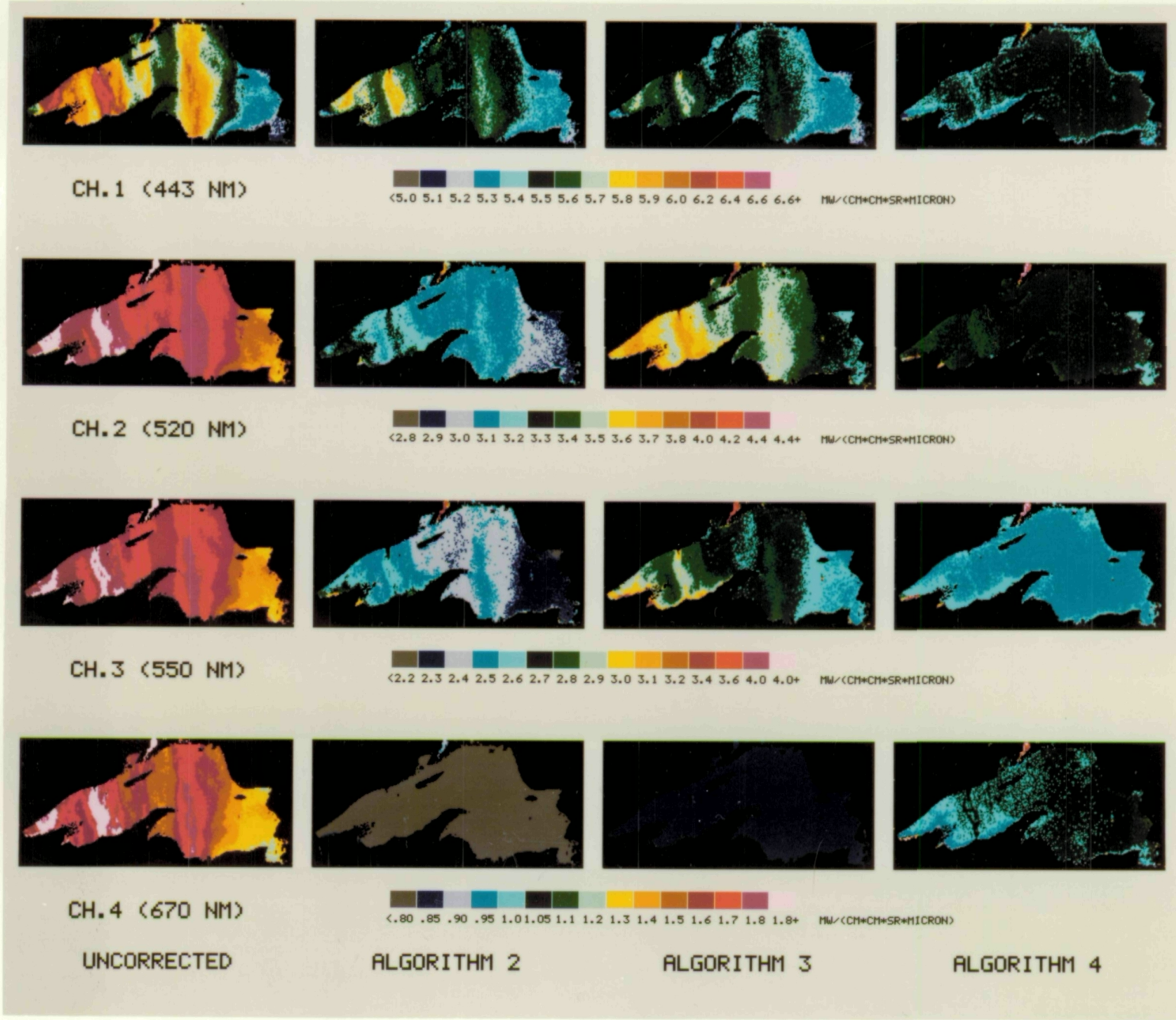

PLATE II

SPATIAL COMPARISON OF ATMOSPHERIC CORRECTION
ALGORITHMS FOR THE LAKE MICHIGAN SUBSCENE

This plate shows a series of color coded radiance maps for each of the first four CZCS channels as collected on June 11, 1980. Shown are the original uncorrected radiance image which does not include any adjustment for sensor deterioration, and the corrected radiance map for each of the following three algorithms: Smith and Wilson [5] (Algorithm 2), Jain's pseudo optical depth algorithm [6] (Algorithm 3), and the residual component algorithm (Algorithm 4). The corrected radiances are shown as transformed to a nadir view geometry and a Rayleigh Atmosphere.

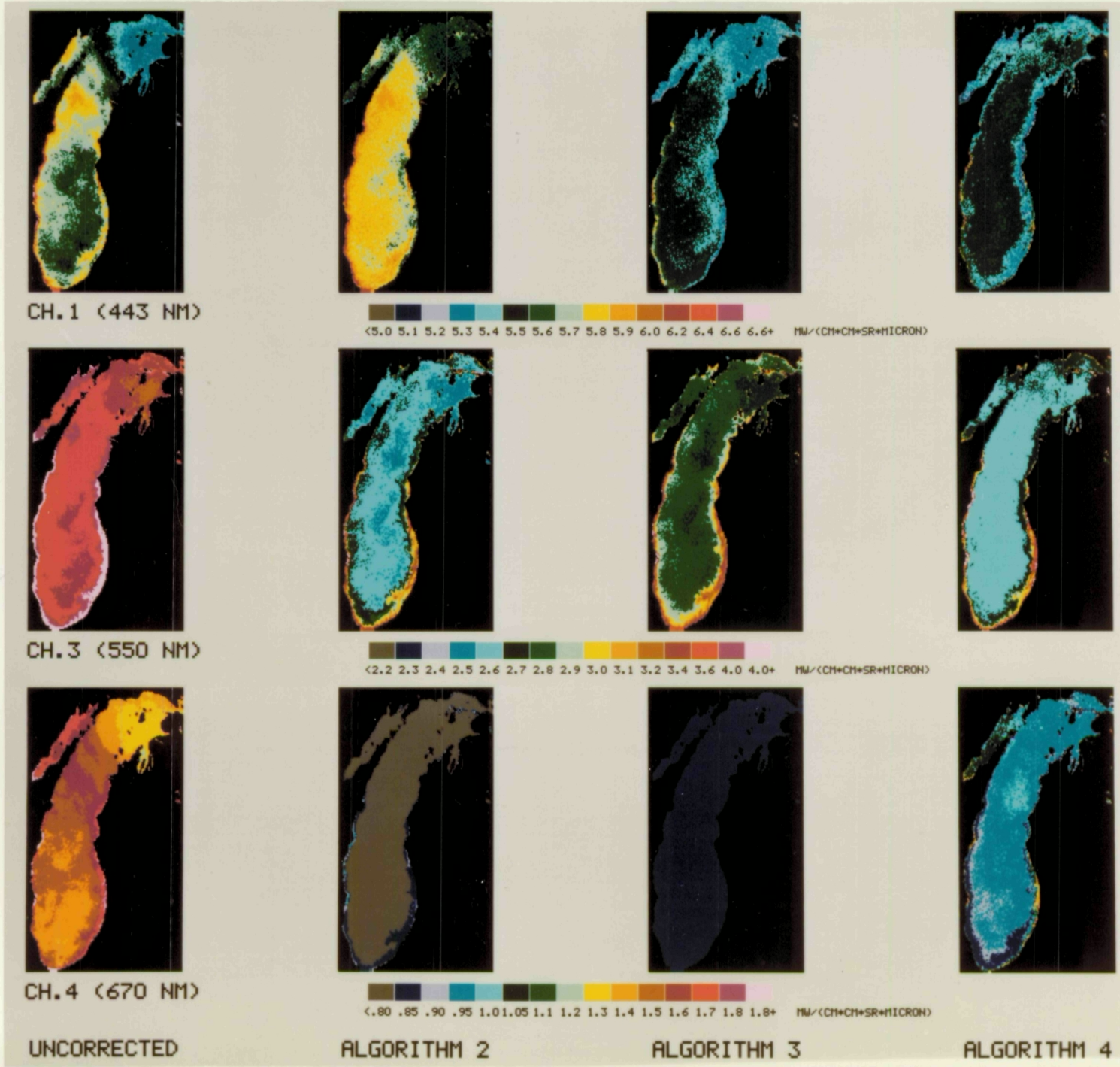

PLATE III

CHLOROPHYLL-A AND SUSPENDED SEDIMENT
CONCENTRATION MAPS, LAKE HURON SUBSCENES

Color coded chlorophyll-a pigment concentration (C mg/m^3) maps are shown in the left panel for Lake Huron (upper), Saginaw Bay (lower left), and Lake St. Clair (lower right). Corresponding suspended sediment maps (SM mg/ℓ) are shown in the right panel. These maps were created from the June 11, 1980 CZCS scene. The suspended sediment algorithm was parameterized to map the high concentrations of suspended sediments in Saginaw Bay. For the Saginaw Bay subscene the predicted very low concentration of less than 0.1 mg/ℓ SM outside the Bay is not considered representative of these waters and was a consequence of the algorithm parameterization.

PLATE IV

CHLOROPHYLL-A AND SUSPENDED SEDIMENT
CONCENTRATION MAPS, LAKE MICHIGAN SUBSCENES

Color coded chlorophyll-a pigment concentration (C mg/m^3) maps are shown in the left panel for Green Bay (left), lower Lake Michigan (middle) and Lake Michigan (right). Corresponding suspended sediment maps (SM mg/ℓ) are shown in the right panel. These maps were created from the June 11, 1980 CZCS scene. The suspended sediment algorithm was parameterized to map the high concentrations of suspended sediments in Green Bay. For the Green Bay subscene the predicted very low concentration of <0.1 mg/ℓ SM outside the Bay is not considered representative of these waters and was a consequence of the algorithm parameterization.

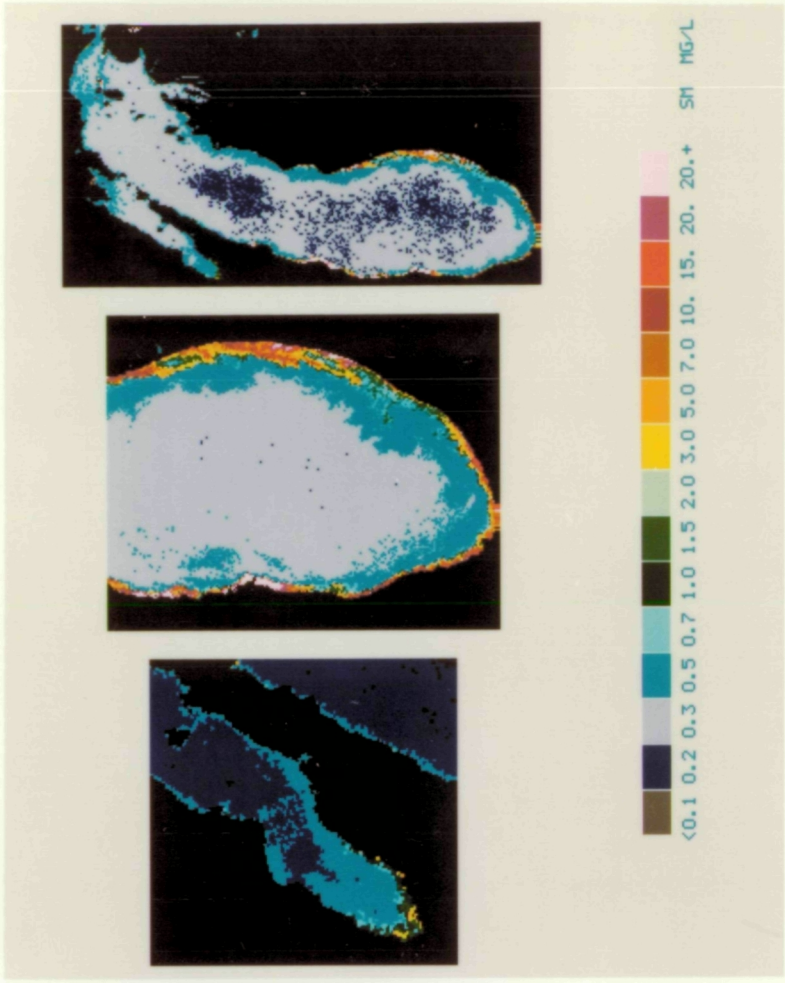

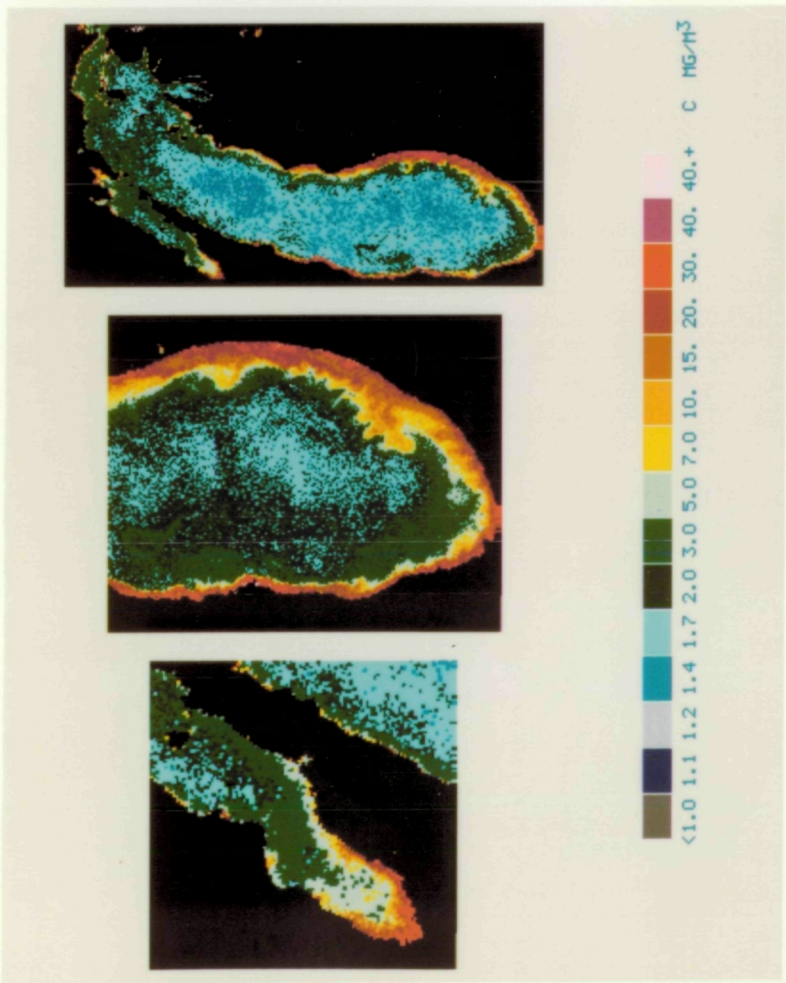

PLATE V

CHLOROPHYLL-A AND SUSPENDED SEDIMENT
CONCENTRATION MAPS, LAKES ERIE AND ONTARIO

Color coded chlorophyll-a pigment concentration (C mg/m^3) maps are shown in the left panel for Lake Erie (upper left), weestern Lake Erie (upper right), and Lake Ontario (lower middle). Corresponding suspended sediment maps (SM mg/ℓ) are shown in the right panel. These maps were created from the July 14, 1980 CZCS scene. The suspended sediment algorithm was parameterized to map the high concentrations of suspended sediments in western Lake Erie. For the Lake Erie and western Lake Erie subscene the predicted very low concentration <0.1 mg/ℓ SM outside the western basin is not considered representative of these waters but were a consequence of the algorithm parameterization. In addition the central portion of Lake Ontario is cloud covered and the mapped concentrations are, therefore, not reliable for this area.

ORIGINAL PAGE
COLOR PHOTOGRAPH

PLATE VI

CHLOROPHYLL-A AND SUSPENDED SEDIMENT
CONCENTRATION MAPS, LAKE SUPERIOR SUBSCENES

Color coded chlorophyll-a pigment concentration (C mg/m^3) maps are shown in the left panel for Lake Superior (upper), Black Bay (lower right), and western Lake Superior (lower left). Corresponding suspended sediment maps (SM mg/ℓ) are shown in the right panel. These maps were created from the August 6, 1980 CZCS scene. The suspended sediment algorithm was parameterized to map the high concentrations of suspended sediments in Black Bay. The predicted very low concentration of <0.1 mg/ℓ SM outside the Bay is not considered representative of these waters and was a consequence of the algorithm parameterization.

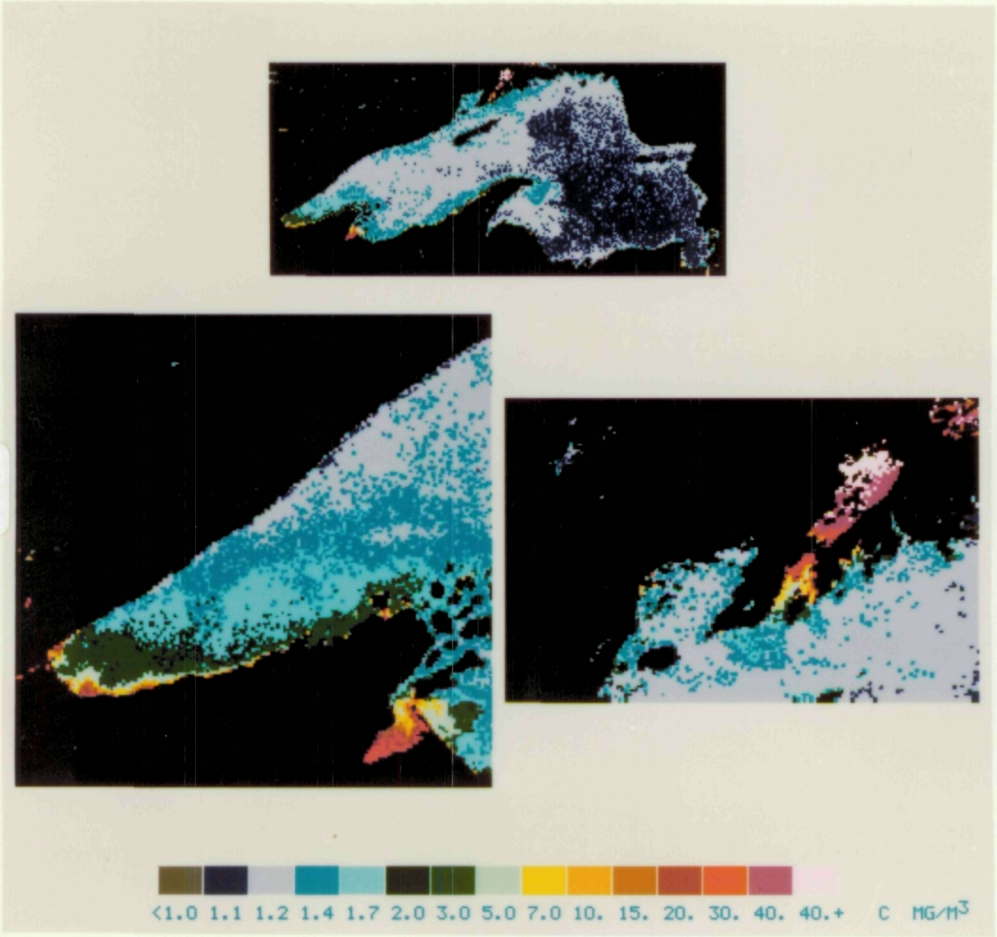
<1.0 1.1 1.2 1.4 1.7 2.0 3.0 5.0 7.0 10. 15. 20. 30. 40. 40.+ C MG/M3

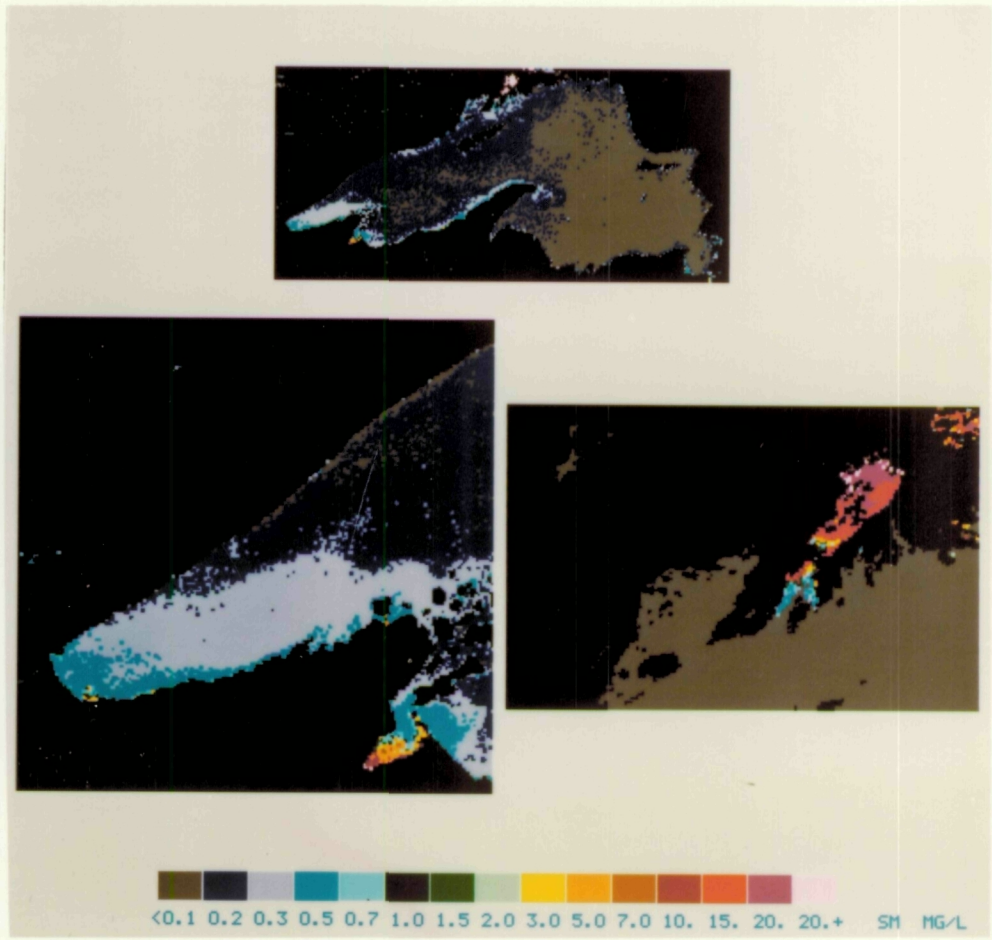
<0.1 0.2 0.3 0.5 0.7 1.0 1.5 2.0 3.0 5.0 7.0 10. 15. 20. 20.+ SM MG/L

PLATE VII

UPWELLING WATER RADIANCE MAPS FOR
LAKE HURON SUBSCENE AT 443 AND 550 NM

This plate shows a color coded water radiance map ($mw/cm^2 \div sr \cdot \mu$) for CZCS bands 1 and 3 (443 and 550 nm). The 443 nm radiance maps are shown on the left panel and the 550 nm maps in the right panel. The upwelling surface radiances as calculated by the atmospheric correction processing have been normalized to a nadir view angle at the top of a Rayleigh atmosphere. The pixel to pixel radiances depict variations in the surface upwelling radiance.

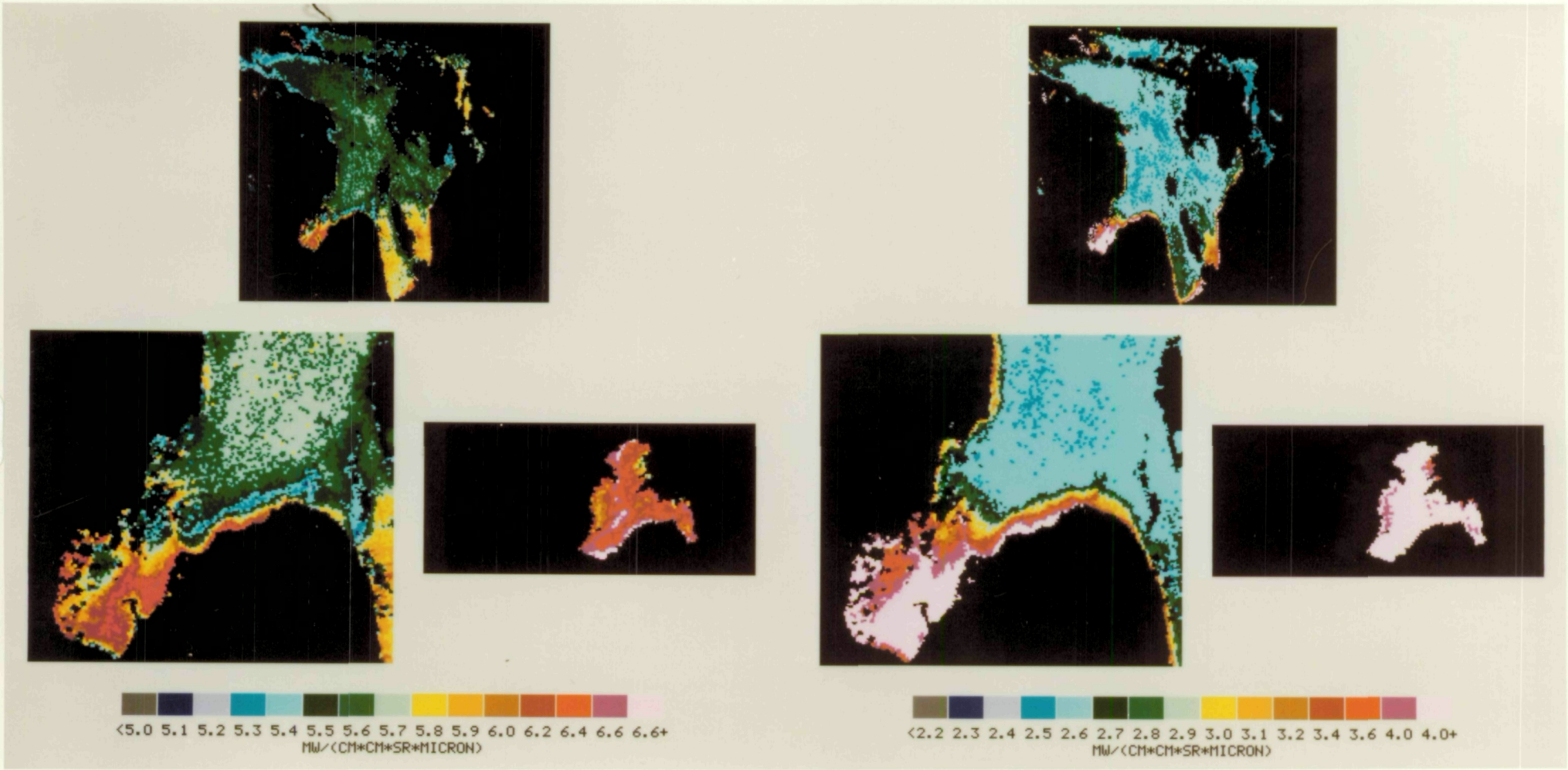
<5.0 5.1 5.2 5.3 5.4 5.5 5.6 5.7 5.8 5.9 6.0 6.2 6.4 6.6 6.6+
MW/(CM*CM*SR*MICRON)
<2.2 2.3 2.4 2.5 2.6 2.7 2.8 2.9 3.0 3.1 3.2 3.4 3.6 4.0 4.0+
MW/(CM*CM*SR*MICRON)

PLATE VIII

CZCS SURFACE TEMPERATURE MAPS FOR
LAKES MICHIGAN AND ERIE SUBSCENES

This plate shows surface temperature over the range from 11 to 25 °C as 1 and 2 degree level slices. CZCS thermal band radiances were calibrated with the available surface measurements. A linear regression model was developed for these data and used to extrapolate to all observed radiance levels. Thus there is greater uncertainty in predicted temperatures at both ends of the scale. The thermal maps on the left are for Lake Erie (upper left), western Lake Erie (upper right) and Lake Ontario (lower middle). Note that the upper portion of Lake Ontario was partially cloud covered for this July 14, 1980 scene. The maps on the right show Green Bay (right), lower Lake Michigan (middle) and Lake Michigan (right). The thermal patterns in Lake Michigan have been shown for this June 11, 1980 scene to be highly correlated to lake bathymetry.

PLATE IX

CZCS SURFCE TEMPERATURE MAPS FOR
LAKES SUPERIOR AND HURON SUBSCENES

This plate shows surface temperature in over the range from 7 to 21 °C as 1 degree increments. CZCS thermal band radiances were calibrated with the available surface measurements. A linear regression model was developed for these data and used to extrapolate to all observed radiance levels. Thus there is greater uncertainty in predicted temperatures at both ends of the scale. The thermal maps on the left are for Lake Superior (upper), western Lake Superior (lower left) and Black Bay (lower right) and were made from the August 6, 1980 scene. The maps on the right show Lake Huron (upper), Saginaw Bay (lower left) and Lake St. Clair (lower right). Note that the upper right hand section of Lake Huron is partially cloud covered for this June 11, 1980 scene.

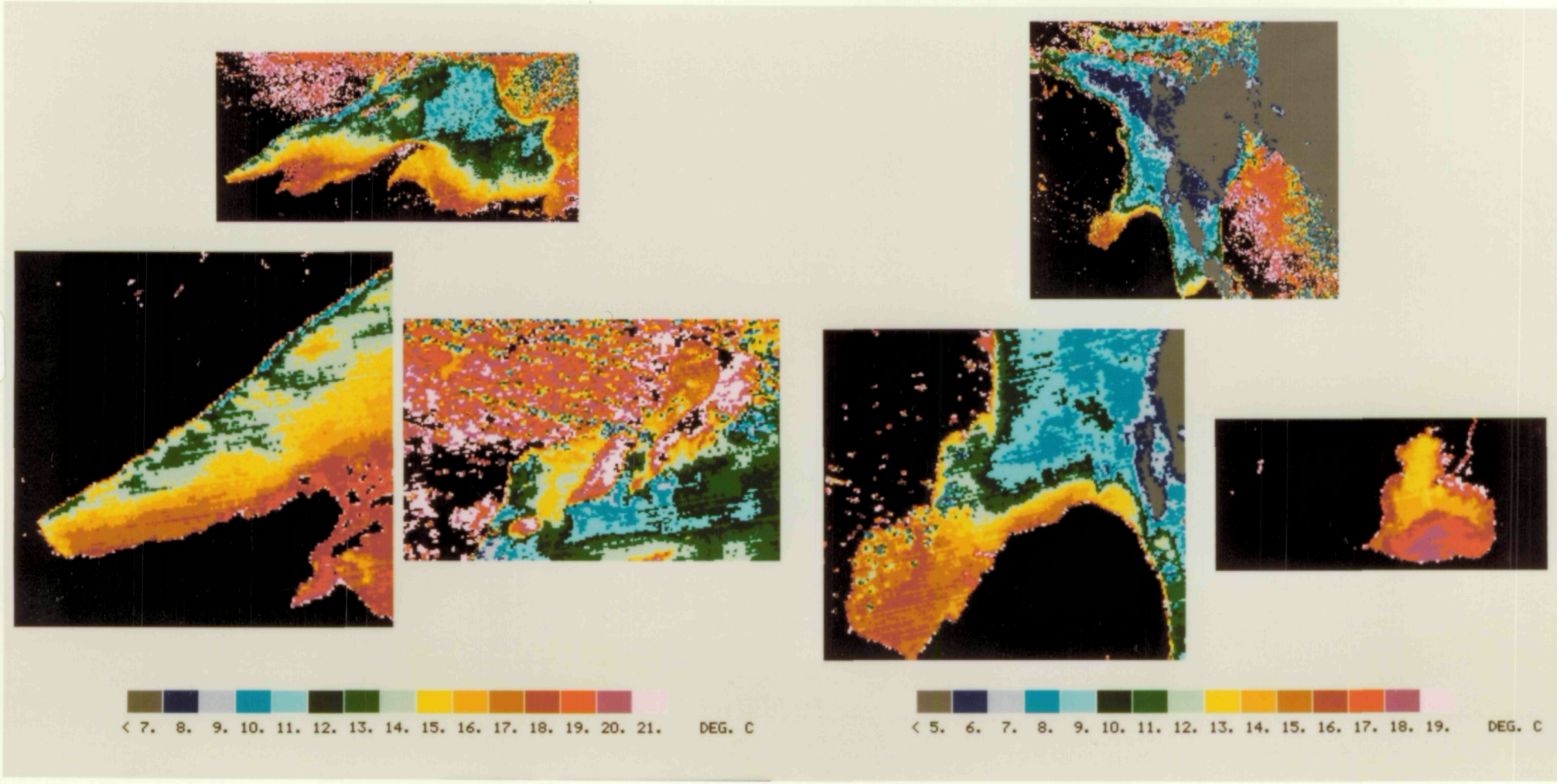
< 7. 8. 9. 10. 11. 12. 13. 14. 15. 16. 17. 18. 19. 20. 21. DEG. C
< 5. 6. 7. 8. 9. 10. 11. 12. 13. 14. 15. 16. 17. 18. 19. DEG. C